Title

ACTIVE MATERIAL REDISTRIBUTION RATES IN ZINC ELECTRODES: EFFECT OF ALKALINE ELECTROLYTE COMPOSITIONS HAVING REDUCED ZINC OXIDE SOLUBILITY

Authors

Nichols, J.T. (Thesis).
McLarnon, F.R.
Cairns, E.J.

Publication Date

1983-11-01

Lawrence Berkeley Laboratory
UNIVERSITY OF CALIFORNIA

APPLIED SCIENCE DIVISION

ACTIVE MATERIAL REDISTRIBUTION RATES IN ZINC ELECTRODES: EFFECT OF ALKALINE ELECTROLYTE COMPOSITIONS HAVING REDUCED ZINC OXIDE SOLUBILITY

J.T. Nichols*, F.R. McLarnon, and
E.J. Cairns

(*M.S. Thesis)

November 1983

APPLIED SCIENCE DIVISION

Prepared for the U.S. Department of Energy under Contract DE-AC03-76SF00098

DISCLAIMER

LBL-17397

ACTIVE MATERIAL REDISTRIBUTION RATES IN ZINC ELECTRODES: EFFECT OF ALKALINE ELECTROLYTE COMPOSITIONS HAVING REDUCED ZINC OXIDE SOLUBILITY

by

James T. Nichols, Frank R. McLarnon, and Elton J. Cairns

November 1983

Berkeley Electrochemical Research Center
Lawrence Berkeley Laboratory
University of California
Berkeley, California 94720

This work was supported by the Assistant Secretary for Conservation and Renewable Energy, Office of Energy Systems Research, Energy Storage Division of the U.S. Department of Energy under Contract No. DE-AC03-76SF00098.

ACTIVE MATERIAL REDISTRIBUTION RATES IN ZINC ELECTRODES: EFFECT OF ALKALINE ELECTROLYTE COMPOSITIONS HAVING REDUCED ZINC OXIDE SOLUBILITY

James Thomas Nichols

ABSTRACT

A series of electrolytes with low hydroxide concentration (~3.5M OH^-) have been tested in 1.35 Ah tri-electrode Zn/NiOOH cells for their ability to reduce zinc redistribution rates. Three electrolytes were evaluated: a 3.5M OH^- electrolyte, a 3.5M OH^--3.4M F^- electrolyte, and a hydroxide-borate electrolyte. The electrolytes were chosen to have a ZnO solubility approximately 25% of that in the standard 30% KOH-1% LiOH electrolyte (7.4 M OH^-). A 6-hour charge rate and a 2.5-hour discharge rate were employed for the Teflon-bonded, zinc oxide electrodes, to which 2% PbO was added to reduce hydrogen evolution. The zinc redistribution rates were found to be lower for the electrolytes with reduced ZnO solubility. In addition, no zinc penetration of the separator occurred for some of the electrolytes, even with overpotentials of 100 to 290 mV. After 125 cycles, none of the cell capacities were limited by the zinc electrode during discharge, less than 2% inactive zinc was found in the zinc electrodes cycled in the hydroxide-fluoride and borate electrolytes.

TABLE OF CONTENTS

Chapter IV, Results & Discussion, cont'd.

Chapter I

Introduction

1. History of the zinc electrode in alkaline electrolyte.

Zn is an attractive negative electrode material for use in secondary batteries with aqueous electrolytes because of both its abundance and relatively light weight.[1] The cadmium electrode is a negative electrode that has seen wide use, has very good reliability and long cycle life, but cadmium is a relatively rare element, obtained as a minor component (0.1 - 0.3%) of zinc ores.[2] Compared to the other secondary battery widely used today, the lead-sulfuric acid battery, the zinc electrode with a NiOOH counter electrode has a demonstrated[1] specific energy of 60-80 Wh/kg at 30 W/kg while the lead acid-battery has a specific energy of 40 Wh/kg.[3]

McBreen and Cairns[1] have published a short history of the various zinc-containing cells that have been investigated and produced. Very briefly summarizing, Volta, in 1800, was constructing Zn-containing primary cells; during the 19th century many types of primary cells were manufactured using Zn as the negative electrode, and PbO_2, air, copper and MnO_2 as positive electrode materials.

For secondary cells the Zn/NiOOH cell was in the literature by 1899, though it received little attention until recent times. Study of the Zn/AgO cell started in the 1920's, and improved cycle life was obtained by using cellulose-containing separators. At the present time Zn/AgO secondary cells with specific energy values of 75 - 120 Wh/kg and lifetimes of 100 cycles[1] are produced for mostly military applications,

where the high cost of the silver is not of significant concern.

Because of the desire to produce large quantities of rechargeable batteries for automotive propulsion,[4] recent years have seen increased emphasis on the Zn/NiOOH cell.[5] Zinc and nickel are desirable because they are sufficiently abundant, and zinc has good resistance to corrosion, a high exchange current density, and light weight. Cycle lifetimes of 155 cycles (at 70 Wh/kg) have been reported for certain charge-discharge regimes and cell constructions,[6] although the precise nature of the cell construction is not known since these reports are not in the open literature. The basic limitations on cycle life have been reported to involve zinc material redistribution, dendrite growth leading to shorting, passivation of Zn, and densification.[1]

The purpose of the research reported here is to study some of these effects in electrolytes different than that primarily used for Zn/NiOOH cells. The electrolytes were chosen primarily to reduce the Zn redistribution rate, but in addition to measuring the rate of redistribution, the electrodes were examined to determine whether differences in morphology existed and whether densification had occurred. Also the quantity of passivated or electrochemically-isolated zinc was determined for some electrodes.

A description of the theories proposed for zinc redistribution is presented in the next section and is followed by Chapter 2 in which a method is described for determining which anion addition to alkaline aqueous electrolytes may result in reduced ZnO solubility.

2. Theoretical models proposed for zinc redistribution

When using the Zn/ZnO negative electrode in alkaline cells, redistribution of Zn across the face of the electrode decreases cell life by reducing the storage capacity.[7,8] As noted above, this is not the only process suspected of reducing the lifetime of Zn-containing secondary cells. The Zn redistribution generally occurs such that the top edge and sides of the Zn electrode lose Zn and ZnO, leaving bare current collector.[7]

Cell capacity is reduced because the counter electrode opposing the bare area cannot be charged or discharged at significant rates. No electrochemical reaction can occur on the bare current collector because ZnO is not available to be reduced during charge of the cell and Zn metal is not available to be oxidized during discharge of the cell. In the absence of any charge-transfer processes at this bare current collector, current cannot flow between the Zn electrode and the counter electrode in this area.* Because charge-transfer processes do not occur in this area of the Zn electrode, the counter electrode can only be charged or discharged through relatively high-resistance current paths to areas on the Zn electrode where charge transfer processes can occur. Thus the counter electrode is not fully charged or discharged and a decreased energy storage capacity is observed.

---

*In actual fact some Zn^{2+} species exists in the electrolyte and is reduced on charge and reoxidized on discharge, but this would be insufficient to significantly charge the counter electrode.

McBreen has proposed a mechanism to account for this Zn redistribution across the face of the electrode.[9] The proposed process involves uneven current distributions which lead to concentration gradients that ultimately lead to the movement of zinc material away from the top and sides of the electrode. These concentration gradients depend on the amount of soluble zinc species in the electrolyte. Concentration gradient-dependent Zn redistribution is consistent with experimental observations.

Another mechanism for Zn redistribution has been proposed by Choi, Bennion and Newman.[10] Their model involves osmotic and electro-osmotic forces which pump water from one electrode compartment to another across the separating membrane. The movement of water causes convective flows that are proposed to carry soluble Zn species in such a way as to give the observed Zn redistribution.

The electro-osmotic flow of water results directly from the current flow of K^+ ions in the KOH electrolyte through the cationic membrane. On discharge, the current flow and water flow is from the Zn electrode toward the counter electrode. At the same time the electrochemical processes at the counter electrode result in an increase in the OH^- concentration in the counter electrode compartment. The increase in KOH in the counter electrode compartment gives rise to an osmotic force that causes water to move across the membrane toward the counter electrode. In addition an opposing osmotic force results from the increase in $Zn(OH)_4^=$ in the Zn compartment; however, the net water flow is toward the counter electrode during discharge. When the cell charges, the net water flow is in the opposite direction.

The result of the electro-osmotic and osmotic flows is a decreasing electrolyte level, thus downflowing in the zinc compartment during discharge and an upflow during charge. During discharge zincate ($Zn(OH)_4^=$) supersaturates the electrolyte and ZnO slowly precipitates. Coupled with the downflow, a solution concentrated in zincate moves toward the lower region of the electrode. During the charge, the flow is upward, but the electrolyte becomes depleted in zincate as Zn metal deposits on the electrode. The difference in the concentration of zincate between the downflowing electrolyte on discharge and the upflowing electrolyte on charge gives a net movement of zinc material toward the lower regions of the zinc electrode as cycling continues.

Both McBreen's current distribution model and Choi, Bennion, and Newman's osmotic pumping model for zinc redistribution are processes involving mass transfer of material, one by diffusion and the other by convection. It can easily be seen then that the rates of zinc redistribution, that is the mass transfer rates, are directly dependent on the concentration of the soluble zinc species. For McBreen's model the higher the absolute concentration of soluble zinc in the electrolyte the greater the differences in concentration. The result will be a more rapid diffusion rate and zinc redistribution rate. In the case of Choi, Bennion and Newman's model, the higher the absolute concentration of soluble Zn, the greater will be the difference in Zn between the discharge downflowing and charge upflowing electrolyte resulting in a more rapid movement of zinc to the lower regions of the electrode.

Both sets of authors mention that supersaturation phenomena are expected to occur in operating cells containing the alkaline zinc electrode. A reduction of the degree of supersaturation (a factor of 2 to 3 times equilibrium concentration) would reduce the rate of shape change according to both models. Hopefully a reduction of the equilibrium concentration would reduce the degree of supersaturation.

The primary goal of the research described in this thesis was to determine methods to reduce the concentration of soluble Zn in the alkaline electrolyte and measure the effect of this reduced Zn concentration on the Zn redistribution rate. In the following chapter, ZnO chemistry in alkaline electrolytes is described and a method to determine the effect of various anions on the solubility of Zn^{2+} species is proposed.

3. References for Chapter I.

1. E.J. Cairns and J. McBreen, in "Advances in Electrochemistry and Electrochemical Engineering," Vol. 11, H. Gerischer and C.W. Tobias, Eds., John Wiley and Sons (1978).

2. C.J. Smithells and E.A. Brandes, Eds., "Metals Reference Book," 5th edition, Butterworth and Co. Ltd., London (1976).

3. J. Miller, J.B. Rajan, F. Hornstra, C.C. Christianson and N.P. Yao, Extended Abstracts, Electrochem. Soc., Vol. 82-2, p.1 (1982).

4. E.J. Cairns, Lawrence Berkeley Laboratory Report No. LBL-13199 (1981)

5. "Final Report Design and Cost Study Zinc/Nickel Oxide Battery for Electric Vehicle Propulsion," Yardney Electric Div., Argonne National Laboratory, Report 2033-76, Argonne, IL (1976).

6. "Annual Report for 1980 R&D for EV Propulsion, Gould," Argonne National Laboratory Report/OEPM 80-14 (1981), available from U.S. Department of Commerce, Springfield, VA.

7. J.J. Murphy, Chem. Technol. 1, 487 (1971).

8. J.J. Lander, "Zinc-Silver Oxide Batteries" A. Fleisher, J.J. Lander, Eds., John Wiley and Sons, New York, 1971, pp. 457-469.

9. J. McBreen, J. Electrochem. Soc. 119, 1620, (1972).

10. K.W. Choi, D.N. Bennion and J. Newman, J. Electrochem. Soc. 123, 1616, (1976).

Chapter II

Solubility of Oxidized Zinc Species in Concentrated KOH.

1. Introduction

The aqueous hydroxyl group forms complexes with Zn^{2+} for which the complex coefficients of formation have been reported.[1,2] Solubility products for zinc hydroxide have also been reported.[1,3,4] From this information one can predict the solubility of zinc hydroxide in concentrated KOH; and given the solubility products between zinc and other anions, the effect of these anions on the solubility of oxidized zinc can be determined. The situation is complicated, however, by the appearance of several crystalline and non-crystalline $Zn(OH)_2$ precipitates and zinc oxide precipitates that can form from zinc-containing alkaline solutions.[1,3]

The solubility of zinc species in alkaline electrolytes, and in fact the structure of zinc oxides and hydroxides has been a subject of much controversy.[5] It was only after considerable effort that the existence of hydroxyl groups in oxidized zinc compounds was proven, and the species present in solution are still subject to debate and much research.[6,7,8]

Equilibrium constants have been difficult to determine, most likely because of the many solid forms of hydroxide and oxide present in precipitates from alkaline solution. It is helpful nonetheless to examine the equilibrium expressions and the presently best-known equilibrium

constants to determine which species, if any, may alter the solubility of oxidized zinc. These expressions allow computation of changes in zinc species concentration as the Zn electrode is charged and discharged, within the limits of the accuracy of equilibrium data and applicability at high concentrations.

A discussion of the solubility of Zn^{2+} species in equilibrium with ε-$Zn(OH)_2$ and ZnO in concentrated hydroxide solutions is presented below. The solubilities predicted from the equilibrium expressions are compared to the reported solubilities for $Zn(OH)_2$. Based on the complex formation constant used to predict $Zn(OH)_2$ solubility, and the solubility product for zinc and another anion, the effect of other anions on the solubility of oxidized zinc in the presence of hydroxyl ions can be estimated. Using the comparison between the predicted $Zn(OH)_2$ solubility and the actual solubility, one can place error limits on the magnitude of the effect of other anions.

2. Zinc oxide solubility and supersaturation in aqueous potassium hydroxide

The dissolution of zinc oxide in KOH solutions requires considerable time to reach saturation unless the slurry is vigorously stirred.[9] Solubilities of ZnO in these solutions have been reported by several workers.[9,10,11,12] These data are shown in Figure II-1 and are in close agreement, though the data from P.R. Mallory Co. presented in reference 11 appear to be high. Supersaturated zinc oxide solutions in aqueous potassium hydroxide have been reported to remain supersaturated with

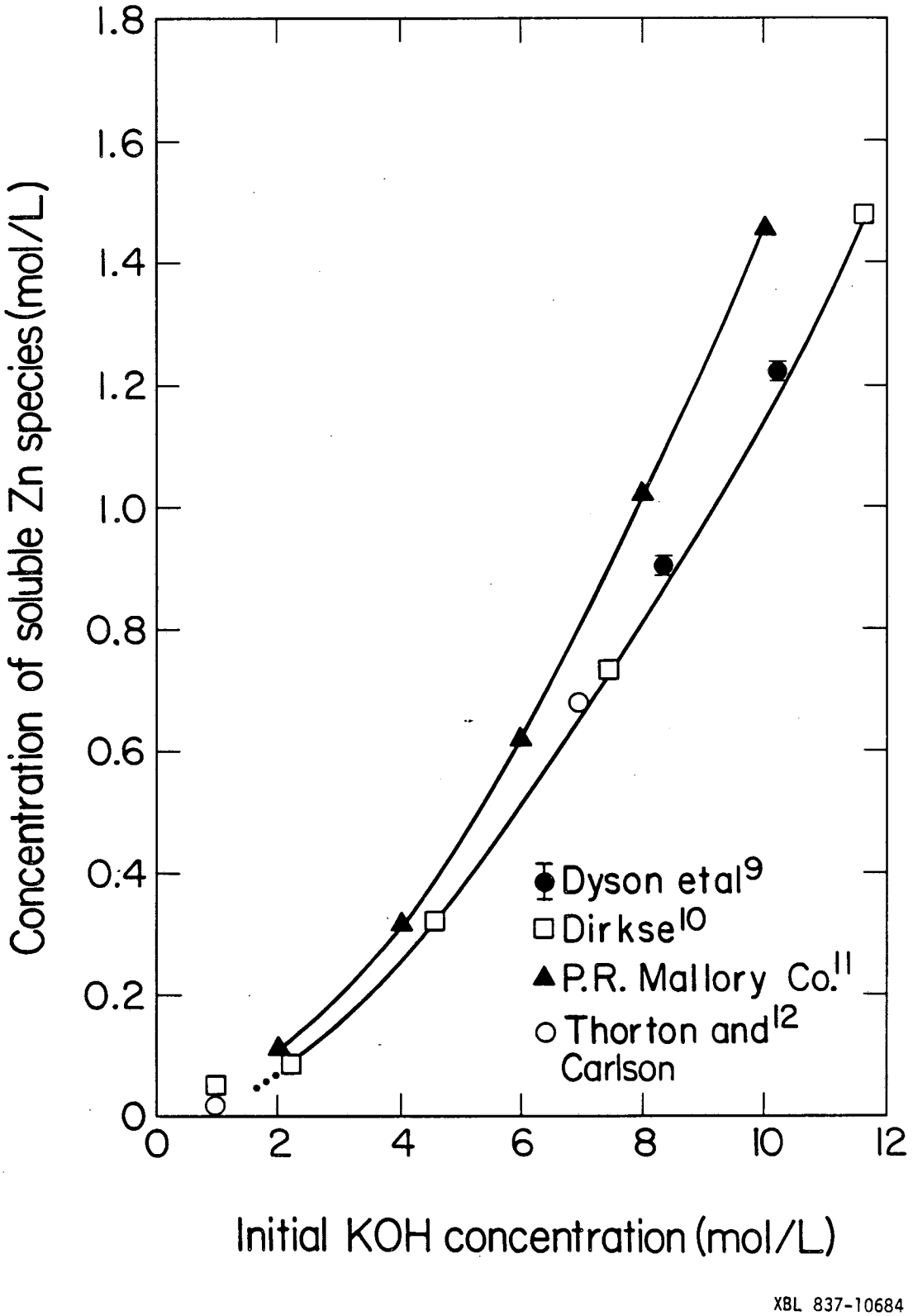

Figure II-1. Solubility of Zinc Oxide at 25°C in Potassium Hydroxide Solutions

respect to ZnO for long periods of time.[6] These supersaturated solutions can be produced by electrochemically dissolving zinc or, to a lesser extent, by dissolving $Zn(OH)_2$ in potassium hydroxide solutions. These slow kinetics are still under investigation.[6] Zinc oxide solubility will be discussed further in section 4 in relation to the formation of hydroxide complexes.

3. Zinc hydroxide solubility in alkaline electrolyte

The solubilities of sparingly-soluble salts are usually reported in the form of solubility products. $Zn(OH)_2$ is such a sparingly soluble salt, and its solubility product has been reported.[1,3,4] The first reference cited contains a summary of these solubility products. The authors note the value varies from 10^{-13} to 10^{-21} but report values of 0.7 to 3.8 x 10^{-17} from various researchers as the best data available for ε-$Zn(OH)_2$. These researchers were sufficiently accurate in reporting experimental procedures that the authors could satisfy themselves of the purity of the ε-$Zn(OH)_2$ used. A "best" value of the solubility product, Ksp, is reported as 3.5 x 10^{-17} for the following expression

$$Ksp = (Zn^{2+})\ (OH^{-})^2 \qquad [2\text{-}1]$$

Equation [2-1] is written in terms of activities and Ksp is used as the thermodynamic equilibrium constant. This can be done because the concentrations were measured in dilute solutions where the activity coefficients are nearly unity. Expressions will be developed here to predict zinc species concentrations in solutions with high ionic

strength where equation [2-1] and the reported solubility product do not rigorously apply. By comparing these predictions to solutions where solubility has been measured, the magnitude of the error in using equation [2-1] can be estimated.

At high hydroxyl-ion concentrations the hydroxyl group is believed to tetrahedrally complex the Zn^{2+} ion.[1,2,6] The overall formation constant, β_4, has been reported as 2×10^{12} to 5×10^{17}. Some of the most recent measurements, at low ionic strength, are 1.4×10^{15}, 3.0×10^{15}, 5.0×10^{17} and 3.7×10^{15}. The 5×10^{17} data point is far from the others and will be disregarded. An average value of 2.7×10^{15} will be used in the calculations to follow.

The overall complex-formation reaction has the following equilibrium expression:

$$\beta_4 = \frac{[Zn(OH)_4^{=}] \; \gamma_{Zn(OH)_4^{=}}}{[Zn^{2+}] \; [OH^-]^4 \; \gamma_{OH^-}^4 \; \gamma_{Zn^{2+}}} \qquad [2\text{-}2]$$

Combining equations [2-1] and [2-2] with a charge balance will eliminate $[OH^-]$ and $[Zn^{2+}]$ from the equations to give the zinc tetrahydroxyl concentration in terms of the metal ion concentration, $[M^+]$; the activity coefficients; β_4; and Ksp.

$$[Zn(OH)_4^{=}] = \frac{M + X/4}{2} - 1/2 \sqrt{\frac{X^2}{16} + \frac{MX}{2}} \qquad [2\text{-}3]$$

where:

$$M = [M^+]$$

$$X = \frac{\gamma_{Zn(OH)_4^{=}}}{(\gamma_{OH^-})^2} \times \frac{1}{\beta_4 Ksp}$$

By comparing the complex-formation constants (not presented here) of the Zn mono-, di-, and trihydroxide it can be determined that the predominant species in concentrated (>1M) hydroxide solutions is $Zn(OH)_4^{=}$, thus equation [2-3] provides a prediction of total soluble zinc in a $Zn(OH)_2$-saturated alkaline solution. The complete derivations are shown in Appendix A.

Other species may form in concentrated solution that are not taken into account by the above analysis. Dimers or polymeric forms[6] of tetrahedrally complexed Zn^{2+} have been proposed. If a significant amount of these species were to form, then a deviation from equation [2-3] would be expected in the direction of larger concentrations of soluble zinc in an electrolyte. Because of the effects of ionic strength on the activity, these polymeric effects are expected to be masked unless they are quite large.

Figure II-2 shows the predicted $Zn(OH)_2$ solubility from equation [2-3], with γ's = 1, compared to experimentally-measured $Zn(OH)_2$ solubility. The predicted values are low, but activities were ignored, and there is a great deal of variation in the reported solubility product and complex formation constant. Furthermore, the dilute-solution equilibrium constants may not apply in the concentrated region to which equation [2-3] applies.

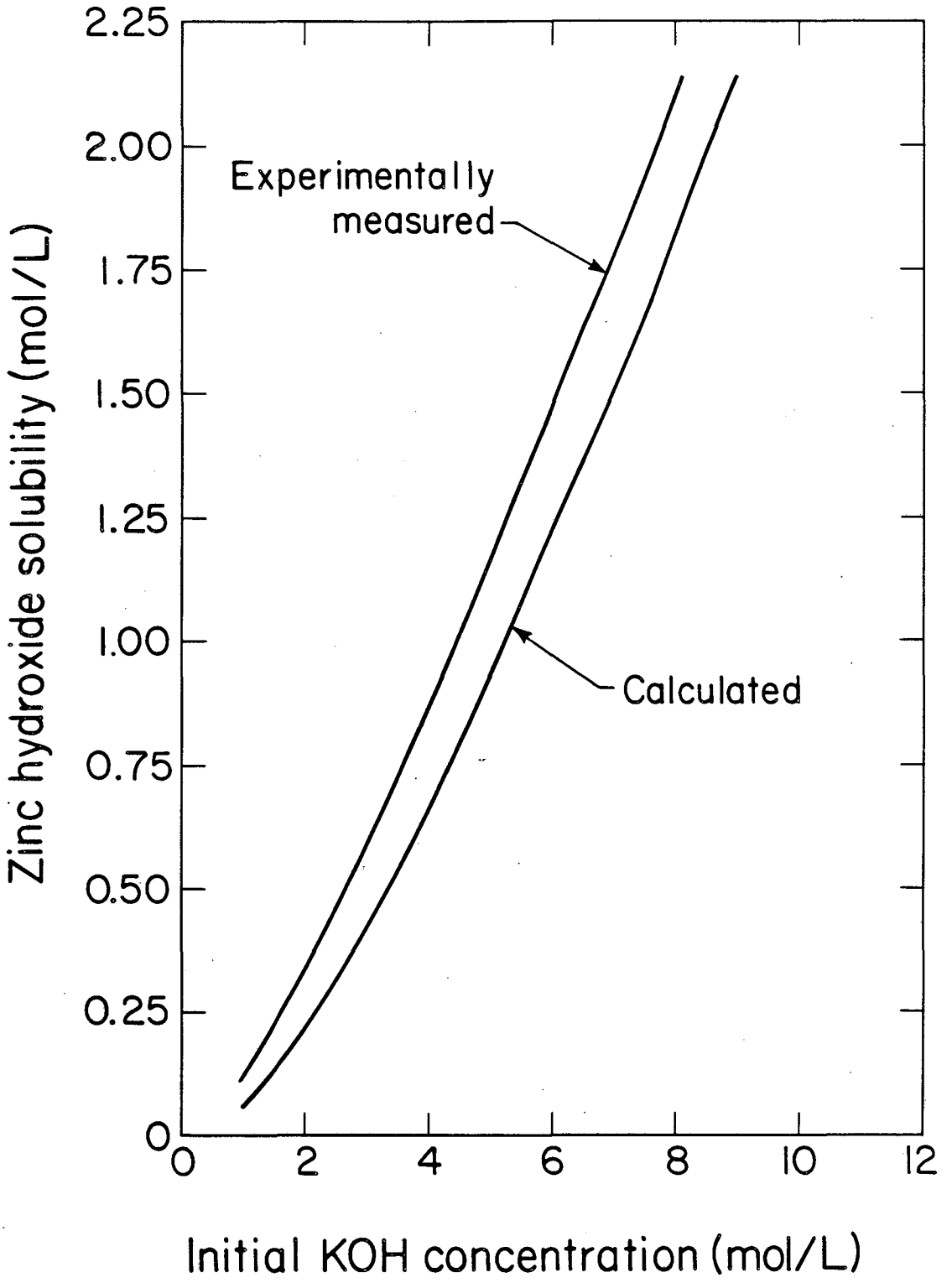

XBL 837-10683

Figure II-2. Comparison of $Zn(OH)_2$ solubility predicted by Equation[2-3] and $Zn(OH)_2$ solubility measured by P.R. Mallory Co.[11]

4. Zinc oxide solubility related to hydroxyl ion complexing.

Using the overall complex-formation equilibrium expression, Equation [2-2], and solubility data for ZnO in aqueous KOH solutions, a solubility product could be calculated. It is obvious that this solubility product would be less than that for $Zn(OH)_2$ by comparing the solubility data for $Zn(OH)_2$ in Figure II-2 with that for ZnO in Figure II-1. Because the activity coefficients are not known, no attempt will be made here to calculate this solubility product using such data.

It is this lower ZnO solubility product that determines the equilibrium concentration of Zn species in concentrated alkaline solutions however. When $Zn(OH)_2$ is dissolved in alkaline solutions, the Zn^{2+} concentration and all other zinc hydroxyl-ion complex species are higher than their equilibrium concentrations with ZnO. Therefore the $Zn(OH)_2$ saturated solution is unstable and ZnO will precipitate, though slowly.[6]

If another anion were present in an alkaline solution, it is conceivable that the Zn^{2+} concentration, in equilibrium with ZnO, would be higher than the equilibrium concentration of Zn^{2+} in the presence of the new ion. In this case the solution would be unstable and the Zn salt of that anion would precipitate. This is the desired result to reduce Zn solubility, i.e. a Zn^{2+} concentration lower than the equilibrium value with respect to ZnO.

In the following section the overall complex-formation expression will be used in conjunction with the solubility products of various salts to predict the $Zn(OH)_4^=$ concentration. If this concentration is less than that of a solution in equilibrium with ZnO, then the anion of

these salts is a candidate additive to reduce zinc solubility in concentrated KOH electrolyte for Zn electrodes.

5. Predicted effect of various anions proposed to reduce Zn solubility

Using the complex-formation expression, equation [2-2], and the solubility product of another anion with zinc, an estimate can be made of the solubility of Zn species in KOH, with due consideration to the effect of ionic strength on the solubility product. The assumption is made in this analysis that there are no other soluble Zn species except those accounted for in the complex formation equation. This is a debatable assumption because investigators cite evidence for other Zn species in concentrated KOH solutions saturated by ZnO.[7] Specifically $ZnO_2^{=} \cdot 2H_2O$ has been proposed.

The data and calculated $Zn(OH)_2$ solubility shown in Figure II-2 indicate that the estimate of zinc hydroxide solubility using the solubility product and the complex formation equilibrium gives a fair estimate of the solubility of $Zn(OH)_2$. One cannot expect this type of calculation to be sufficiently accurate to prove or disprove the existence of $ZnO_2^{=} \cdot 2H_2O$. The complex-formation equilibrium expression only predicts the concentration of $Zn(OH)_4^{=}$; if $ZnO_2^{=} \cdot 2H_2O$ exists, then its concentration would depend on another equilibrium and its presence would increase the amount of soluble zinc in the KOH solution. If the estimate of $Zn(OH)_4^{=}$ concentration were highly accurate, then any additional soluble zinc over the estimate could be attributed to $ZnO_2^{=} \cdot 2H_2O$ (or other soluble species). But such is not the case, because the

solubility estimate is only an order-of-magnitude estimate.

The zinc solubility, as $Zn(OH)_4^=$, will be calculated for the anions sulfide and phosphate, $ZnO_2^= \cdot 2H_2O$ notwithstanding. ZnS and $Zn_3(PO_4)_2$ are two of the most sparingly soluble salts of zinc with solubility products of $1 \cdot 10^{-21}$ and $9.1 \cdot 10^{-33}$, respectively.[4] ($Zn(OH)_2$, ZnO and $ZnCO_3$ are some other sparingly soluble zinc compounds.) In the calculation to follow, it will be shown that PO_4^{3-} has no influence on the solubility of oxidized Zn in strong KOH, but $S^=$ may have some effect. Due to unknown activity coefficients, equilibrium constants, and existence of other species, the exact effect on solubility can be determined only by measurement of solubility in an $OH^-/S^=$ electrolyte.

Since the solubility product for zinc phosphate is so small, the concentrations are small under the conditions that apply when the solubility product is determined, thus the activity coefficients are near unity. In this case the solubility product, Ksp_{PO_4}, can be taken to be the thermodynamic equilibrium constant. The equilibrium expression for zinc phosphate is:

$$Ksp_{PO_4} = (PO_4^{3-})^2 \ (Zn^{2+})^3 \qquad [2-4]$$

The following derivation, using the overall complex-formation expression, Equation [2-2], will be valid for strong KOH where the predominant species in solution is $Zn(OH)_4^=$.

The $Zn(OH)_4^=$ concentration is proportional to the Zn^{2+} concentration, which is assumed to be fixed by Equation [2-4]. If the calculated solubility is higher than that for ZnO in equilibrium with the KOH solution, then the assumption is false. That is, the Zn^{2+} concentration is fixed at a lower concentration by the equilibrium with ZnO, and $Zn_3(PO_4)_2$ will not be present. If $Zn_3(PO_4)_2$ is initially present, it will dissolve and ZnO will precipitate to the extent permitted by the mass balance. Either all of the zinc phosphate will dissolve or hydroxyl ions will be depleted.

Combining Equations [2-2] and [2-4] gives an expression from which the hydroxyl-ion concentration can be eliminated by introducing an expression for the charge balance. The resulting expression is valid for any physically-obtainable hydroxide and phosphate concentration. The reaction of phosphate to biphosphate is ignored to give a "best case" calculation. The loss of phosphate by reaction to biphosphate will increase the Zn^{2+} ion concentration according to Equation [2-4] and thus the $Zn(OH)_4^=$ concentration according to Equation [2-2].

For the special case of zinc phosphate dissolving in a hydroxide solution, three zinc ions are produced for two phosphate ions. The phosphate is thus eliminated from the expression to give:

$$[Zn(OH)_4^=]^5 = (\tfrac{9}{4})\,\beta_4^3\, Ksp_{PO_4}\,([M^+]-4[Zn(OH)_4^=])^{12}\,\frac{(\gamma_{OH^-})^{12}}{\gamma_{PO_4^{-3}}^2\;\gamma_{Zn(OH)_4^=}^3} \qquad [2\text{-}5]$$

Where $[M^+]$ is the initial alkali cation (and OH^-) concentration before addition of the zinc phosphate. The complete derivation is contained in

Appendix A.

Table II-1 contains results from the solution of implicit Equation [2-5] for various initial MOH concentrations assuming activity coefficients of 1. It can be seen that the zinc solubility is approximately $[M^+]/4$, as one would expect for an extremely high solubility. The solubility is limited only by the amount of hydroxyl ion present to complex the zinc ion.

TABLE II-1

$[M^+]$ (M)	$[Zn(OH)_4^=]$ (M)
1	0.243
2	0.490
4	0.984
6	1.48
8	1.98
10	2.48

Zinc sulfide is another sparingly-soluble salt of Zn^{2+}. The equilibrium solubility expression is:

$$(Zn^{2+}) = \frac{Ksp_S}{(S^=)} \qquad [2\text{-}6]$$

The solubility product is $1 \cdot 10^{-21}$. Sulfide is a strong base, but for the purposes of this discussion, the presence of an equilibrium with bisulfide will be ignored.

Again, assuming the zinc tetrahydroxyl ion is the major species, Equation [2-6] can be substituted into the complex-formation Equation [2-2] for (Zn^{2+}). Introducing the charge balance to eliminate the OH^- and the mass balance to eliminate the $S^=$ for the situation of dissolving ZnS in a hydroxide-containing solution gives

$$[Zn(OH)_4^=] = \frac{8[M^+] + \frac{1}{\sqrt{A}} - \sqrt{\left(\frac{16[M^+]}{\sqrt{A}} + \frac{1}{A}\right)}}{32} \qquad [2\text{-}7a]$$

$$A = \frac{Ksp_S \beta_4 (\gamma_{OH^-})^4}{\gamma_{Zn(OH)_4^=} \gamma_{S^=}} \qquad [2\text{-}7b]$$

The detailed derivation is presented in Appendix A. For all activity coefficients set equal to one, the solubility is 0.074M in 7M MOH.

The density corrections have been left out of the above derivation because the uncertainties in the complex-formation constant and activity coefficients are more significant in comparison. The presence of bisulfide was ignored for convenience; its effect will now be considered.

The dissociation constant for bisulfide is 1.2×10^{-15}, [4] so in 7M KOH, with a hydroxyl ion activity[7] of 20, the ratio $(S^=)/(HS^-)$ is approximately 2. As sulfide converts to bisulfide, hydroxyl ions are produced; the combined effect is to increase the $Zn(OH)_4^=$ concentration. The presence of any other complexes such as those involving bisulfide will further increase the solubility. The solubility expressed by Equation [2-7] therefore represents the minimum solubility.

In conclusion, it was shown in Section 3 that zinc hydroxide solubility can be predicted, to within a factor of ten, by using solubility products and complex-formation coefficients determined in dilute solutions. This level of accuracy is sufficient to use the complex formation constant and solubility products of other zinc salts to screen possible KOH electrolyte additives to reduce oxidized zinc solubility. Phosphate does not appear to substantially reduce the oxidized zinc solubility but sulfide appears to have a large effect. The use of sulfide in a cell is not practical however. Sulfide oxidizes to sulfur at the potential of the NiOOH electrode and probably would not remain in its reduced form through the life of the cell.

6. Candidate electrolytes for reducing Zn redistribution rates

As noted in the Introduction, the rate of zinc redistribution of a Zn electrode cycled in alkaline electrolyte should be related directly to the concentration of soluble zinc species in the electrolyte. A reduction of the zinc species concentration should lead to a reduction in the zinc redistribution rate, all other parameters remaining constant. The most insoluble compounds of zinc were noted to be ZnO, $Zn(OH)_2$, ZnS and $Zn_3(PO_4)_2$. The zinc oxide solubility has been shown in Figure II-1. Zn redistribution rates of electrodes containing ZnO have been determined to be too high for long-lived zinc electrodes.[13] Zinc hydroxide dissolves and reprecipitates as ZnO. This is commonly referred to[14] as aging of $Zn(OH)_2$. The effects of sulfide and phosphate addition to the KOH electrolyte have been estimated earlier in this chapter and found to be unacceptable for use in secondary alkaline Zn

cells. The phosphate appears to have little effect in reducing the zinc species concentration and sulfide will oxidize at the potential of the nickel electrode.

Another technique to reduce the zinc concentration is obvious from examination of Figure II-1: the reduction of the hydroxide concentration. It has been reported that the zinc redistribution rate is reduced when the hydroxide concentration is reduced.[15] These observations were made at concentrations higher than the 31% KOH commonly used for alkaline Zn/NiOOH cells. Lower KOH concentrations have not been used because of the lower utilization of the $Ni(OH)_2$ in the nickel oxide counter electrode.[11] In addition, the conductivity is reduced[16] in KOH solutions below 31%.

Another potential problem for Zn electrodes discharged in electrolytes with lower hydroxide concentration is an increased tendency toward passivation. Dirkse[14] summarizes the speculation of some researchers that as hydroxyl ions are depleted at the surface of the Zn electrode, the dissolved zinc precipitates as $Zn(OH)_2$ and passivates the electrode. Another proposed mechanism is the precipitation of ZnO or $Zn(OH)_2$ from a supersaturated electrolyte in the vicinity of the electrode surface. In either case, a reduction of the KOH concentration will give an electrolyte from which ZnO or $Zn(OH)_2$ will form sooner and at a lower current density. Dirkse has questioned[14] this precipitation model, and work continues toward the understanding of the nature of zinc passivation.

To reduce the zinc concentration in KOH electrolyte, several modified electrolytes have been used, but none have been found to give reduced solubility, high conductivity, and high counter-electrode utilization at the same time. $Ca(OH)_2$ has been used by several researchers to reduce the hydroxide concentration,[17,18] and at lower hydroxide concentration F^-, $PO_4^{\equiv}$ and BO_3[12,19-24] have been tested for various proposed advantages. Oxalates have also been used in attempts to reduce zinc concentration.[19]

A borate and a fluoride containing electrolyte with a low KOH concentration were chosen for the experiments reported here. Figure II-3 shows the ZnO solubility in some of these combinations in relation to the hydroxide concentration of the initial electrolyte. It is obvious for most electrolytes shown that the added anion has no significant affect on the ZnO solubility. The solubility appears to be determined solely by the hydroxide concentration.

The alkalinity of the borate-containing electrolyte is unknown, but the range of possible hydroxide concentrations includes the hydroxide concentration of a KOH electrolyte with the same ZnO solubility. No attempt has been made here to calculate the free hydroxyl-ion concentration in the borate-containing electrolytes using the boric acid dissociation constants.

The electrolytes used in this work are shown in Table II-2. A reduced hydroxide concentration of 3.5M was chosen as a factor of approximately two lower than the standard 30% KOH-1% LiOH electrolyte. An experiment involving the 3.5M OH^- electrolyte without any other anion

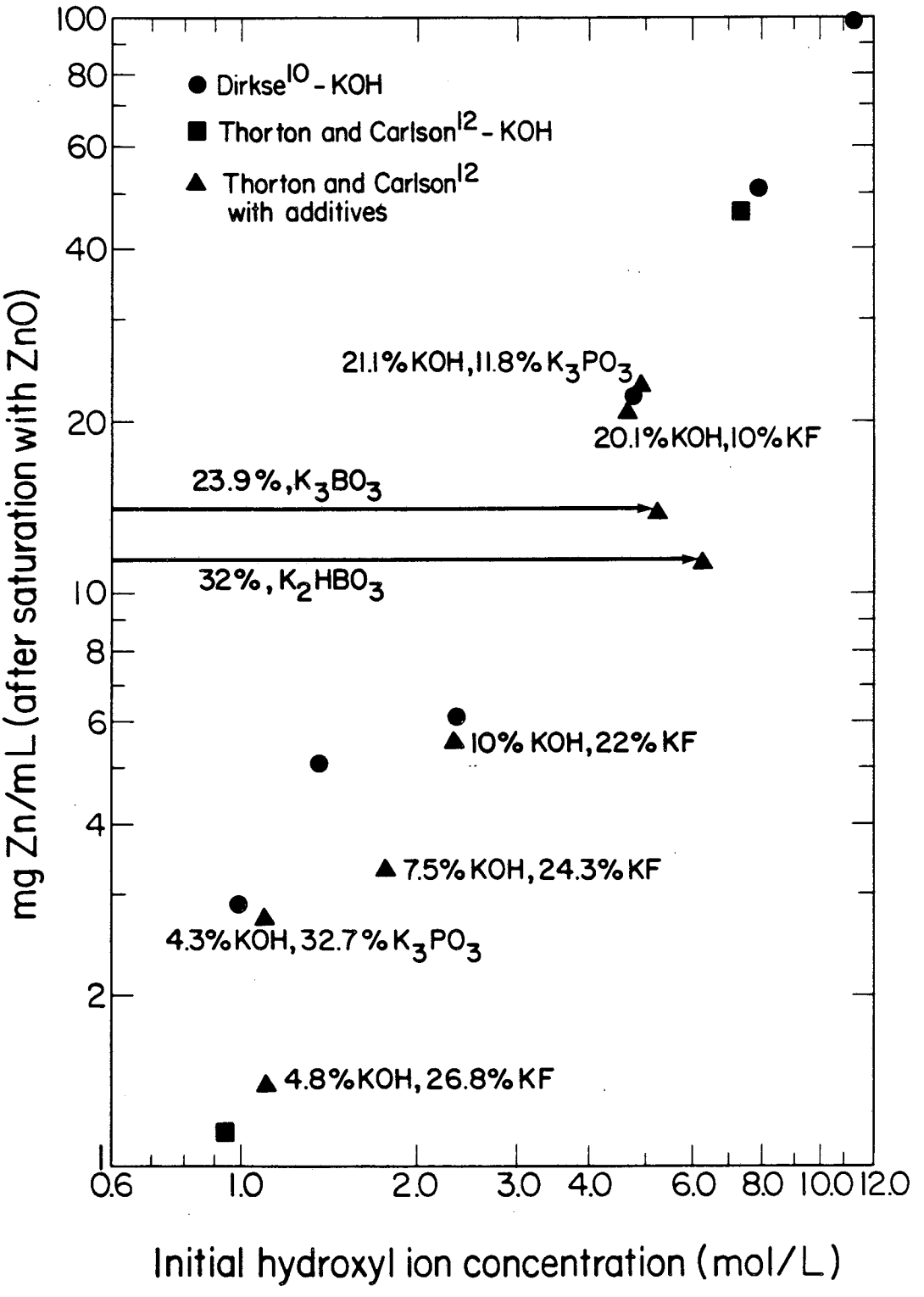

XBL 834-1666

Figure II-3. Solubility of ZnO in alkaline electrolytes with F^-, BO_3^{3-}, and PO_4^{3-} compared to solubility of ZnO in KOH electrolytes. Arrows for borate-containing electrolytes indicate possible range of free hydroxyl ion concentration.

was chosen to aid in judgement of the effect of the chosen anions. The fluoride anion concentration is approximately the same as the hydroxyl ion concantration. The borate electrolyte was chosen to have a ZnO solubility similar to the 3.5M OH^- electrolyte and the OH^--F^- electrolyte. Based on the work of Thorton and Carlson,[12] a K_3BO_3-Li_3BO_3 electrolyte with no additional hydroxyl ion was chosen.

Table II-2

Electrolyte Compositions[a]

Standard:	30% KOH, 1% LiOH (7.4M OH^-), ZnO saturated
Low KOH:	14.4% KOH, 1.12% LiOH (3.5M OH^-), ZnO saturated
Fluoride-containing:	15.3% KOH (3.5M OH^-), 15.0% KF, ZnO saturated, LiF saturated
Borate-containing:	21.5% K_3BO_3, 1.13% Li_3BO_3, (1.7M BO_3^{3-}), ZnO saturated

[a]The wt% and molarities shown in the table are the compositions before addition of ZnO to the electrolyte.

Based on the information presented in this chapter a set of electrolytes were chosen that have the potential to increase the cycle life of an alkaline secondary cell containing the Zn electrode by lowering ZnO solubility. Fluoride- and borate-containing electrolyte were chosen, and experiments were conducted to determine the effects on cell performance. The parameters measured were the rate of zinc redistribution, the state of charge at the end of the cycling experiment, the electrode potential, the cell capacity during cycling, the quantity of electrochemically-unavailable Zn at the end of the cycling experiment and the Zn morphology. Some of these parameters were also determined for a 3.5M OH^- electrolyte containing no additional anions.

7. References for Chapter II

1. R.A. Reichle, K.G. McCurdy and L.G. Hepler, Can. J. Chem. 53 , 3841 (1975).

2. A.O. Gubeli and J. Ste-Marie, Can. J. Chem. 45, 827 (1967).

3. M. Pourbaix, "Atlas of Electrochemical Equilibrium in Aqueous Solutions," French portions translated by J.A. Franklin, 2nd Eng. Edition, Nat. Assoc. of Corr. Eng., Houston, TX (1974).

4. R.B. Fischer and D.G. Peters, "Chemical Equilibria," W.B. Saunders, Pub., Philadelphia (1970).

5. H.E. Brown, "Zinc Oxide," The New Jersey Zinc Co., New York (1957).

6. T.P. Dirkse, J. Electrochem. Soc. 128, 1412 (1981).

7. N.A. Hampson, G.A. Herdman and R. Taylor, J. Electroanal. Chem. 25, 9, (1970).

8. S.K. Sharma and M.D. Reed, J. Inorg. Nucl. Chem. 38, 1971 (1976).

9. W. Dyson, L. Schreier, W. Sholette and A. Salkind, J. Electrochem. Soc. 115, 566, (1968).

10. T.P. Dirkse, J. Electrochem. Soc. 106, 154, (1959).

11. S.U. Falk and A.J. Salkind, "Alkaline Storage Batteries," John Wiley and Sons, New York, p. 586 (1969).

12. R.F. Thorton and E.J. Carlson, J. Electrochem. Soc. 127, 1448 (1980).

13. J.J. Murphy, Chem. Tech. 1, 487 (1971).

14. T.P. Dirkse, in "Power Sources 3, Proc. of 7th Int. Symp.," D.H. Collins, Ed., Oriel Press, Newcastle-Upon-Tyne, England (1970).

15. G.A. Dalin, M. Sulkes, and Z. Stachurski,in Proc. 18th Annual Power Sources Conf., PSC Publications Committee, Atlantic City (1964).

16. "Landolt Bornstein Phys. Chem. Tab.", W.A. Roth and K. Scheel, Eds., Julius Springer, Verlag, Berlin (1923).

17. Japanese Patent 80,137 (October 27, 1980).

18. European Pat. Office, Publication of Pat. App. 0028879A2, (May 20, 1981).

19. M. Cenek, O. Kouril, J. Sandera, A. Touskova and M. Calabek, in Proc. 10th Int. Power Sources Symp., Power Sources 6, D.H. Collins, ed., Academic Press, New York, p. 215 (1977).

20. U.S. Patent 4,224,391 (Sept. 23, 1980).

21. U.S. Patent 4,247,610 (Jan. 27, 1981).

22. U.S. Patent 3,849,199 (Nov. 19, 1974).

23. Japanese Patent 26,044 (March 18, 1975).

24. F.A. Schneider, "Power Sources 4, Proc. of 8th International Symposium," p. 115, D.H. Collins, Ed., Oriel Press, Newcastle-Upon-Tyne, England (1973).

Chapter III

Experimental Equipment and Procedures

1. Cell Cycling Regime

The Zn electrodes were cycled between NiOOH counter electrodes. A cycling regime was chosen that would correspond (as closely as practical) to the use pattern of a battery intended for electric vehicle propulsion,[1] where an overnight charge is typical and commuter-type travel is expected with a discharge time of 2 to 4 hours. The details of construction of these electrodes are presented in later sections; the compositions of the electrolytes have been given previously and are described in more detail in later sections.

A charge time of 6 hours and a discharge time of 2.5 hours were chosen. No attempt was made to simulate the high-rate discharge expected for short acceleration periods in electric vehicle use, nor was the long rest time between charges and discharges simulated; this allowed the required data to be attained in a reasonable time. As the cell capacity declined, the charge current was maintained at a constant level giving shorter charge and discharge times. Constant current is a possible charge method for an automobile propulsion battery, but it is obviously not feasible for the discharge. A typical driving profile is much more difficult to implement and therefore was not used. The currents were 225 mA on charge and 540 mA on discharge, and currents were maintained constant to within 1 mA of the desired currents. To enable direct comparison of the different electrolytes selected, the

cells were operated for the same number of cycles or until failure. The criteria for a failed cell were capacity loss to less than 60% of the original value, or shorting. Cycling continued to approximately 125 cycles if the cell did not fail.

The end of discharge was determined to be when the Zn electrode design capacity had been achieved or when the cell potential reached 1.1 volts, whichever came first. The total amount of charge put into the cell on each cycle was 104% of the coulombs delivered on the previous discharge. The extra four percent of charge was necessary because the NiOOH electrode is inefficient during charge, producing some oxygen rather than only charging the nickel.*

As noted, the nickel electrode is about 4% inefficient, but the zinc electrode is nearly 100% efficient. The result is that the Zn electrode becomes more fully charged than the nickel electrode on each cycle. Since the Zn electrode is designed with extra ZnO, the net effect is a gradual conversion of the excess ZnO to Zn. The gain in Zn metal would be about 4% of the amount of charge during each cycle if the Zn electrode were 100% efficient. The Zn electrode does evolve some hydrogen,[2] and the oxygen produced by the nickel electrode can partially dissolve in the electrolyte and reach the Zn electrode where it can react with the Zn. This gives a gain in Zn metal of some (unknown) amount less than 4%. The increase in Zn can continue only until the ZnO is consumed, at which point some other electrochemical reaction must occur, i.e. the

* The four percent value was chosen based on experience from preliminary cell cycling.

production of H_2.

In all cells used in these experiments, a rise in Zn electrode overpotential near the end of charge was observed, and taken as an indication of depletion of ZnO. When possible, the excess ZnO was restored by discharging the cell to below 1.1 volts. When the cell is discharged in this manner, additional Zn metal is oxidized and and ZnO precipitates at the negative electrode, and water is decomposed to form hydrogen gas and hydroxyl ions at the nickel electrode. This procedure was used as needed; the frequency varied from cell to cell. The cycling regime for all experiments is presented in Table III-1.

Table III-1

Summary of Cell Cycling Conditions

Charge current	225 mA
End of charge	After passing 104% of previous discharge coulombs
Discharge current	540 mA
End of discharge	Cell potential of 1.1 volts or a cell discharge of 1.35 Ah, whichever came first
Rest time	10 minutes
Length of experiment	125 cycles or until failure
Failure criterion	< 60% of design capacity or internal shorting
Restore ZnO reserve	As necessary to reduce overpotential on Zn electrode during charge

2. Cell Cycling Equipment

The charge and discharge regimes specified in the previous section were maintained by a combination of analog and digital equipment. The current was maintained at a digitally-set level to within 0.25 mA by the analog equipment and monitored to an accuracy of ±1 mA. Lawrence Berkeley Laboratory's Department of Instrument Science and Engineering designed[4] the analog equipment and provided access equipment to a Digital Equipment Corporation LSI-11/23 computer. Analog-to-digital equipment also allowed cell and reference-electrode potentials to be measured to an accuracy of ±2 mV for a source resistance less than 5kΩ.

Programming for the computer was completed by M. Katz[3] and was designed to provide the logical decisions required to cycle the cells as specified in Section 1 and to record necessary data. The computer program was designed to cycle one cell per channel, or two cells in series connected to each channel. When cycling two cells in series, the discharge is ended when either cell reaches the 1.1 volt cutoff limit. All other potential or charge limits are monitored for each cell, and charging or discharging is ended when these limits are exceeded.

Continuous operation was required and implemented by providing a communication pathway between the program cycling the cells and a program receiving information entered through the keyboard. The program receiving keyboard information could be removed from the memory when necessary and replaced by programs designed to manipulate data without interfering with the cell-cycling program. The cell-cycling system is more fully elsewhere.[4]

3. Cell Design

A. Electrode specifications

Manufacture of the zinc electrodes was accomplished through the use of a filter-table method described in Appendix B. The composition was primarily zinc oxide with some polymeric binder material to improve the electrode integrity. To obtain data comparable to that obtained from battery electrode stacks, the zinc electrode was sandwiched between two nickel oxide electrodes. The zinc electrode then functions with current flow on both faces as would occur in a stack of alternating zinc and nickel oxide electrodes.

The size of the electrodes was arbitrarily chosen to match the 62-mm tall and 70-mm wide nickel electrodes available for preliminary experiments. A wide variety of electrode thicknesses have been used by various researchers and manufacturers. The thicknesses have ranged from 0.7 to 2.0 mm.[2,5-8] For the experiments reported here, a thickness of 0.8 mm was used.

Zinc electrode utilization as a function of porosity has been examined at fifteen-minute discharge rates for 2-mm thick electrodes.[9] The utilization was found to vary from almost zero, at 58% porosity, to a maximum of 76% utilization, at 82% porosity, defined on a metals basis. From 82% porosity to 75% porosity the decrease in utilization is about 15%. Zinc electrodes with a porosity of 76% were used in the experiments described in this thesis. At higher porosities the electrodes were too fragile and difficult to handle.

Typically a Zn/NiOOH cell contains more ZnO than NiOOH. The Zn/NiOOH ratio, expressed in equivalents, can range from 2.0 to 6.[6,10,11] The higher values correspond to experimental cells. A value of 3.0 was used in the cell-cycling experiments described in this thesis, and is typical of current cell-design practice. With a ratio of 3, the zinc electrode was cycled over 33% of its theoretical capacity when the nickel electrode was cycled over its full capacity using the charge and discharge conditions shown in Table III-1.

Because Zn is thermodynamically unstable in the alkaline electrolyte used in zinc-electrode-containing cells,[12] the Zn metal corrodes with the simultaneous evolution of hydrogen. To reduce the corrosion rate, various materials are added to decrease the kinetic rate constant for hydrogen evolution. Mercury has historically been added to reduce the rate of evolution of hydrogen,[13] but other metals have also been tested. Additional metals found to have ability to reduce the rate of hydrogen evolution are Pb, Tl, and Cd[2]. Due to mercury's toxicity, lead was chosen for the Zn electrodes described herein. The lead was added at a level of 2 wt% of the total PbO, ZnO, and binder mass.

The binder is a polymeric material which may also improve the electrode's ability to accept charge[14] and may reduce the extent of Zn redistribution.[10,13] For these electrodes, polytetrafluoroethylene (PTFE) was used at a level of 4 wt% of the total ZnO, PbO, and binder mass.

A copper current collector was used because of its high electronic conductivity and relatively low cost. Silver has been used for Zn electrode current collectors[2,10,11] in some applications but is prohibitively costly in any large-volume commercial battery. Iron has been suggested as a current collector;[15] however, it leads to significant increases in the hydrogen evolution rate from Zn electrodes.[2] The copper current collector was of the expanded mesh type both to reduce weight and to provide an active-material interconnection between the two electrode halves. The mesh was an Exmet type 3-Cu 6-4/0* onto which a 13-μm lead layer was electroplated from a lead fluoroborate solution, to reduce the rate of hydrogen evolution.[16,17]

Table III-2 contains a summary of the zinc electrode parameters and Table III-3 shows porosity, quantity of ZnO and electrode thickness. The selected cell dimensions and a Zn/NiOOH ratio of three resulted in a Zn electrode design capacity of 4.05 Ah. The eight electrodes shown in Table III-3 were produced with less than 4% variation in the mass of ZnO.

---

* Exmet Corp., Bridgeport, Connecticut.

Table III-2

Zinc Electrode Design Specifications

Cell design capacity	1.35 Ah
Zn/NiOOH equivalent ratio	3.0
Hydrogen gas suppressant	2 wt% PbO
Binder	4 wt% PTFE
Dimensions	70 by 62 by 0.8 mm
Current collector	Pb-plated copper mesh

Table III-3

Actual Zinc Electrode Capacity and Porosity

Electrode	ZnO (Ah)	ZnO (g)	Porosity (as metals basis)	thickness (mm)
A	4.10	6.215	76.5%	0.84 ±0.02
B	4.01	6.081	76.3%	0.81 ±0.02
D	4.03	6.116	76.0%	0.81 ±0.02
E	3.94	5.984	77.3%	0.84 ±0.03
F	4.03	6.111	76.5%	0.83 ±0.03
G	4.10	6.221	75.5%	0.81 ±0.02
H	4.02	6.099	76.9%	0.84 ±0.02
J	4.08	6.198	75.8%	0.81 ±0.02

The nickel oxide electrodes supplied by Eagle Picher* were made of sintered nickel powder on a nickel screen, into which nickel hydroxide was deposited using a proprietary process. The nickel hydroxide loading was reported as 56-57 mg/cm^2. Each nickel electrode had a 1-cm wide, 0.13-mm thick nickel tab, spot welded to a corner. The nickel tab covered 1 cm^2 of the electrode and contained six spot welds. Before spot welding, six holes were punched into the tab using an awl with a 0.7 mm cylindrical, pointed tip. The tab was degreased with hexane, followed by isopropanol, and then water. The tab with its rough-edged punched holes was pressed onto the nickel electrode using an Arbor press. The ragged edges of the holes protruded completely through the nickel electrode to provide a good surface for spot welding. These protrusions melted during spot welding, incorporating plaque and screen into the melt. In addition to the tabs, a Ni wire was spot welded to the electrode next to the reference cell (see Section B). The purpose of this wire was to obtain a potential measurement free of the voltage drop through the tab and spot welds.

The manufacturer recommended, for the first few (formation) cycles, a 20-hour charge at a current sufficient to charge the electrode in 10 hours, and a discharge at the normal rate. Because of the zinc electrode, the nickel electrodes were discharged at the 2.5-hour rate to the potential where hydrogen was evolved, and discharging continued at the 10-hour rate until the zinc was discharged as indicated by a cell potential of 0.0 volts. This procedure is called "formation" and is

---

* Eagle Picher Industries, Inc., Colorado Springs, Colorado.

necessary in order to obtain the maximum utilization of the nickel hydroxide.

B. Cell Case Design

The cell cases were composed of four parts machined from acrylic sheet and rod. The portion containing the zinc and nickel electrodes consisted of two sheets machined flat to within 0.03 mm separated by a 6.60-mm thick frame-shaped spacer with inner dimensions 1.5 mm larger than the electrodes on each side and the bottom, machined flat and parallel to within 0.05 mm. One face of the cell case contained a 0.5-mm capillary and was drilled and tapped at that location for a reference-cell attachment. The reference-cell case consisted of a 4.7-mm column containing an Hg/HgO reference electrode, a fill port and a 0.86-mm dia, 3.2-cm long capillary all machined in one piece from an acrylic rod. A platinum wire passed through the lower portion of the column making contact with the mercury without contacting the electrolyte. In this configuration, mixed potentials involving oxygen were avoided. The details are shown in drawings in Appendix C. A photograph of an assembled cell is also shown.

Acrylic was chosen for its resistance to strong alkali solution and its stiffness. The other cell parts also required resistance to strong alkali. Those parts and compositions are: "O"-ring: carbon-filled ethylene-propylene copolymer; packing to fill excess space: polyethylene; reference-cell fill plug: nylon; terminals: nickel; screws: Ni-plated 304 stainless steel; fill tubing: 300 series stainless steel or nickel, and capillary packing: an acrylic fiber, Orlon.

The use of stainless steel was kept to a minimum to avoid iron contamination of the Zn electrode. The fill tubing was usually stainless steel since its contact time with the electrolyte was minimal whereas the tab screws could be expected to be splashed with electrolyte frequently. The terminals, fill tubing and platinum were attached to the cell case using an amine-epoxy resin with a 24-hour setting time.

C. Separator and Wick

To prevent cell shorting, a separator of some type is required.[18] Membrane-type separators[10,13] and microporous separators[13] have been used. For these experiments, three layers of Celgard 3401* were chosen. This series of Celgard separator has the smaller pore size (the 3500 series has the larger pore size) and contains a proprietary wetting agent. The wetting agent is necessary because the polypropylene material is hydrophobic.

The separator was heat sealed around the Zn electrode. To minimize the number of seals, but also to provide a backup seal, two seals were made on the Celgard at each edge. The two inner layers were sealed together, trimmed, and the outer layer sealed around the first two. Usually the seal could not be made within the 1.5 mm space available between the electrode and the case, so the sealed separator was folded into the 1.5 mm space during assembly. To keep zinc dendrites from growing over the top, the separator was sealed along the tab for 1.5 to 2 cm.

---

* Celanese Fibers Corp., Summit, NJ.

As noted earlier (Section 1), the nickel electrode evolves oxygen near the end of charge. The oxygen becomes saturated with water, and over a long period of time, the nickel electrode may dry out. To prevent this, a material capable of wicking electrolyte from surrounding areas is wrapped around the nickel electrode. In these experiments, non-woven nylon, Pellon 2502K4[a] was used. It was compressed to 0.15mm thick in an assembled cell. The wick was washed in Alconox[b] detergent, rinsed and dried before cutting to shape.

4. Electrolyte Makeup and Analysis

The compositions of the electrolytes for these experiments were presented in Chapter II. A medium and a low hydroxide concentration were chosen to determine the effect of hydroxide concentration. A 14.4% KOH-1.1% LiOH electrolyte has roughly 1/2 the hydroxyl-ion concentration of a 30% KOH-1% LiOH electrolyte. The fluoride and borate electrolytes were chosen to have approximately the same hydroxyl ion concentration as the low KOH solution.

The carbonate content is often not measured by experimenters but may influence the cell performance.[19] It was desirable for these experiments to achieve the lowest possible carbonate levels in the electrolyte. A procedure is available to determine carbonate levels in $CO_3^=$-OH^- solutions; however, fluoride and borate are involved in acid-base reactions and their presence interferes with the titration so that $CO_3^=$

[a] Pellon Corp., Chelmsford, MA.

[b] Alconox Inc., New York.

cannot be analyzed by the procedure. To determine the quantity of carbonate introduced by the electrolyte makeup procedures, the two KOH-LiOH electrolytes were analyzed for carbonate. The fluoride and borate electrolyte makeup was assumed to introduce a similar amount of carbonate to the electrolyte. The carbonate analysis methods are described in Appendix D.

The electrolytes were made up and stored in polyethylene containers cleaned with detergent to remove hydrocarbons. Each bottle was set up with a siphon tube, to a valve, and a vent tube connected to a CO_2 scrubber. The 1/8-inch tubing was either polypropylene or polytetrafluoroethylene, and the valves were 316 stainless-steel with Teflon seats, except for the valve on the KF electrolyte bottle. All wettable parts in the valve for the KF electrolyte were composed of Teflon. The CO_2 scrubber contained Ascarite.[a]

The potassium hydroxide was obtained as a 46.3% solution,[b] rather than the usual pellet form. The pellets contain a few percent carbonate whereas the KOH solution contained only 0.04 wt% K_2CO_3. The solution also contained 1 ppm Fe and 2.5 ppm Ni. The water for the electrolyte was deionized to 15 MΩ-cm resistivity, stored in a stoppered glass bottle and used in less than two hours. The LiOH[c] purity was reported as 98% by acidimetry.

---

[a] Ascarite, Arthur H. Thomas Co., Philadelphia, PA.

[b] J. T. Baker Chem. Co., Phillipsburg, NJ

[c] Matheson, Coleman and Bell Manufacturing Chemist, Stock # LA349, Norwood, Ohio.

To prevent absorption of significant quantities of CO_2 from the air, contact of the electrolyte with air must be minimized. This was accomplished by siphoning the 46.3% solution from the storage bottle (similarly vented through a CO_2 scrubber) into the 600 to 1000 mL makeup bottle and keeping the makeup bottle tightly capped except for addition of chemicals. Prior to siphoning the 46.3% solution into the makeup bottle, a quantity of KOH solution was allowed to pass through the valve to clear any corrosion products from the 316 stainless-steel valve. After use, the valve exit was flushed with 5% acetic acid to prevent the buildup of carbonate. Weighings were made after the addition of each chemical to verify that the proper quantity had been added. The electrolyte was made to within 0.25% of the composition specified.

Following makeup of the 30% KOH-1% LiOH and the 14.4% KOH-1.1% LiOH electrolyte, the carbonate content was analyzed by the procedure outlined in Appendix D. Table III-4 shows the results of the analysis for carbonate and hydroxide. The K and Li were not analyzed, the hydroxide was analyzed and the proportion of KOH and LiOH was determined based on the ratio of K and Li added to the electrolyte. The 0.1000M HCl±0.0003M titrant was prepared by the UCB College of Chemistry Microchemical Analysis Laboratory.

Table III-4

Electrolyte	KOH (wt%)	LiOH (wt%)	samples	carbonate as K_2CO_3 (wt%)	samples
30% KOH-1% LiOH	30.22±0.20*	1.007±.007*	3	0.053±.009*	4
14.4% KOH-1.1% LiOH	14.57±0.72*	1.13±.053*	2	0.044	1

* 95% confidence interval plus titrant bias of 0.3% shown

To prevent absorption of carbon dioxide during cell cycling, the cell vent was connected to a manifold purged with air. The air was passed through a 1 M NaOH gas scrubber at approximately 0.5 L/min. For the potassium fluoride electrolyte, $KF \cdot 2H_2O$ was obtained[a] with 0.01 wt% K_2CO_3, 5 ppm Fe, and 0.03 wt% K_2SiF_6 as impurities. Since $KF \cdot 2H_2O$ is highly hygroscopic, a concentrated solution of KF was made from the crystals and analyzed with atomic absorption for K by the UCB Microchemical Analysis Laboratory. (The analysis indicated that the crystal composition was within 0.1 % of $KF \cdot 2H_2O$.) The necessary 46% KOH solution was then siphoned into the bottle and LiOH added. The LiOH crystals dissolved; however, a precipitate persisted. A LiF precipitate was suspected. Analysis of the electrolyte by the Microchemical Analysis Laboratory for lithium using atomic absorption showed only 20 μg/mL of lithium indicating that LiF had precipitated. The final composition reported is based on the assumption that all of the LiOH dissolved and LiF precipitated.

The borate-containing electrolye was made up by adding a quantity of H_3BO_3 to the makeup bottle with sufficient water to dissolve it. The KOH was added slowly and the bottle was weighed frequently to obtain the proper amount of KOH, finally the LiOH was added to obtain the final composition. The H_3BO_3 purity was reported to meet ACS reagent-grade standards.[b]

---

[a] Mallincrodt, Paris, Kentucky
[b] J.T. Baker Chem. Co., Phillipsburg, NJ

Following makeup of each of the electrolytes, reagent grade ZnO* was added in sufficient quantity to saturate the electrolyte. The slurry was stirred for at least 5 days at room temperature. During the stirring and storage period, the room temperature varied from 18°C to 28°C.

The densities of the fluoride- and borate-containing electrolytes, before saturation with zinc oxide, were determined by weighing a volume of electrolyte metered from a burette. A 20-mL sample was used so that an accuracy of 0.25% could be obtained (a ± one drop accuracy). The burette was calibrated with water, density-corrected for temperature[12]. The temperature was measured to an accuracy of ±1°C and deviated less than 2°C from the calibration temperature when measuring the electrolyte volume. A period of 2 hours was allowed for the electrolyte in the burette to reach equilibrium with the room temperature. The samples were weighed to an accuracy of 0.2 mg which is more than 2 orders of magnitude better than the volume measurement.

The densities of the zinc-oxide-containing electrolytes and the fluoride-containing electrolyte were determined by weighing a 0.250 mL (±0.4%) sample of the electrolyte to the same 0.2 mg accuracy (better than 1 part in 1000). A syringe was used to fill the 0.25 mL pipette, and care was taken to insure that stopcock grease from the syringe did not contact the pipette, that paper fibers from the tissue used to wipe the pipette after filling did not remain on the pipette, and that heat from contact with the hands did not significantly affect the measurement

* Mallincrodt, Paris, Kentucky

temperature. The pipette was not touched with the hands at any time. When separating the pipette from the tubing connecting it to the syringe the pipette was held momentarily in tissue; this may have slightly heated the pipette. The pipette was cleaned between uses with deionized water, followed by reagent-grade anhydrous acetone.

The same sample used to obtain the density of the zinc-oxide-saturated electrolyte was analyzed for zinc by atomic absorption following dilution and neutralization. All samples were prepared by the method described below except the electrolyte from cell HIGHB. A measurement of the volume of electrolyte from cell HIGHB was not obtained and is the reason for reporting an accuracy of ±3% for this analysis (see Chapter IV, Section 1).

After the filled pipette had been weighed, the sample was discharged into a 50-mL volumetric flask. Deionized water was then drawn into the pipette three times and discharged into the flask. After each discharge the outside of the pipette was washed with deionized water from a wash bottle. Sufficient nitric acid was then added to the unstable solution to neutralize the hydroxide and zincate, and to raise the acidity sufficiently to maintain the zinc in solution. A dilution accuracy of 0.25-mL is the accuracy to be expected for a 50-mL volumetric flask. The atomic absorption analysis has an accuracy of about 1.0%, so the Zn analysis has been assumed to be accurate to 1.5 % in the absence of statistical data.

5. Cleaning and Assembly Procedures

The following cleaning procedures were used to eliminate foreign hydrocarbons and carbonate precipitates from the cell materials. Prior to epoxying the terminals and fill tubing to the acrylic cell case, the metal parts were degreased using rinses of hexane, isopropanol and water.

Prior to assembling the cell, the cell cases, terminal screws, polyethylene packing, reference cell, and nylon fill plug were washed with detergent and rinsed with water. The materials were then rinsed with 5% reagent-grade acetic acid solution to remove any carbonates, such as those from water stains, and finally rinsed with water. The `O'-rings were washed with detergent and rinsed with water.

To prevent gas from blocking the capillary to the reference cell, the 0.5-mm hole was packed with an acrylic yarn. This was accomplished by drawing a portion of the yarn through the hole with 0.13-mm nylon monofilament. It was found that if the packing material did not fill the hole as tightly as possible, by using a thick enough portion of the yarn, gas bubbles could enter the capillary, which then increased the capillary resistance, and yielded incorrect reference potential readings.

The packing tightness of the electrode stack was chosen by trial and error based on the appearance of the zinc redistribution in preliminary experiments. Where significant movement of zinc toward the bottom occurred the packing was assumed to be too loose. The final packing was chosen to compress the Pellon wick to 0.15 mm. The polyethylene packing

sheets were cut to the exact dimension of the inner width of the cell case to eliminate any extra electrolyte reservoirs and at least 1 cm higher than the top of the electrode stack. The corner areas of a 0.38-mm thick polyethylene sheet in the packing were removed to allow sufficient room for the thicker tab areas of the electrodes.

After attaching the reference electrode compartment to the cell case, the cell was leak-checked under vacuum. If the cell could maintain an absolute pressure of less than 10 mm Hg for 5 minutes after evacuation, the seals were considered tight enough. The reference electrode compartment was then filled with Hg and HgO and the cell was weighed. The cell was then evacuated again and filled with electrolyte to above the polyethylene sheets. The vacuum was slowly released and electrolyte was added as necessary to maintain the electrolyte level above the polyethylene sheets. The cell had to be reasonably leak tight for two reasons: to be sure the electrode pores were filled and to fill the reference electrode compartment. After the excess electrolyte was removed, the cell was reweighed and allowed to stand for at least 24 hours to allow electrolyte to soak into all the pores.

6. Post-Cycling Tests

After the cells reached 120 to 130 cycles, they were examined to determine the zinc redistribution, state of charge, dendrite penetration and quantity of electrochemically-inactive zinc. The redistribution was determined by obtaining an X-ray image of each electrode after cycling. To determine the quantity of electrochemically inactive zinc, the electrode was first discharged with the separator removed to discharge any

zinc blocked by bubbles trapped under the separator. The remaining zinc could be inactive because it is either passivated or electrically isolated from the current collector. By the state of charge is meant the Ah of zinc metal remaining in the electrode at the end of the final charge or discharge.

When discharging the zinc electrode (with the separator removed) in the cell with excess electrolyte, some of the discharged zinc can enter the excess electrolyte and supersaturate it, rather than precipitating in the electrode. Because of this possible loss of zinc oxide, the redistribution had to be determined prior to discharging the electrode in excess electrolyte.

To most accurately determine the state of charge and quantity of electrochemically inactive zinc, the entire electrode should be used. It was desirable, however, to observe the extent of dendrite penetration through the separator and to examine the electrode morphology using the Scanning Electron Microscope (SEM). Electrodes were disassembled in both the charged and discharged states for these observations. The SEM sample-preparation procedures are described in the next section. To insure that sufficient samples were available for the SEM study, half of each electrode was saved for this purpose.

After obtaining the X-ray image of the electrode disassembled in the charged state, half of the electrode was discharged in excess electrolyte with the separator removed, to obtain some indication of the state of charge of these electrodes. The quantity of electrochemically inactive zinc was also measured in this electrode half. The possible error

in determining the state of charge of the charged electrode is obvious considering that the redistribution may not produce a symmetrical electrode. A similar statement can be made about the measurement of the electrochemically inactive zinc for each electrode; however, based on the results shown in Chapter IV, the error for this measurement is not believed to be significant. An accurate measurement of the quantity of electrochemically active zinc was obtained in four of the cells by discharging the available zinc completely and then discharging the electrode in excess electrolyte after obtaining the X-ray image. The electrochemically-inactive zinc was measured in half of the electrode.

Summarizing the procedure for the discharged cell of each of the four electrolytes: discharge at the 2.5-hour rate to 1.1 volts, discharge at the 10-hour rate to 0.0 volts, disassemble, obtain X-ray image, remove separator and discharge in excess electrolyte at the 10-hour rate to 0.0 volts, wash, dry, bisect the electrode, and determine the quantity of electrochemically inactive zinc in one half of the electrode. The procedure for the other four electrodes in the charged state was: disassemble in the charged state, obtain X-ray image, bisect the electrode, wash and dry one half, discharge the other half at the 10-hour rate to 0.0 volts in excess electrolyte with the separator removed, wash, dry, and determine the quantity of electrochemically inactive zinc. These procedures are diagrammed in Figures III-1 and III-2; the cell names are defined in Chapter IV, Table IV-1.

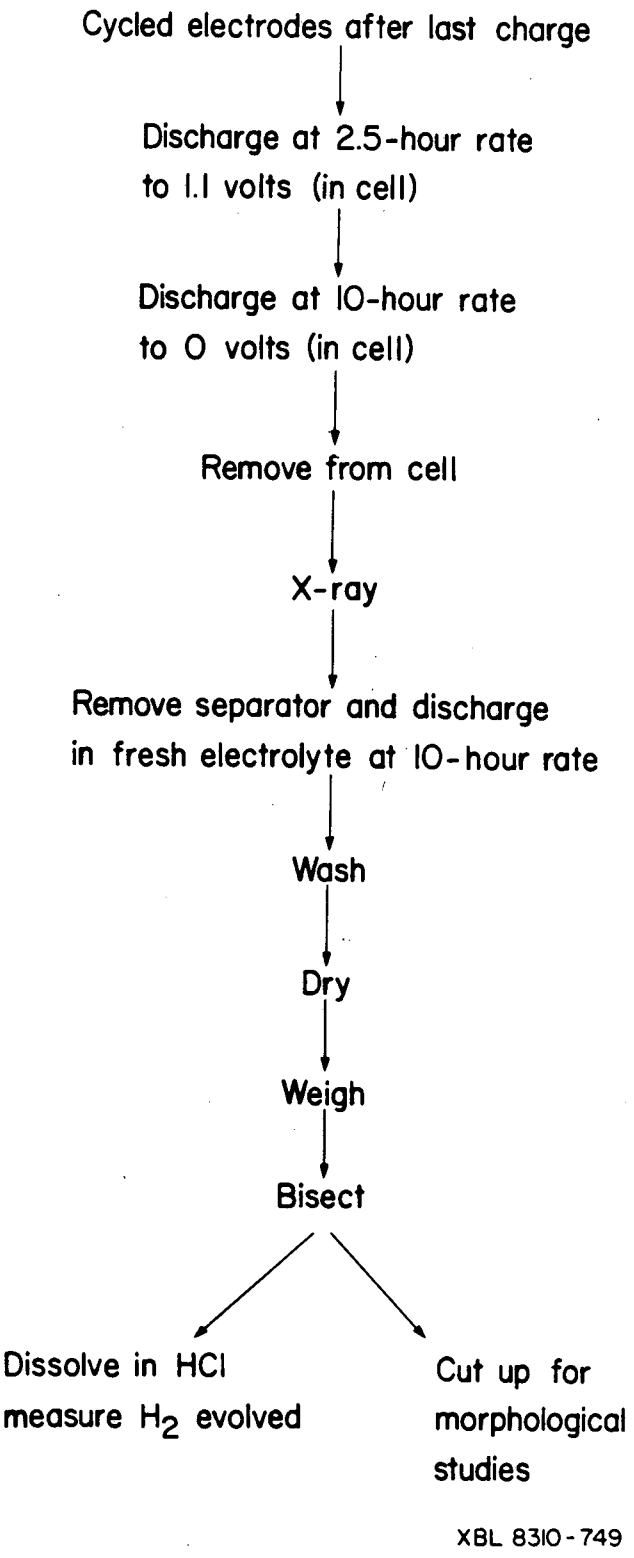

Figure III-1. Post-Test Analysis Procedure for Electrodes HIGHD, LOWA, KFF, and B03H.

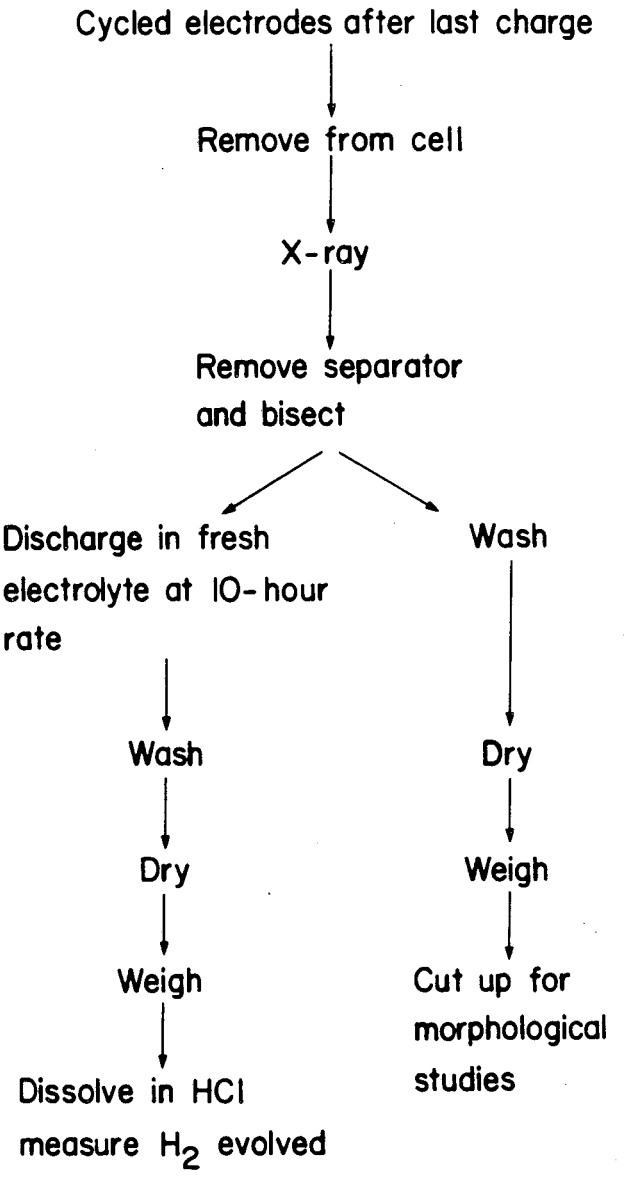

XBL 8310-3314

Figure III-2. Post-Test Analysis Procedure for Electrodes HIGHB, LOWE, KFG, and B03J.

The electrodes of some of the cells were washed by spraying deionized water over the electrode as it lay in a Buchner funnel. A thin rubber gasket was cut to block the area not covered by the electrode. After washing in this manner, the electrode was soaked in deionized water for about two hours. The method was not adequate so the other electrodes were washed by only soaking the electrode in deionized water for about eight hours. The water was changed from four to six times during the period. When using the Buchner funnel the additional handling caused portions of the electrode to flake off. This lost material was not easily recovered. Those electrodes washed by each procedure are identified in the results chapter. After washing, the electrodes were dryed by applying a high vacuum for at least 24 hours.

The X-rays were obtained using a machine manufactured by Profax Co. with 500-mA maximum current and 140-keV maximum energy using a 2.5-mm aluminum filter and tungsten anode. Cronex-4-Ready Pack* film was used, which required 100-mAs of exposure at the 60-keV energy chosen for these zinc electrodes. Because the X-ray equipment was available only during non-use times for its primary mission, the X-ray images were obtained 1 to 3 days after cell disassembly. The electrode thus remained in its electrolyte out of the cell case for this period of time. During this time the electrode was stored in a nitrogen-filled polyethylene bag kept in nitrogen-purged glove bag.

---

* E.I. Dupont de Nemours and Co., Wilmington, DE

The cell used to discharge the zinc electrode, after the separator was removed, contained a discharged Ni electrode as a counter electrode. The Ni electrode evolved hydrogen during the Zn electrode discharge. The zinc electrode was discharged until a cell potential of 0.0 volts was achieved, which corresponded to a Zn electrode potential of approximately -1.05 volts versus an Hg/HgO reference electrode, varying for each electrode. The cell case was 7.5 x 6.1 x 1.0 cm, and contained the same type of ZnO-saturated electrolyte in which the zinc electrode was cycled. The Zn and Ni electrodes were separated by a distance of 4-mm and held in place by 1.75-mm slots in the sides and bottom of the acrylic case. A sheet of wicking material was used to electrically isolate the two electrodes. After discharging to 0.0 volts, some of the zinc electrodes were turned around to determine if zinc remained on the side of the electrode facing away from the counter electrode. No additional zinc could be discharged from these electrodes.

The quantity of electrochemically-inactive zinc was determined by measuring the quantity of hydrogen produced when immersing the electrode in acid. Hydrochloric acid does not dissolve copper or lead,[12] so the hydrogen is a direct result of the dissolution of zinc metal. The experiment consisted of measuring, before and after adding 6 M HCl, the quantity of gas in a closed system containing the electrode. An Erlenmeyer flask was connected through a two-holed stopper to the top of an inverted burette filled initially with water. A burette containing the HCl was connected to the flask through the other stopper hole. The following assumptions were made: the gases behaved as ideal gases, the quantity of hydrogen dissolved in the water was negligible and the gas

was saturated with water. (The gas became saturated with water as it passed through the small quantity of acid present in the flask). The surface of the water in the burette was small so the water in the burette could not contain an appreciable quantity of H_2. While the hydrogen dissolving in the acid produced an unknown error, its possible magnitude is considered later.

To measure the hydrogen, the inverted burette was vacuum filled with water and the discharge end connected to the Erlenmeyer flask containing half of the electrode and a magnetic stirrer bar. The stopcock on the burette was then opened and sufficient time was allowed for the temperature of the system to equalize. The flask and tubing volume were previously measured and the burette volume was known. Using PV=nRT, the number of moles of gas was determined. The atmospheric pressure was obtained from a mercury manometer. The pressure in the system was corrected for the height of the column of water in the burette and the partial pressure of water. After addition of the HCl to the flask, a similar set of measurements and pressure corrections were made, also after allowing sufficient time for the temperature to equalize. The total volume, after adding HCl, was taken to be the known flask volume minus the volume of acid added plus the measured volume of gas in the burette.

At 1 atm. pressure and 20°C, an error of $4 \cdot 10^{-5}$ moles of hydrogen is approximately equivalent to 1 mL of gas, or a change in temperature of 2°C, or an error in pressure measurement of 7 cm of water (5 mm Hg). An error of this size would amount to 2.6 mg of zinc. The volume measurement was more accurate than 1mL and the pressure measurement better than

1 cm of water. A temperature error of $2^{o}C$ is possible if sufficient time for temperature equalization was not allowed. If the gas were not quite saturated with water, then the assumed correction for a water vapor pressure of about 25 mm Hg could lead to an error of several mm Hg. If the acid were saturated with hydrogen at 1 atm. and had the same Henry's law constant as water, then $4 \cdot 10^{-5}$ moles of hydrogen would have dissolved in 50 mL. However, because the acid contained a high concentration of dissolved material, it is not likely that it contained as much as $4 \cdot 10^{-5}$ moles of hydrogen. The error in measured hydrogen is likely to be then on the order of $4 \cdot 10^{-5}$ moles due to errors in temperature and water saturation; errors in pressure measurement or dissolved hydrogen in the strong acid electrolyte are likely to be less significant.

7. Sample Preparation and Equipment for SEM and Microanalysis Studies

The electrode handling procedures through drying each electrode are described in the previous section. This section contains a description of those procedures peculiar to the preparation of electrode samples for the Scanning Electron Microscope (SEM).

The SEM used for microanalysis requires a pressure of 10^{-6} torr; the samples must be very dry to achieve these pressures. Porous materials are particularly difficult to dry because they generally adsorb a significant amount of water due to their high surface areas. Zinc oxide is not considered to be hygroscopic, but the zinc oxide used to make the eight electrodes contained about 5% water before drying.

A vacuum system was set up with a liquid-nitrogen cold trap to dry these electrodes. To keep pump oil away from the electrodes while drying them, the isolation valve to the pump was closed when the pump's ultimate pressure was reached. The valve was opened as necessary to maintain the vacuum as air leaked in. This prevented pump oil vapor or mist from moving toward the vessel containing the electrodes. The vacuum system employed here did not seal completely, and overnight the leakage amounted to about one torr from a maximum vacuum of 20 mtorr.

Oil on samples subjected to electron bombardment will polymerize and decompose, leaving a carbon residue that limits SEM resolution.[20] Oil of sufficient thickness to be disastrous will deposit on all surfaces in an SEM's vacuum chamber if any oil droplets are present on samples, including oils from the hands.

The samples dried as described above were acceptable for the two SEM's used; however, the procedure did not produce sufficiently-dry samples for the ultra-high (10^{-9} torr) vacuum required for the Scanning Auger Microscope (SAM). Additional drying in a vacuum oven for 3 hours at a maximum vacuum of 30 mtorr and 80°C dried the electrode sample sufficiently for the SAM. After the samples were dried, they were stored in polyethylene bags. All utensils and cutting boards that came in contact with the electrodes were cleaned with hexane followed by ethanol.

The SEM Analytical Electron Microscope* (SEM-AEM) is a low magnification machine capable of good resolution at < 1000X and occasionally to

* Advanced Metals Research Corp., AMR-1000.

5000X with these type of samples. The microanalysis was accomplished with an Energy Dispersive Spectrometer (EDS) for X-ray detection. An EDS detector is capable of element detection at the 0.2% level.

The high resolution ISI-SEM* is capable of producing good images at magnifications of 10^5. These magnifications were not obtainable with these electrode samples as discussed in the results chapter. The SEM has a tungsten filament electron gun.

The SAM performs surface analysis of less than 0.8 nm depth by measuring Auger electrons. The detector of the Perkin-Elmer SAM is a single channel, electron gun coaxial type which acquires Auger electrons produced by a typically 2-keV, $1.7 \cdot 10^{-7}$-A, 1-μm electron beam. The large beam diameter limits elemental mapping to areas the size of tens of micrometers. Because of this high surface sensitivity, contaminants of monolayer thickness must be avoided.

* International Scientific Instruments (ISI), DS130.

8. References for Chapter III

1. E.J. Cairns, Lawrence Berkeley Laboratory Report No. LBL-13199 (1981).

2. Otto Wagner and Albert Himy, in Proc. of the 27th Power Sources Symp., PSC Publications Comm., Red Bank, NJ (1976).

3. M.H. Katz, "Computer Control of Electrochemical Experiments with Application to Zinc/Nickel Oxide Cells," (MS Thesis), LBL-15546 (1982).

4. M.H. Katz, J.E. Katz, J.T. Nichols, F.R. McLarnon, and E.J. Cairns, J. of Power Sources, Vol. 10, No. 2, pp. 149-165 (1983).

5. D.C. Hamby, N.J. Hoover, J. Wirkkala, and D. Zahnle, J. Electrochem. Soc. 126 2110 (1979).

6. Yardney Electric Division "Final Report Design and Cost Study Zn/NiOOH Battery for Electric Vehicle Propulsion," Argonne National Laboratory Report No. ANL 2003-76, Argonne, Illinois (1976).

7. Gould, Inc.,"Develop Ni/Zn Battery Suitable for Electric Vehicle Propulsion," Report 762-003-1 prepared for Argonne National Laboratory, Argonne, Illinois (1977).

8. M. Klein and D. Dube, "Design and Cost Study of Ni/Zn Batteries for Electric Vehicles," Energy Research Corporation, Report for Argonne National Laboratory, Argonne, Illinois (1976).

9. C.M. Shepherd and H.C. Langelan, J. Electrochem. Soc. 109, 657 (1962).

10. J. McBreen, J. Electrochem. Soc. 119, 1620 (1972).

11. K.W. Choi, D. Hamby, and D.N. Bennion, J. Electrochem Soc. 123, 1628 (1976).

12. "CRC Handbook of Chemistry and Physics," 55th ed., Chemical Rubber Co. Press, Cleveland (1974).

13. E.J. Cairns and J. McBreen, in "Advances in Electrochemistry and Electrochemical Engineering," Vol. 11, H. Gerischer and C.W. Tobias, Eds., John Wiley and Sons, (1978).

14. U.S. Patent 3,630,781 (December 28, 1971).

15. European Patent Office, Pub. of Pat. App. 0028879A2 (May 20, 1981).

16. J. Bockris and N. Pentland, Trans. Faraday Soc. 48, 833 (1952).

17. T.S. Lee, J. Electrochem. Soc. 118 1278 (1971).

18. J.J. Lander and J.E. Cooper, Air Force Aero. Prop. Lab., Wright-Patterson Air Force Base, Tech. Rep. AFAPL-TR-71-32 (October 1971).

19. S.U. Falk and A.J. Salkind, "Alkaline Storage Batteries," John Wiley and Sons, New York, (1969).

20. O.C. Wells, A. Boyde, E. Lifshin, and A. Rezanowich, "Scanning Electron Microscopy," McGraw-Hill Book Co., New York, (1974).

Chapter IV

Results and Discussion

The ultimate goal of alkaline zinc electrode research is to improve the life of cells using the zinc electrode, without sacrifice of performance. One of the major reasons for short cell life has been, as presented in Chapter I, the redistribution of the zinc material across the zinc electrode as the cell is cycled. The result is a loss of capacity. There are several other life-limiting phenomena observed, such as cell shorting, zinc densification, and zinc passivation.[1] Their interrelations and relation to the redistribution phenomenon remains unclear. Concentrating for the moment on the redistribution problem, a potential solution is to reduce the concentration of the zinc species in the electrolyte. As indicated by both redistribution models presented in Chapter I, the concentration of zinc species has a direct bearing on the rate of mass transfer of the zinc. A reduction of zinc concentration would therefore reduce the driving force for mass transfer which should reduce the redistribution rate.

One approach to the reduction of the solubility of zinc species in the electrolyte would be the addition of an anion to form a salt of reduced solubility. However as shown in Chapter II, none of the common inorganic, sparingly-soluble salts for which data are available is appropriate, with the possible exception of the sulfide salt of zinc. The sulfide ion is oxidizable in the environment of the alkaline cell

though, making its use undesirable.

Another approach is to reduce the hydroxide-ion concentration of the electrolyte. This certainly reduces the zinc concentration, but the reduced hydroxide concentration lowers the conductivity and may lead to quicker formation of passivating films on discharging zinc (see Section II-6). The conductivity can be increased by addition of soluble salts, and the presence of additional ions may have positive effects on the development of passivating films.

The major thrust of these experiments is to obtain measurements of zinc redistribution rates when using altered alkaline electrolytes. Additionally, measurement of other characteristics is desirable to improve understanding of processes occurring in the alkaline zinc electrode. Additional observations undertaken were the measurement of electrochemically unavailable zinc metal (due to passivation or isolation), determination of the state of charge, determination of the morphology, and measurement of electrode potentials during cell cycling.

The electrolyte compositions chosen for these experiments are shown in Chapter II, Table II-2 and the zinc electrode specifications are shown in Chapter III, Tables III-2 and III-3. The cells are identified by a series of letters indicating the electrolyte composition and the identity of the zinc electrode. The electrolyte is identified by the first part of the cell name and the Zn electrode is identified by the last letter of the cell name. The standard electrolyte containing the high OH^- concentration (7.4 M) is identified by HIGH, the low OH^- concentration electrolyte (3.5 M) without any additional anions by LOW, the

fluoride-containing electrolyte by KF, and the borate-containing electrolyte by BO3. Table IV-1 shows the cell names for the eight cells constructed for the experiments described herein.

Table IV-1
Electrolyte Composition and Associated Cell Name

Cell Name	Electrolyte[a]
HIGHB	7.4 M OH^-
HIGHD	7.4 M OH^-
LOWA	3.5 M OH^-
LOWE	3.5 M OH^-
KFF	3.5 M OH^- with F^-
KFG	3.5 M OH^- with F^-
BO3H	1.7 M $BO_3^{\equiv}$
BO3J	1.7 M $BO_3^{\equiv}$

[a] Species concentration before addition of ZnO.

The charge and discharge cycling regime used is fully described in Chapter III , Section 1; the chosen regime was executed by a computer as described in Chapter III, Section 2. A six-hour charge and a 2.5-hour discharge were chosen for the 1.35-Ah capacity cell. The discharge was limited to 1.35 Ah or a 1.1 volts cell potential, except during Ni electrode formation and ZnO reserve restoration. The pairs of cells with identical electrolytes were cycled in series unless the capacities of the two cells differed significantly. For these experiments, all pairs were cycled in series until the desired number of cycles were achieved or the cell failed. Each electrolyte was tested in two cells to establish the consistency of observed shape change and cycling behavior. Many variables can affect the redistribution rates, so it is important to establish reproducibility by the use of duplicate tests.

1. Electrolyte

The zinc oxide solubility was determined for each of the electrolytes. As noted in Chapter II, this solubility is expected to depend only on the hydroxide concentration. The solubility of ZnO in these electrolytes is shown in Table IV-2 with the densities. These data can be compared to those of other researchers as shown in Chapter II, Figure II-3. The measured solubilities compare favorably, though the value for the 14.4% KOH electrolyte appears to be high.

Table IV-2
Electrolyte Density and ZnO Solubility

Electrolyte[c]	Hydroxide[c] Concentration	Density (g/mL)	Temperature (°C)	Zn content (mg Zn/mL)
30% KOH- 1% LiOH, ZnO sat.	7.4M	1.339 ± 0.4%[a]	21 ± 1	50.8 ± 1.5%
14.4% KOH 1.12% LiOH ZnO sat.	3.5M	1.156 ± 0.4%[a]	21 ± 1	16.0 ± 1.5%
15.3% KOH- 15.0% KF Li sat.	3.5M	1.290 ± 0.25%[b] 1.284 ± 0.4%[a]	23.5 ± 1 23 ± 1	0
15.3% KOH- 15.0% KF, Li sat. ZnO sat.	3.5M	1.328 ± 0.4%[a]	21 ± 1	12.6 ± 1.5%
21.5% K_3BO_3 1.13% Li_3BO_3	-	1.251 ± 0.25%[b]	25 ± 1	0
21.5% K_3BO_3 1.13% Li_3BO_3 ZnO Sat.	-	1.265 ± 0.4%[a]	21 ± 1	14.4 ± 1.5%

a) 250-μL pipette technique
b) Burette technique
c) The electrolyte composition shown with the ZnO-saturated electrolyte is the composition before adding the ZnO.

The densities were determined as described in Chapter III, Section 4. The caustic-fluoride electrolyte density was measured by both weighing a filled micropipette and weighing a burette-metered quantity of electrolyte. The KOH-LiOH electrolyte density was not determined; it is available in the literature.[2] Following cycling of the cells, a sample of electrolyte after the last discharge was obtained with a syringe. The density, zinc content, and location of the sample are presented in Table IV-3.

The mass of electrolyte initially added to each cell is shown in Table IV-4. Also shown in Table IV-4 is the difference between the initial cell dry mass and the final cell wet mass. This difference is the electrolyte in the cell minus the loss of oxygen from the cell. Oxygen loss from the cell is due to oxygen evolution at the nickel-oxide electrode, and corresponding zinc oxide conversion to zinc metal. For those cells completely discharged (HIGHD, LOWA, KFF, and BO3H), the mass difference is the electrolyte mass, though not the electrolyte mass prior to discharging to 0.0 volts. For charged cells, the difference is the electrolyte mass less the mass of missing oxygen. That is, the mass of oxygen evolved from the cell during the production of zinc metal when added to the difference shown in Table IV-4 is equal to the electrolyte mass.

Table IV-3
Final Electrolyte Density and Zn Content for Each Cell

Cell	Electrolyte Density (g/mL)	Temp (°C)	Zn content of electrolyte (mg/mL)[a]	sample location[b]	cycle number	open circuit time[c] (h)
HIGHB	--	--	4.5±3%	Ni	34	.5
HIGHD	1.381±0.4%	22±1	63.6±1.5%	Zn	122	2.25
LOWA	1.141±0.4%	25±1	11.5±1.5%	Ni	124	2
LOWE	1.144±0.4%	25±1	11.0±1.5%	Ni	123	2.75
KFF	1.310±0.4%	26±1	13.8±1.5%	Ni	130	1.25
KFG	1.324±0.4%	26±1	12.0±1.5%	Ni	129	2
BO3H	1.293±0.4%	23±1	15.2±1.5%	Ni	125	2
BO3J	1.303±0.4%	26±1	16.0±1.5%	Ni	124	1.75

a) Except cell HIGHB where weight percent is reported
b) Ni electrode side of separator or Zn electrode side of separator
c) Time after current stopped that sample was taken

Table IV-4
Electrolyte Added to Each Cell and
Difference Between Initial and Final Cell Mass

Cell	Initial electrolyte mass[a], g	Difference between final wet and initial dry cell mass[a], g
HIGHB	12.5	13.0
HIGHD	12.0	11.0
LOWA	11.6	12.2
LOWE	11.4	11.8
KFF	12.2	10.8
KFG	11.9	11.0
BO3H	11.8	11.1
BO3J	12.0	11.0

a) excluding electrolyte in the reference cell compartment

From comparisons of Table IV-3 and Table IV-2 it can be seen that the cycling conditions for these cells were such that highly supersaturated conditions were not obtained throughout the electrolyte. Heavily supersaturated electrolytes close to the Zn electrode have been observed.[3] Supersaturated conditions were probably not observed here because samples close to the zinc electrode were difficult to obtain.

The only sample obtained from inside the separator was that for cell HIGHD, and even this sample was not obtained close to the electrode material. The sample was obtained near the top of the electrode but the zinc material had redistributed to near the bottom of the electrode as shown in Section 3.

To allow time for the concentration gradients to relax, an open-circuit rest period of two hours was chosen. This appears to be an appropriate time because open circuit cell potentials were found to reach a constant level in about two hours. A supersaturated electrolyte would not significantly change in composition in this time from precipitation of ZnO. These strong alkaline, ZnO-supersaturated solutions return to equilibrium only slowly over a period of hundreds of days.[4]

The overall objective of these reduced hydroxide-concentration electrolytes was to reduce the concentration of soluble zinc species in the electrolyte, and as can be seen from Table IV-2 this was achieved as expected. A zinc concentration reduction of about a factor of four was obtained in the ZnO-saturated electrolyte, though data on the extent of supersaturation was not obtained. One must conclude that the electrolyte in regions away from the zinc electrode does not supersaturate to any appreciable extent in cells operated at an average discharge current density of 6.2 mA/cm^2.

2. Post-Test Examination

The two cells containing the 3.5-M OH^- electrolyte, LOWA and LOWE, were cycled for 124 cycles to a final capacity of 62% of design capacity (1.35 Ah). Cell LOWE was disassembled in the charged state, and

examination of the separator showed that a small amount of zinc had penetrated the separator. Some zinc was also found in the wick. Cell LOWA, which was discharged to 0.0 volts before disassembly, had some zinc outside the separator at one corner, even though the cell was in the discharged state. The zinc probably penetrated the separator through a defective seal.

The two cells containing the standard 7.4 M OH^- electrolyte were cycled until failure due to shorting. Cell HIGHB shorted after 26 cycles, and cycling stopped after 34 cycles. Cell HIGHD continued until it shorted after 118 cycles. Cell HIGHB was disassembled in the charged state to determine if the cell had in fact shorted. A short was found 1.5 cm from the top edge and 4.5 cm from the tab side of the electrode. The short contacted the Ni electrode at a spot slightly smaller than 1 mm in diameter. Slight tugging was required to remove the wick from the Ni electrode. The wick of cell HIGHD contained some zinc material, even though it was disassembled after discharging to 0.0 volts. Zinc was also present outside of the separator at both lower corners of the zinc electrode.

The cells with the fluoride-containing electrolyte were cycled in series for the number of cycles intended. Cell KFF was disassembled in the discharged state after 130 cycles, and cell KFG was disassembled in the charged state on the 130th cycle. The final capacity of these cells was 69% of the design-value of 1.35 Ah. Cell KFF was discharged to 0.0 volts and upon disassembly no zinc was observed in the wick, nor in corner or edge areas where zinc was found in cells of the other electrolytes. The separator of cell KFG was extremely clean, and the only spot

of material (assumed to be zinc) was at the corner against the tab of the nickel electrode. In the outer layer of separator, the spot was approximately 0.1 mm in diameter. The separator of this electrode had not been penetrated in the seal areas.

The cells using the borate-containing electrolyte were cycled in series until their planned disassembly on the 125th cycle. The final capacity was 74% of 1.35 Ah. Cell B03H was disassembled after discharging to 0.0 volts, and cell B03J was disassembled in the charged state. Some bubbles were noted behind the separator when cell B03H was disassembled; no zinc appeared in the wick. Cell B03J contained a small amount of zinc in the lower corners but none was in the wick of this charged cell. The outer layer of separator contained no zinc at all.

Overall, the fluoride-containing cells showed the least zinc penetration of the separator. The borate-containing cells were similarly free of penetration, with the exception of some zinc in the lower corners outside of the separator. This is probably due to small defects in the seal, so one would have to conclude that the extent of penetration of the separator was essentially equivalent to that in the fluoride electrolyte, i.e. close to zero. The KOH-LiOH, 3.5 M OH^- electrolyte cells showed definite signs of penetration, and the 7.4 M OH^- electrolyte cells had penetration of the separator sufficient to short the cell.

3. Cell Capacity and Zinc Redistribution

The primary objective is to improve the capacity retention of secondary cells using the alkaline zinc electrode. It has been proposed earlier that the zinc redistribution directly limits the cell capacity, and that this capacity loss can be mitigated by reducing the concentration of zinc in the electrolyte. The capacity losses actually observed for these experiments are shown in Figures IV-1 and IV-2 for the standard electrolyte and the electrolytes with reduced zinc concentration. Only four curves are shown because cells with identical electrolytes were cycled in series.

The capacity versus cycle number curves contain several discontinuities, most of which arise from the procedure used to restore the ZnO reserve (see Chapter III, Section 1). In the case of cell HIGHD, the sharp decline in capacity at cycle 118 is due to shorting. This curve also shows a sharp decline at cycle 26 due to the shorting of cell HIGHB in series with cell HIGHD. Following restoration of the ZnO reserve, the nickel electrode was sometimes undercharged and sometimes overcharged. Cell HIGHD cycles 55 and 84 and cell BO3H cycle 25 show undercharge while cell LOWA cycles 50 and 87 show overcharge.

Overall the cells with the standard 7.4M OH^- electrolyte had a higher capacity until shorting. The cells with the borate electrolyte initially achieved the design capacity of 1.35 Ah, but declined to roughly 10% less than the standard electrolyte for the majority of the cycling period. The cells with the 3.5M OH^- electrolyte had a capacity that was initially lower and remained lower throughout the period. This

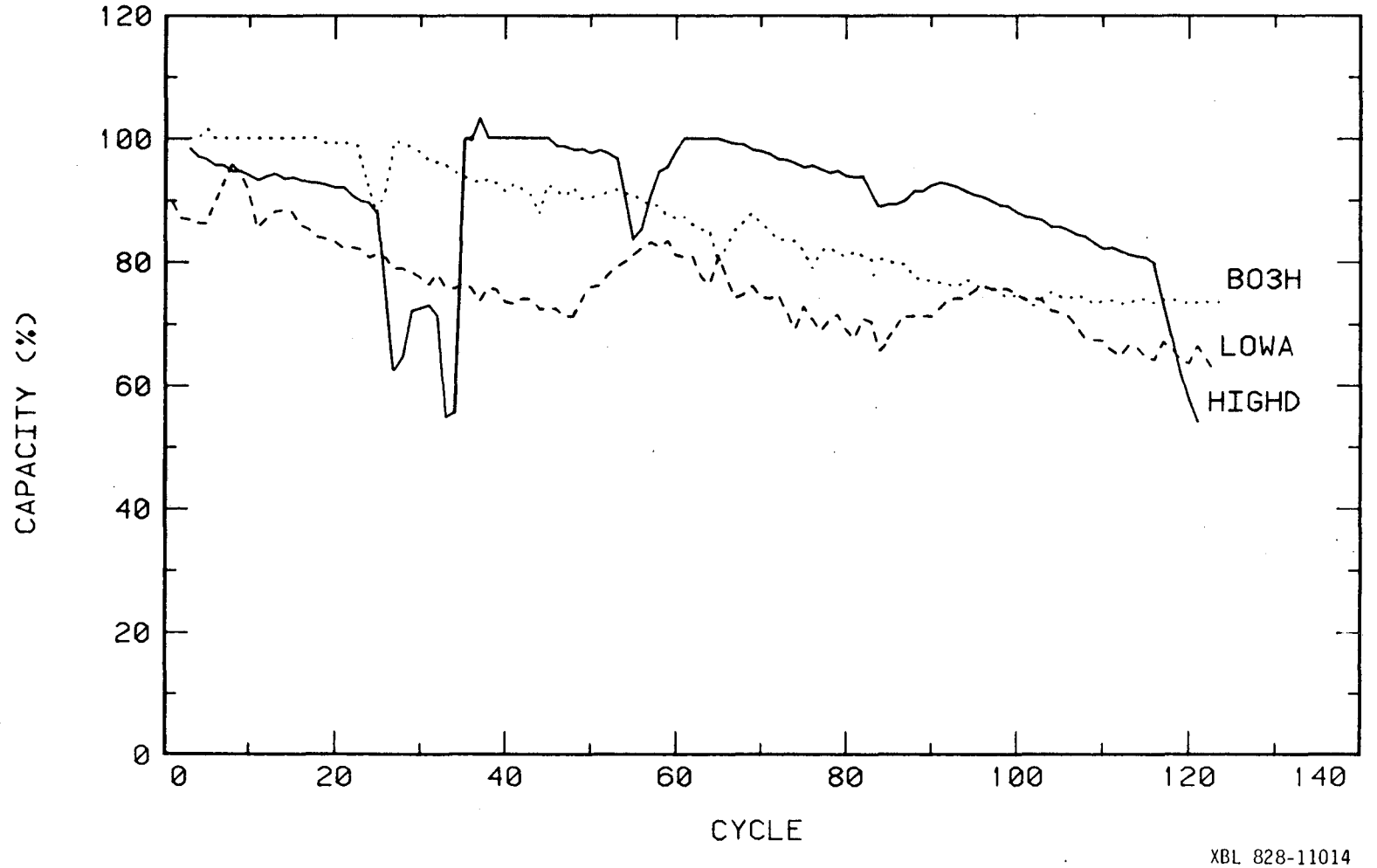

Figure IV-1. Comparison of capacities of cells BO3H, LOWA and HIGHD. 100% capacity is equivalent to a discharge of 1.35 Ah. A normal discharge is to a cell potential of 1.1 volts or 1.35 Ah, whichever is reached first.

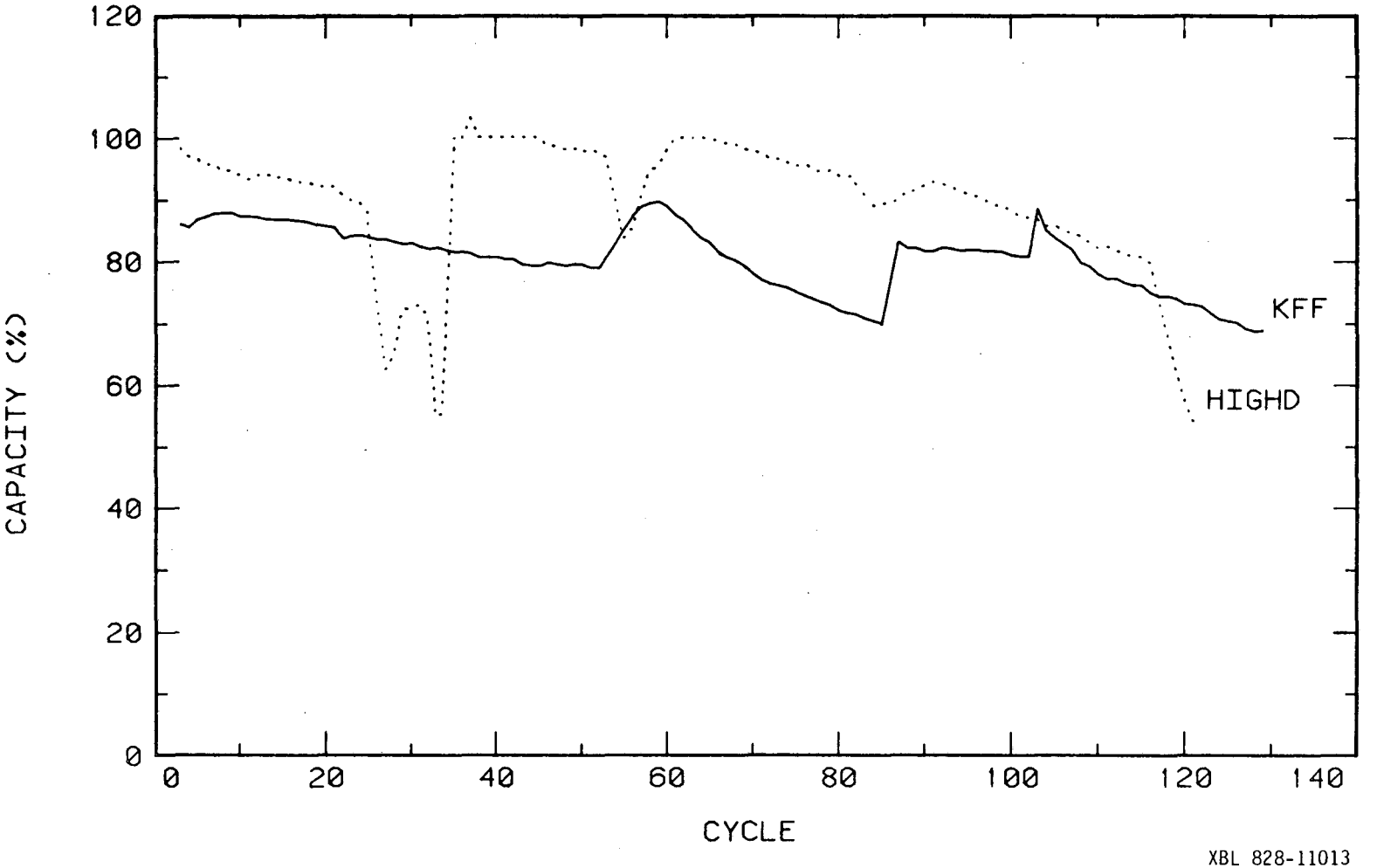

Figure IV-2. Comparison of capacities of cells KFF and HIGHD. 100% capacity is equivalent to a discharge of 1.35 Ah. A normal discharge is to a cell potential of 1.1 volts or 1.35 Ah, whichever is reached first.

is probably caused by reduced utilization of the Ni electrode[2] due to the lower hydroxide concentration. The cells containing the caustic-fluoride electrolyte had the lowest initial capacity, probably caused by a combination of two factors: reduced hydroxide concentration and the lack of lithium in the electrolyte. The lithium is added to the electrolyte of Ni electrode-containing cells to improve the utilization of the NiOOH,[2] but lithium was not soluble in the fluoride electrolyte. The discontinuities in cell KFF's capacity data will be discussed in the following section.

Capacity reduction could be attributable to capacity loss of the NiOOH electrodes, densification or passivation of zinc,[1] internal shorting or zinc redistribution. The post-cycling examination revealed that cell HIGHB had shorted and similar loses in capacity and coulombic efficiency (<95%) were observed for cell HIGHD; thus it is believed to have shorted as well. The observed capacity loss for the other six cells is not believed to have resulted from shorting, based on the post-test examination presented in the previous section. Possible densification and passivation will be discussed in a following section where it will be shown that little inactive zinc was present.

The actual zinc redistribution is shown in the X-ray images of Figures IV-3 through IV-10, and the measured area loss and capacity loss are presented in Table IV-5. The image obtained before cycling the electrode is necessary to establish the original distribution of zinc oxide. Various defects in the original distribution of zinc oxide have been reported to accelerate the zinc redistribution.[5] Figures IV-3 through IV-10 show the initial zinc oxide distribution to be fairly

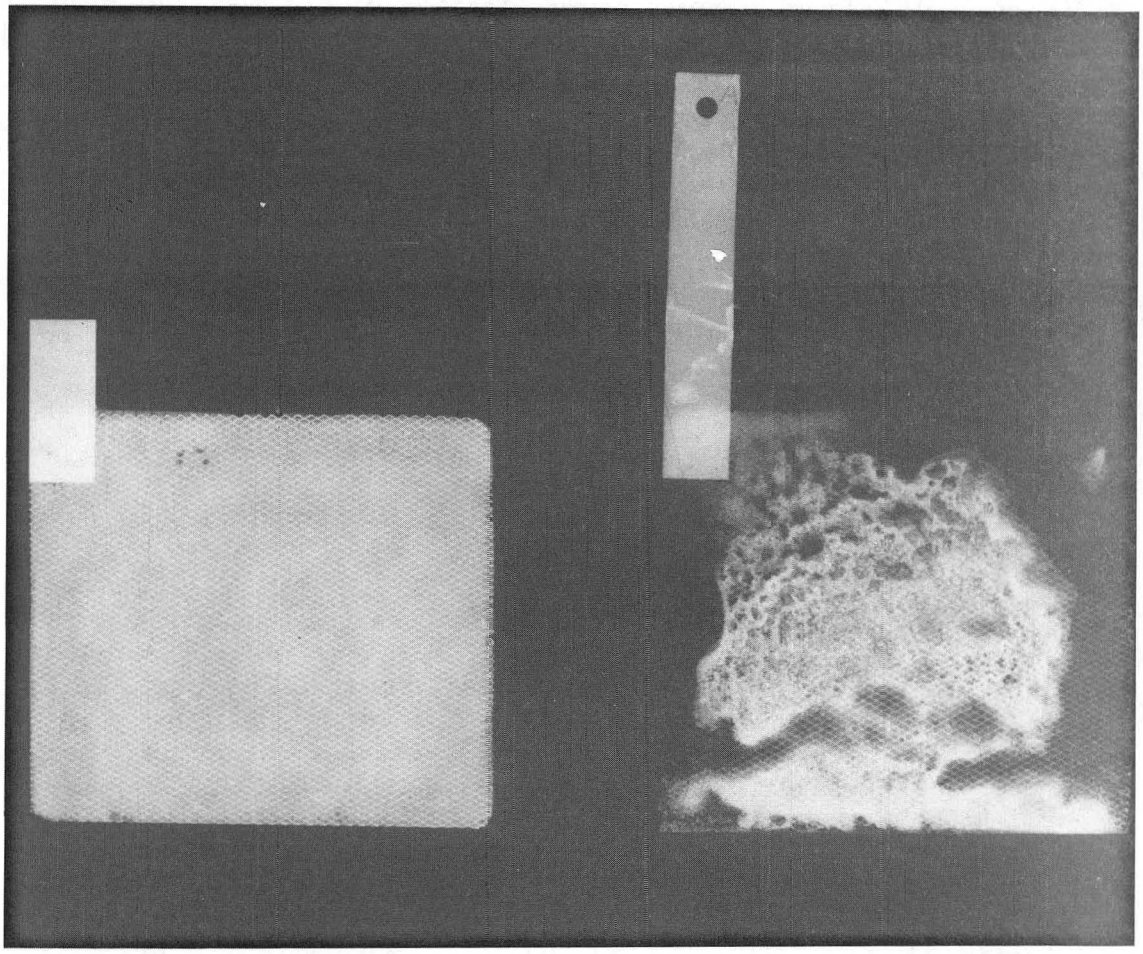

XBB 827-6073

Figure IV-3. X-ray Image of Zinc Electrode LOWA. 1.35 Ah design capacity electrode, with three times theoretical ZnO, cycled between two NiOOH counter electrodes at an average depth of discharge of 76.2% of design capacity in a 14.4% KOH-1.1% LiOH, ZnO-saturated electrolyte. The electrode is shown before cycling and in the discharged state after cycle 124 with an estimated 36% loss of area. The magnification is 0.81, the X-ray energy was 60KeV and the dose was 100 mAs.

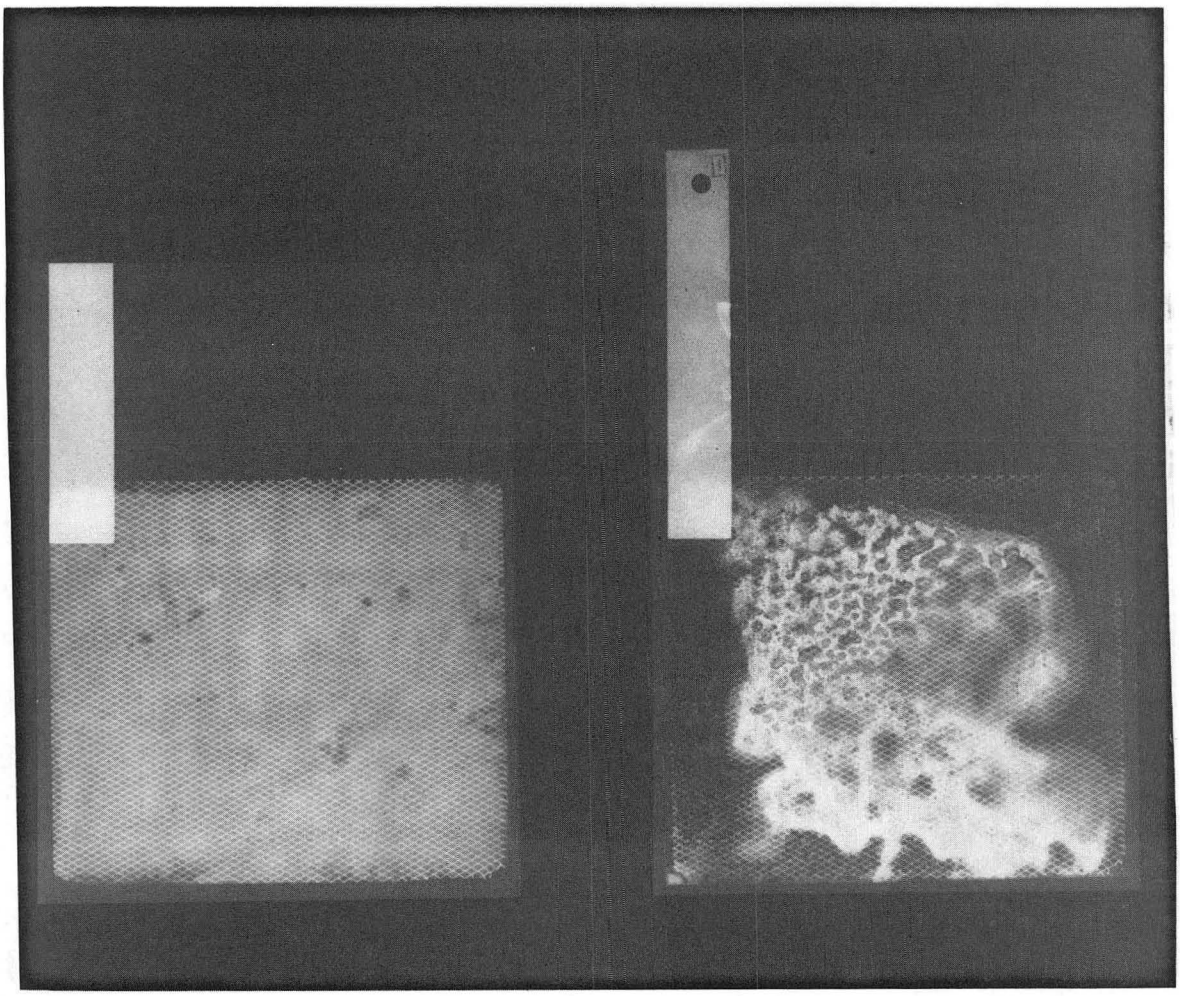

XBB 827-5926

Figure IV-4. X-ray Image of Zinc Electrode LOWE. 1.35 Ah design capacity electrode, with three times theoretical ZnO, cycled between two NiOOH counter electrodes at an average depth of discharge of 76.2% of design capacity in a 14.4% KOH-1.1% LiOH,ZnO-saturated electrolyte. The electrode is shown before cycling and in the charged state on cycle 124 with an estimated 39% loss of area. The magnification is 0.86, the X-ray energy was 60 KeV and the dose was 100 mAs.

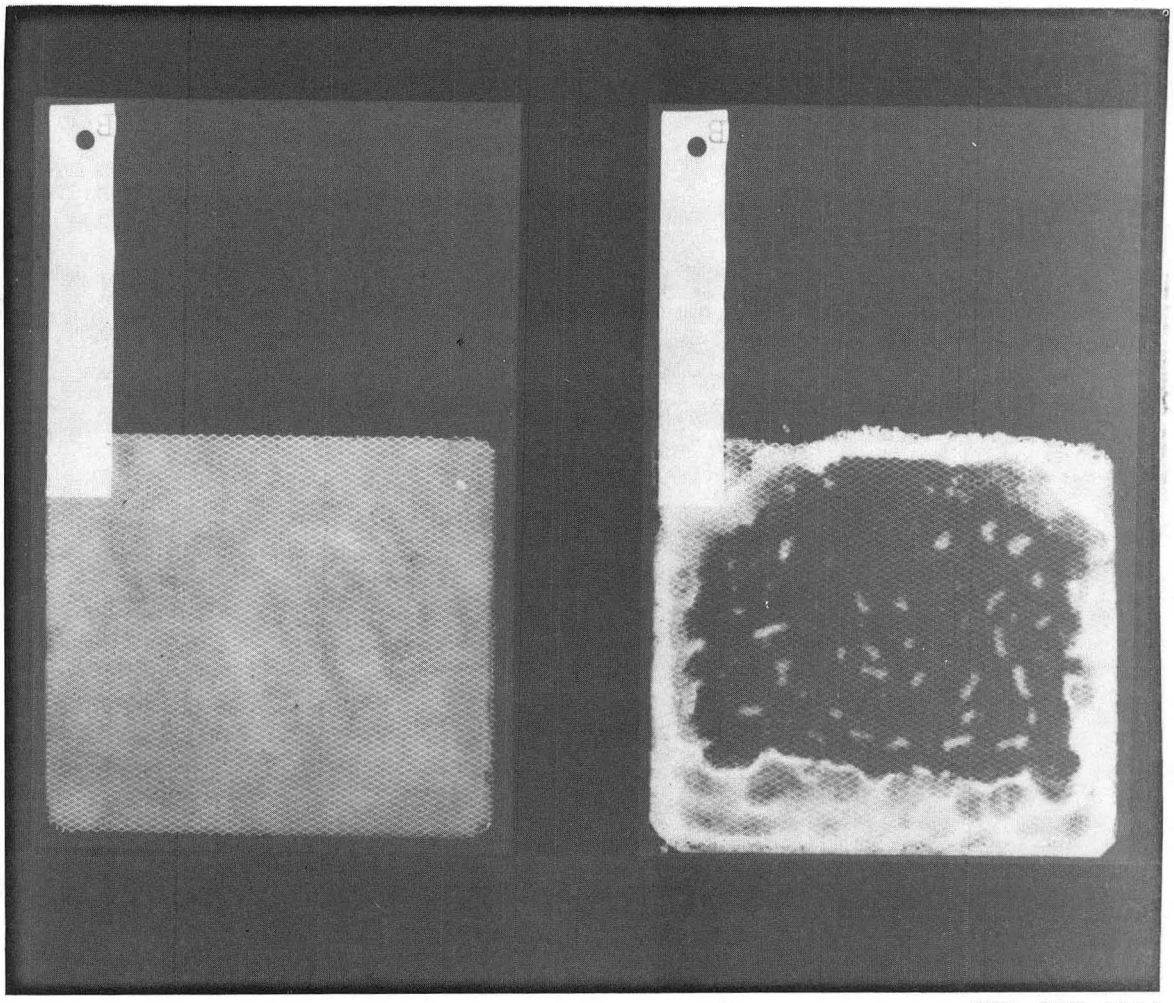

XBB 827-5924

Figure IV-5. X-ray Image of Zinc Electrode HIGHB. 1.35 Ah design capacity electrode, with three times theoretical ZnO, cycled between two NiOOH counter electrodes at an average depth of discharge of 94.2% of design capacity in a 30% KOH-1% LiOH,ZnO-saturated electrolyte. The electrode is shown before cycling and in the charged state on cycle 34 with an estimated 52% loss of area. The magnification is 0.84, the X-ray energy was 60 KeV and the dose was 100 mAs.

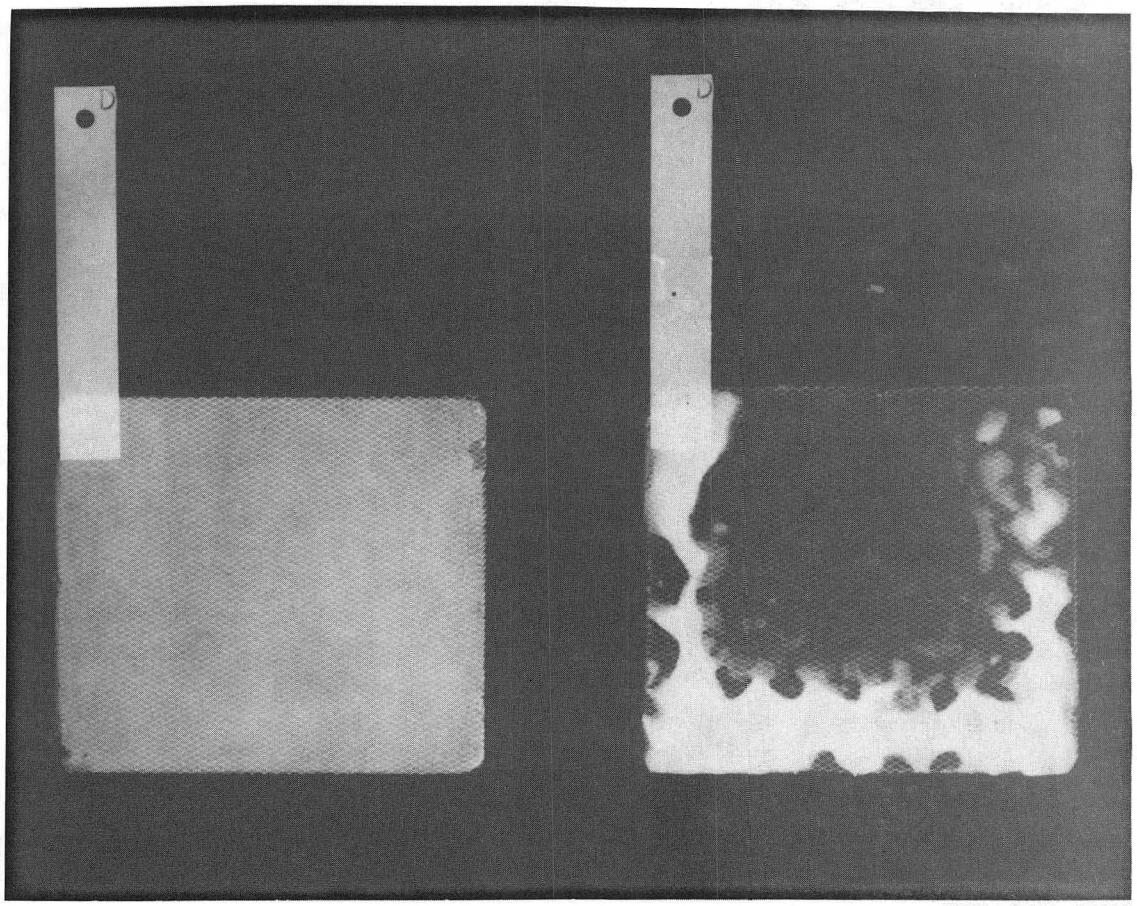

XBB 827-6075

Figure IV-6. X-ray Image of Zinc Electrode HIGHD. 1.35 Ah design capacity electrode, with three times theoretical ZnO, cycled between two NiOOH counter electrodes at an average depth of discharge of 93% of design capacity in a 30% KOH-1% LiOH,ZnO-saturated electrolyte. The electrode is shown before cycling and in the discharged state after cycle 122 with an estimated 56% loss of area. The magnification is 0.81, the X-ray energy was 60 KeV and the dose was 100 mAs.

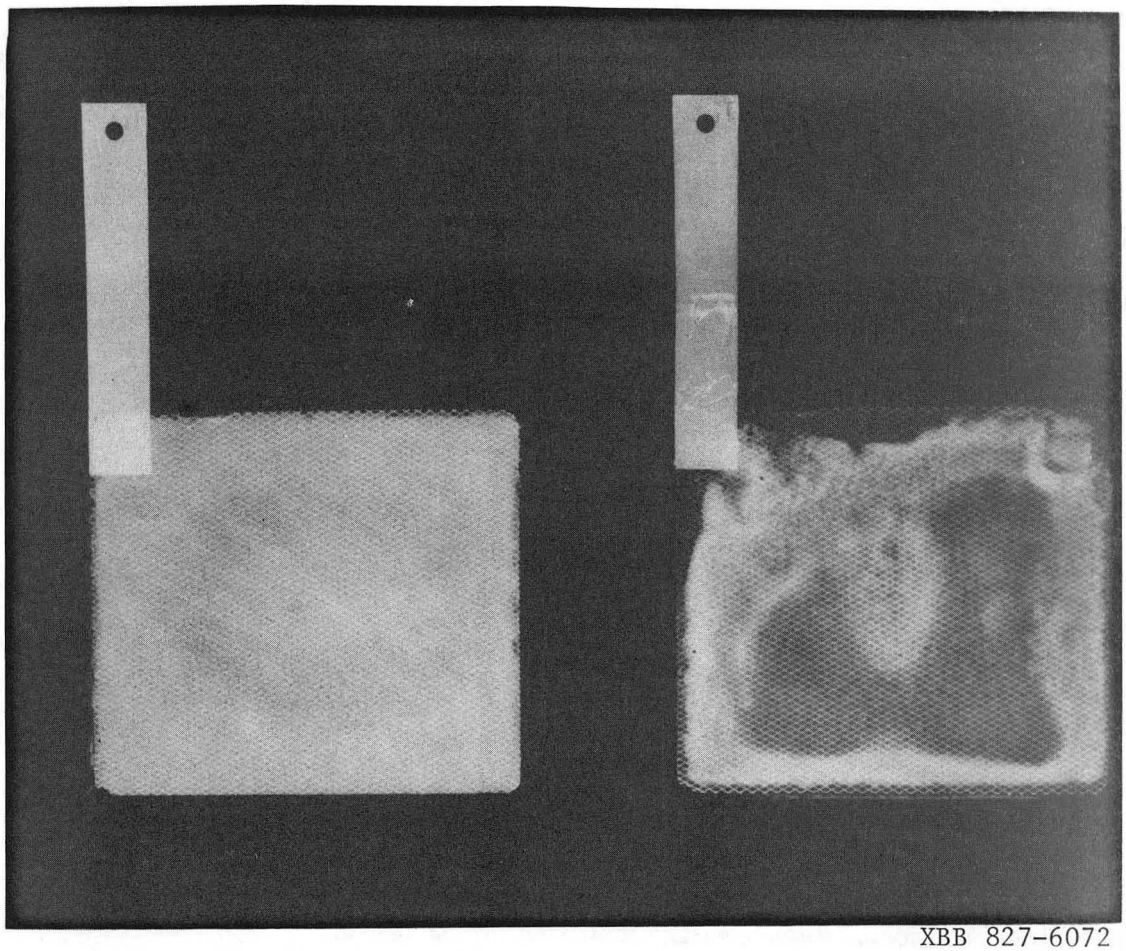

XBB 827-6072

Figure IV-7. X-ray Image of Zinc Electrode BO3H. 1.35 Ah design capacity electrode, with three times theoretical ZnO, cycled between two NiOOH counter electrodes at an average depth of discharge of 88.8% of design capacity in a 21.5% K_3BO_3-1.13% Li_3BO_3,ZnO-saturated electrolyte. The electrode is shown before cycling and in the discharged state after 125 cycles with an estimated 11% loss of area. The magnification is 0.80, the X-ray energy was 60 KeV and the dose was 100 mAs.

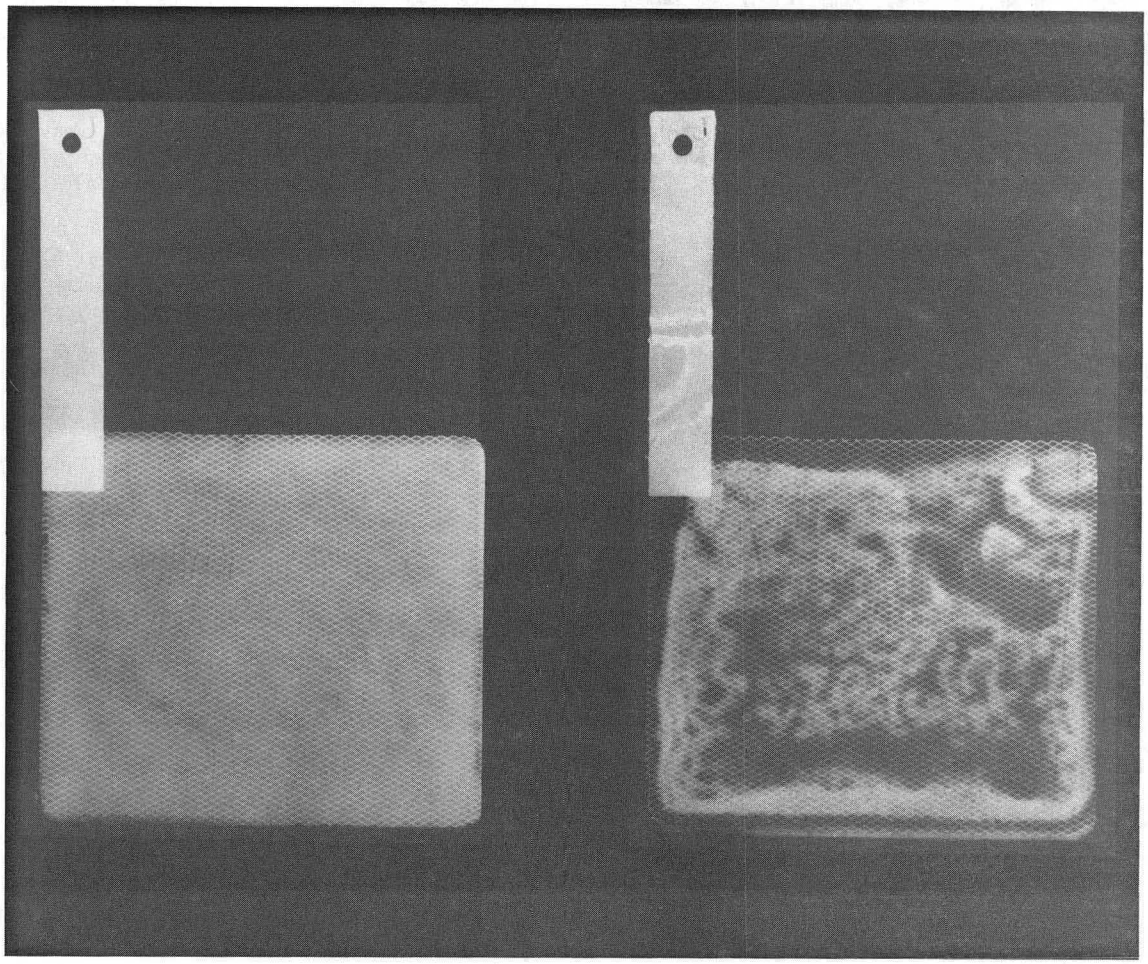

XBB 827-5927

Figure IV-8. X-ray Image of Zinc Electrode B03J. 1.35 Ah design capacity electrode, with three times theoretical ZnO, cycled between two NiOOH counter electrodes at an average depth of discharge of 88.8% of design capacity in a 21.5% K_3BO_3-1.13% Li_3BO_3, ZnO-saturated electrolyte. The electrode is shown before cycling and in the charged state on cycle 125 with an estimated 14% loss of area. The magnification is 0.86, the X-ray energy was 60 KeV and the dose was 100 mAs.

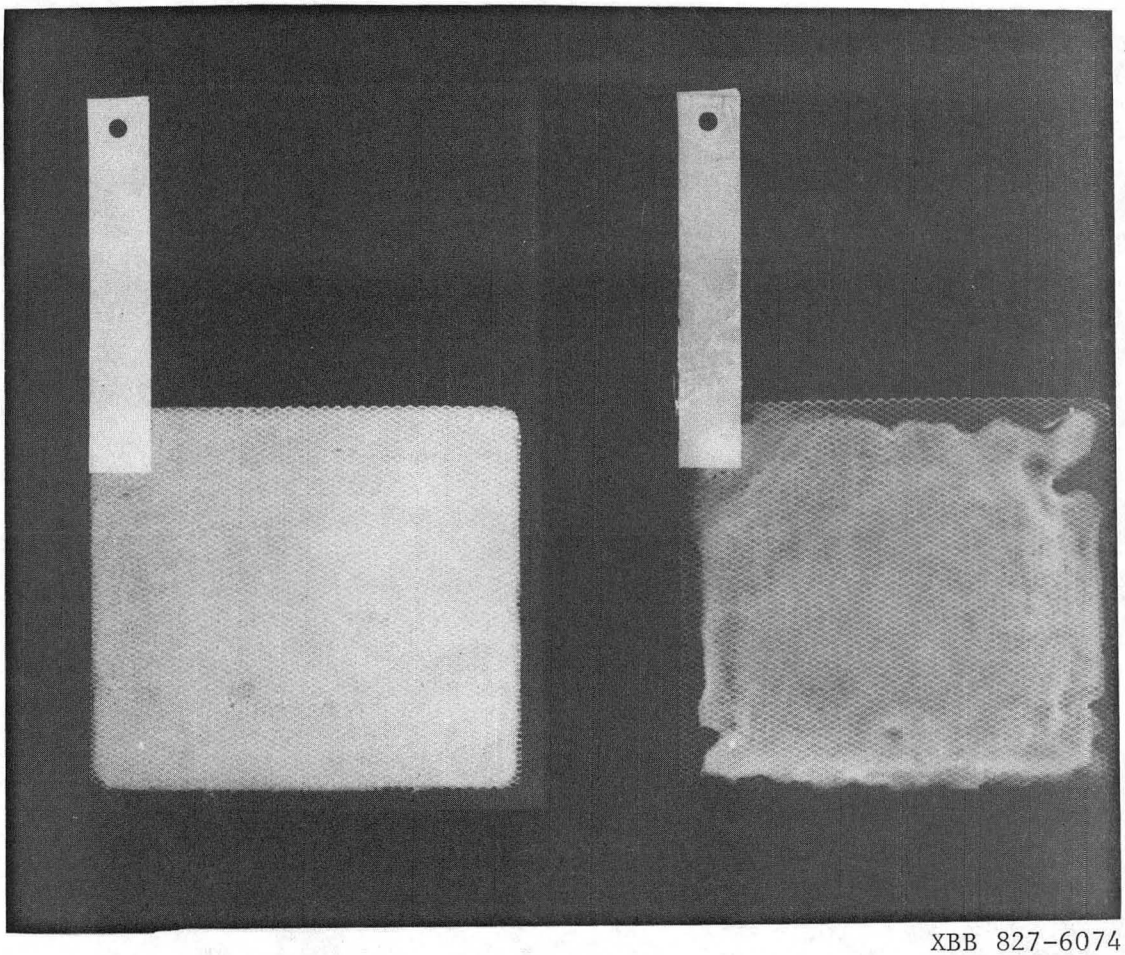

XBB 827-6074

Figure IV-9. X-ray Image of Zinc Electrode KFF. 1.35 Ah design capacity electrode, with three times theoretical ZnO, cycled between two NiOOH counter electrodes at an average depth of discharge of 82.5% of design capacity in a 15.3% KOH-15.0% KF, Li-saturated, ZnO-saturated electrolyte. The electrode is shown before cycling and in the discharged state after cycle 130 with an estimated 13% loss of area. The magnification is 0.81, the X-ray energy was 60 KeV and the dose was 100 mAs.

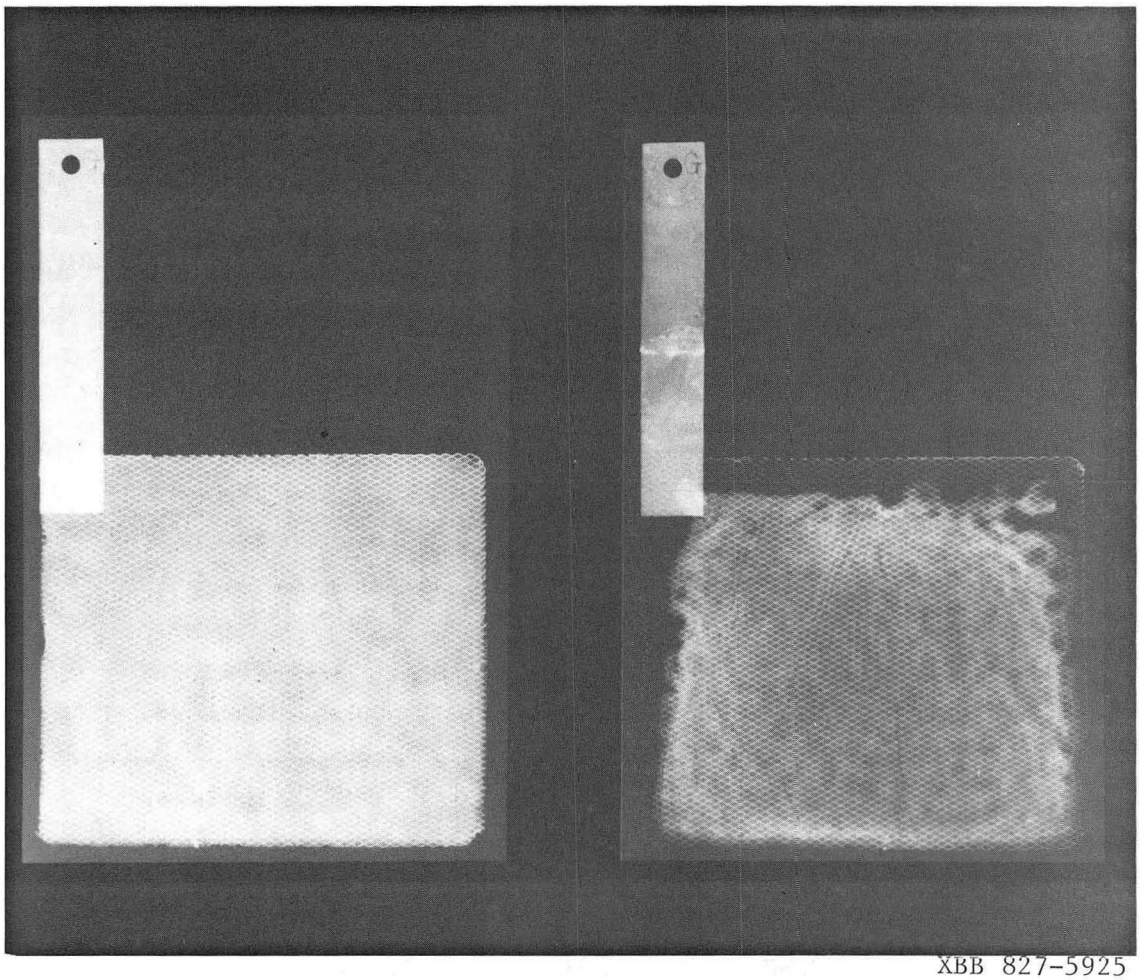

XBB 827-5925

Figure IV-10. X-ray Image of Zinc Electrode KFG. 1.35 Ah design capacity electrode, with three times theoretical ZnO, cycled between two NiOOH counter electrodes at an average depth of discharge of 82.5% of design capacity in a 15.3% KOH-15.0% KF, Li-saturated, ZnO-saturated electrolyte. The electrode is shown before cycling and in the charged state on cycle 130 with an estimated 18% loss of area. The magnification is 0.86, the X-ray energy was 60 KeV, and the dose was 100 mAs for the uncycled electrode and 150 mAs for the cycled electrode.

uniform, with only some small defects. The defects do not seem to correlate with the absences or accumulations of zinc material in the cycled electrode.

The values reported in Table IV-5 are the percentage of area shown on the X-ray to contain no Zn or ZnO. Others[6,7] have reported that this bare area is generally found around the edges of the electrode with the Zn and ZnO accumulated toward the middle of the electrode. These estimates are of course subjective, particularly in the case of the borate electrode. For these electrodes the thinned areas in the central portion of the electrodes were not counted as loss areas.

Table IV-5
Estimate of Loss of Zn Electrode Area and Capacity Loss

Electrode	Area loss, %	Capacity loss, %
HIGHD	56%	47.6% (22.7%)[a]
HIGHB	52%	44.4% (10.9%)[a]
LOWA	36%	35.3%
LOWE	39%	35.3%
KFF	13%	23.3%
KFG	18%	23.3%
BO3H	11%	27.4%
BO3J	14%	27.4%

a) capacity loss before shorting is shown in parenthesis.

The high OH^- concentration electrolyte cell had the most extensive zinc redistribution and the low OH^- concentration electrolyte the next most. The F^- and BO_3^{-3} electrolyte-containing cells showed a reduced redistribution rate, but the Zn in the electrodes from the cells containing caustic-borate electrolyte had thinned considerably in the central areas. The low OH^- concentration electrolyte without the additives cannot be quite as directly compared to the others. Cell LOWA and LOWE

were not packed as tightly as the other six cells. The thicknesses of these cell stacks were 6% more than the others, 2.74 mm versus 2.59 mm, and the tightness of packing has been reported to influence the redistribution rate.[1] The redistribution rate could be expected to be less in a tighter packed cell, but it is unlikely that this difference in packing thickness could have reduced the redistribution by the 20% necessary to match the redistribution rate shown by the caustic-fluoride and borate electrolytes.

It had been proposed earlier that the capacity loss is due to the redistribution of the zinc. If that is so, then one should observe a correlation between the amount of redistribution and the capacity loss. Another possible reason for capacity loss is a decrease in the NiOOH electrode's ability to accept charge. These two possible mechanisms will now be discussed.

The second column of Table IV-5 contains the cell capacity loss (at the end of the experiments) as a percentage of the maximum capacity. The low KOH electrolyte cells, LOWA and LOWE, have a capacity loss that correlates well with the theory that only the portion of the electrode opposite Zn material can be discharged. These cells had a 35% capacity loss versus a 36% and 39% area loss. The cells containing caustic-borate electrolyte have a capacity loss that exceeds the area loss. This could be due to NiOOH electrode capacity loss, but the X-ray images in Figures IV-7 and IV-8 show thinned areas covering 20-30% of the electrode area. The thinned areas may contain insufficient material to fully charge or discharge the opposing Ni electrodes. The cells containing the fluoride electrolyte are reasonably close to the capacity loss

expected for the amount of area loss. Examination of Figure IV-2 shows the capacity of the fluoride-containing cells is erratic and declining at the last few cycles. This will be shown in the following section to be an artifact caused by cycling the two cells in series; the nickel electrode could not be as fully charged or discharged as might have been possible if the cells had been cycled individually.

The three low-hydroxide electrolytes may support the theory of a direct correlation between area loss and capacity loss; however, the high-hydroxide electrolyte does not appear to agree with this theory. Cell HIGHD retained 77% of its capacity until just before shorting. The zinc is unlikely to have redistributed significantly during the four cycles after shorting. The redistribution area loss was nearly 56% while the capacity loss (from cycle 37 to 116) was only 23%. The loss was actually larger than 23% but cell HIGHD's maximum capacity early in life could not be determined because cell HIGHB limited the discharge. If one assumes a linear relation for capacity loss versus cycle number, then the capacity loss from the early cycles to cycle 116 would be about 34%. This behavior has been observed by Seiger:[8] capacity losses of only 20% were observed for cells with zinc electrodes cut to represent 50% loss of area. Even though the capacity loss of cell HIGHD relative to area loss is greater than that reported by Seiger, it is still significantly less than would be expected from the loss of area.

A more informative way to look at this data is to compare the ratio of initial capacity retained to the zinc electrode area retained. This ratio is presented in Table IV-6. A value of one for the ratio would imply a direct 1:1 correlation between zinc electrode area and cell

capacity. A value less than one means the capacity has decreased more rapidly than the zinc electrode area has decreased. The ratio had a value near one for cells LOWA and LOWE, but cells BO3H and BO3J had values less than one. This lower capacity retention has been addressed and is believed to be due to areas of the zinc electrode with insufficient zinc material to fully charge the opposing portions of the nickel-oxide electrode. The lower value of the capacity retention ratio for cells KFF and KFG was at least partially due to cycling the two cells in series. Six of the cells then have capacity-retention-to-area-retention ratios close to or slightly less than one. The seventh cell, HIGHD, cycled in 7.4 M OH^- electrolyte, had a capacity retention ratio 50% or more higher than the others.

Table IV-6
Comparison of Cell Capacity Retention

Cell	Ratio of initial capacity retained to area retained
HIGHD	1.50
LOWA	1.01
LOWE	1.06
KFF	0.88
KFG	0.94
BO3H	0.82
BO3J	0.84

If the nickel electrode can be charged to a higher level than the zinc-electrode area loss would indicate for cell HIGHD, then one must explain the lower capacity observed in the other cells. Passivation, isolation, and densification of zinc have been proposed to limit the Zn capacity, and as mentioned in the previous section, the passivation could be more severe in cells with lower KOH concentration. If regions

of the Zn electrode contained passivated, isolated or densified zinc, the Zn electrode may not appear to be limiting (i.e. showing excessive over-potential) but the opposing Ni electrode may not be charged for lack of charge transfer processes occurring on the opposing Zn electrode. It will be shown that the fluoride and borate electrodes did not have passivated, isolated or unreactive densified zinc, and that the Zn electrodes cycled in 3.5 M OH^- and 7.4 M OH^- electrolytes probably did not have any such inactive zinc either. The decreased ability to charge the nickel electrode must then be attributed to either the decreased hydroxide concentration affecting the ability of the Ni electrode to accept charge or the reduced conductivity or both. It is difficult to determine the amount of NiOOH electrode capacity loss versus the capacity loss resulting from Zn electrode area loss from these data. The capacity of the NiOOH electrodes was not measured after disassembling the cells.

Another observed effect on zinc redistribution rates is the amount of excess zinc in the zinc electrode.[1] These cells were designed with three times the theoretical amount of zinc when cycled at the 1.35-Ah design capacity. The cells were to be cycled at this 1.35-Ah capacity; however, the Ni electrode did not have sufficient capacity. The average depth of discharge (DOD) is presented in Table IV-7. The ranking of DOD from greatest to least is high OH^-, borate, fluoride and low OH^-.

Table IV-7
Average Depth of Discharge

Electrode	Depth of discharge, %
LOWA	76.2
HIGHD	93.0
KFF	82.5
BO3H	88.8

The average depth of discharge for cell KFF is only 11% lower than cell HIGHD but the zinc redistribution of cell KFF is considerably less, 13% versus 56%. The deviation of the average depth of discharge from cell HIGHD to cell BO3H is only 4% but again the redistribution of zinc is considerably less for cell BO3H, 11% versus 56%. Cells LOWA and LOWE had the least DOD and considerable shape change. The differences in DOD are slight and no obvious trend existed. It is probably safe to conclude that the lower DOD did not account for the large difference in the redistribution rate.

The conclusion one can reach from these results is that the zinc redistribution is greatly improved by the lowered zinc oxide solubility obtained by reducing the hydroxide concentration. The capacity retention of the cell containing the high OH^-, however, was much better than one might expect from the more rapid zinc redistribution. The capacity retention of the cell containing the high OH^- concentration as a percentage of maximum capacity was less than the fluoride-containing electrolyte though, and probably less than the borate-containing electrolyte. The ability of the high-hydroxide electrolyte cells to maintain capacity, despite extensive zinc redistribution, appears to be due to the high hydroxide concentration, high conductivity, or both.

4. Electrode Potential Measurements

The electrode potentials were measured through the use of an Hg/HgO reference electrode described in Chapter III, Section 3B. The zinc electrode potential during open circuit was obtained for most of the cells in the charged state and the Ni electrode open circuit potentials in the charged and discharged state. For the zinc electrode, the potential was -1.33 V to -1.34 V, the exception being cell HIGHD which had an open circuit potential of -1.355. Reliable open circuit potential data for the zinc electrode were not obtained for cell HIGHB, but the potential appeared to be approximately -1.33 volts. No open-circuit potentials in the charged state were obtained for cell KFF.

The nickel-oxide electrode has a state-of-charge dependent open-circuit potential. In the charged state the potential is approximately 0.51 V vs Hg/HgO, and in the discharged state approximately 0.31 vs Hg/HgO. A large variation was obtained from one electrolyte to another. The nickel-oxide electrode open-circuit potentials in the discharged state were obtained following a discharge at 0.54 A to a cell potential of 1.1 V. The open-circuit potentials in the charged state were obtained following a 4% overcharge at 225 mA for cells HIGHD, LOWA, and LOWE; and following a 50% overcharge at 135 mA for cells KFG, BO3H, and BO3J. The open-circuit potentials are presented with the cell and electrode potentials in Figures IV-11 through IV-18. The zinc electrode

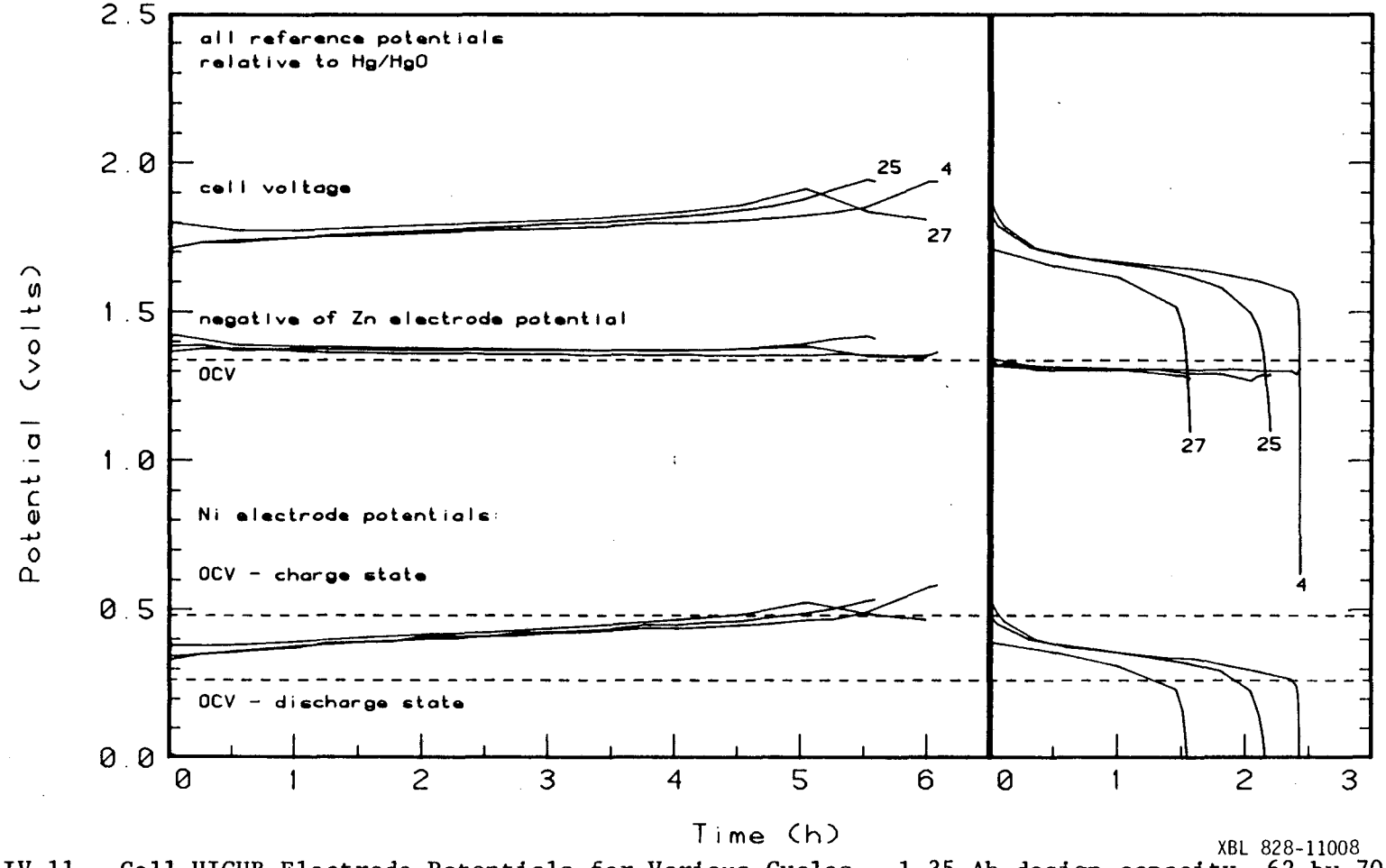

XBL 828-11008

Figure IV-11. Cell HIGHB Electrode Potentials for Various Cycles. 1.35 Ah design capacity, 62 by 70 mm Zn electrode with three times theoretical ZnO, cycled between two NiOOH counter electrodes in a 30% KOH-1% LiOH, ZnO-saturated electrolyte. The 225 mA charge is shown at the left and the 540 mA discharge is shown at the right with apparent shorting during the charge of cycle 27. Irregularities in the electrode potentials are due to bubbles in the reference electrode capillary causing a high-resistance path. The reference capillary was at the back side of the Ni electrode.

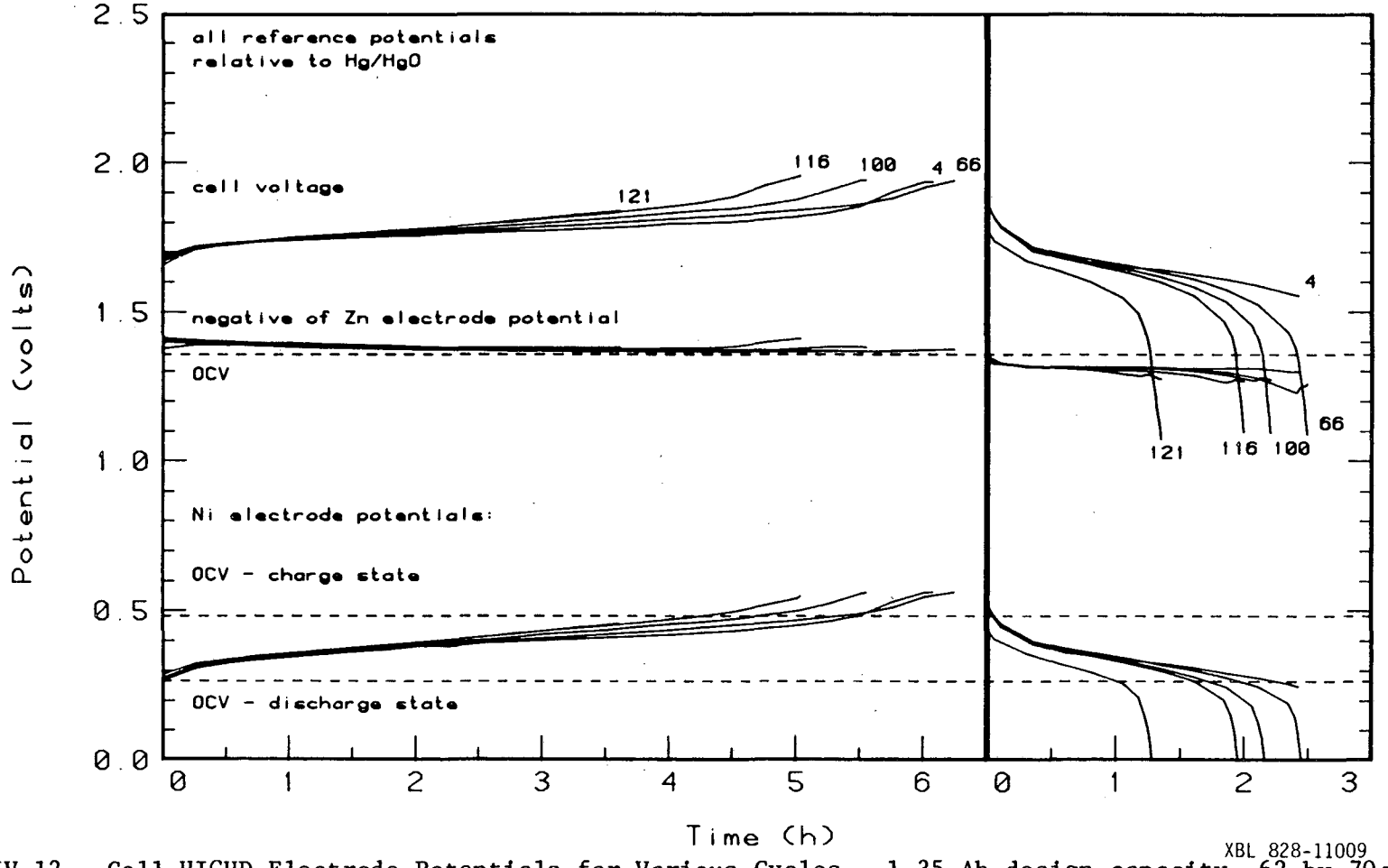

XBL 828-11009

Figure IV-12. Cell HIGHD Electrode Potentials for Various Cycles. 1.35 Ah design capacity, 62 by 70 mm Zn electrode with three times theoretical ZnO, cycled between two NiOOH counter electrodes in a 30% KOH-1% LiOH,ZnO-saturated eletrolyte. The 225 mA charge is shown at the left and the 540 mA discharge is shown at the right. The reference capillary was at the back side of the Ni electrode.

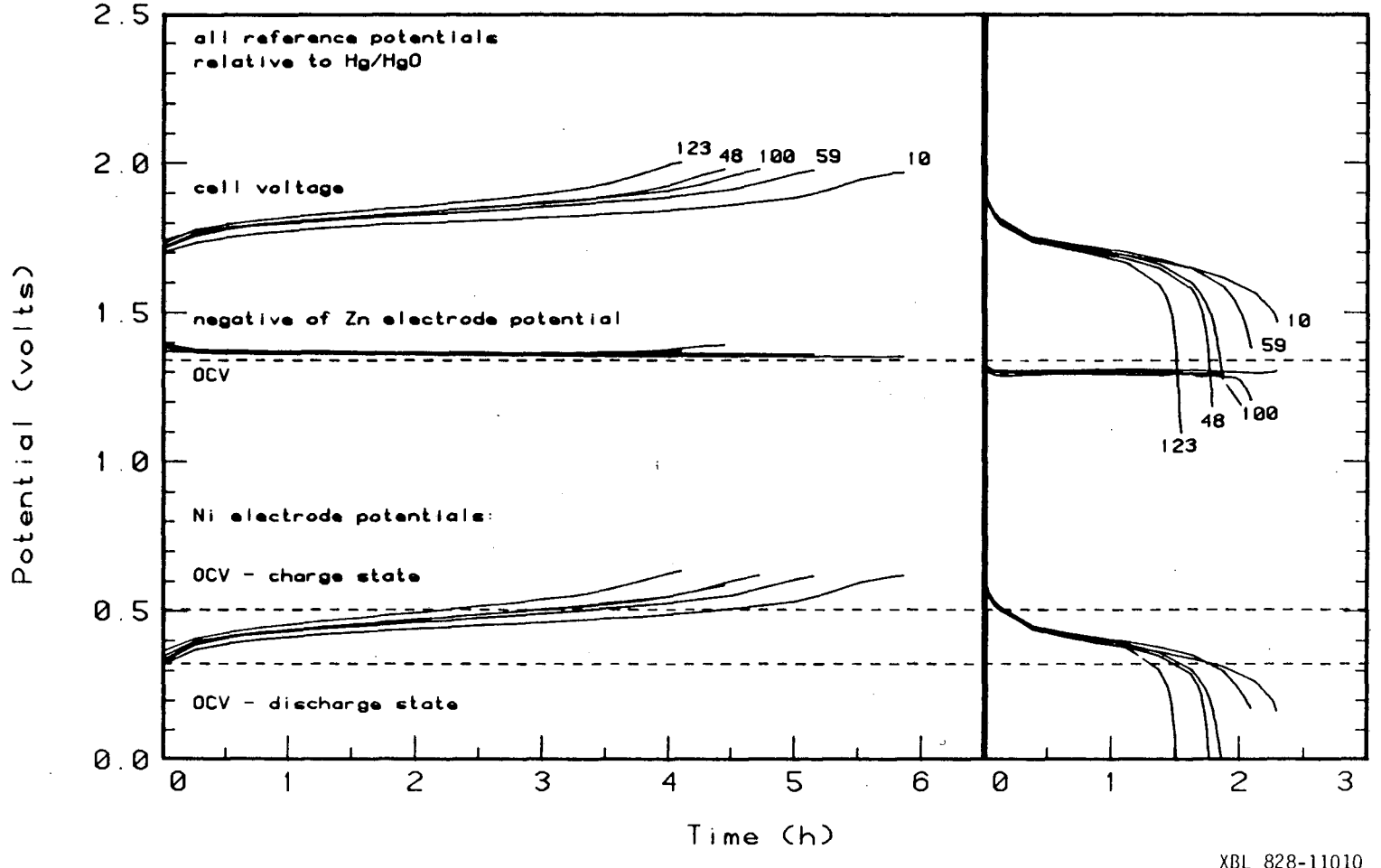

XBL 828-11010

Figure IV-13. Cell LOWA Electrode Potentials for Various Cycles. 1.35 Ah design capacity, 62 by 70 mm Zn electrode with three times theoretical ZnO, cycled between two NiOOh counter electrodes in a 14.4% KOH-1.1 LiOH,ZnO-saturated electrolyte. The 225mA charge is shown at the left and the 540 mA discharge is shown at the right. The reference capillary was at the back side of the Ni electrode.

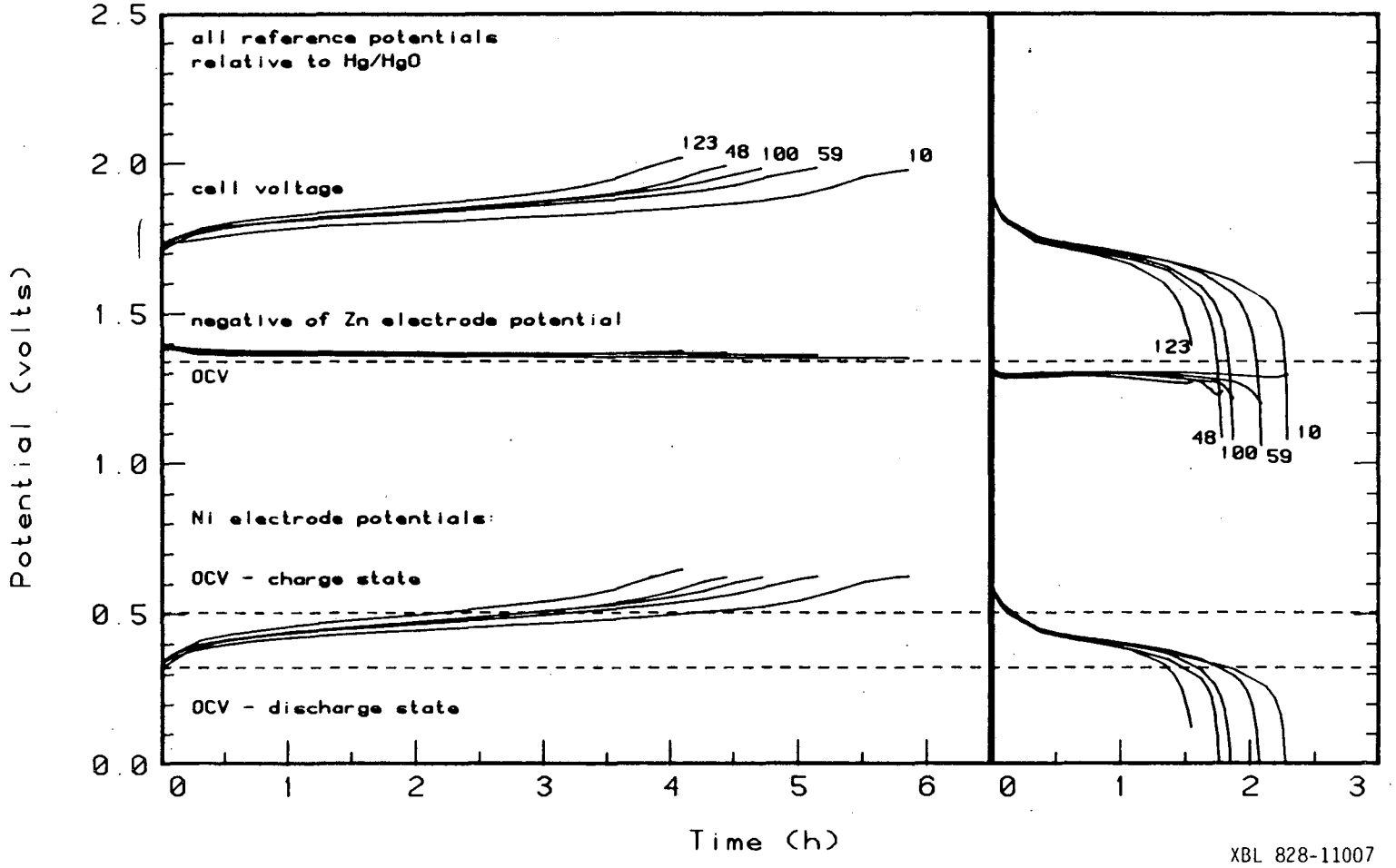

XBL 828-11007

Figure IV-14. Cell LOWE Electrode Potentials for Various Cycles. 1.35 Ah design capacity, 62 by 70 mm Zn electrode with three times theoretical ZnO, cycled between two NiOOH counter electrodes in a 14.4% KOH-1.1% LiOH,ZnO-saturated electrolyte. The 225 MA charge is shown at the left and the 540 mA discharge is shown at the right. The reference capillary was at the back side of the Ni electrode.

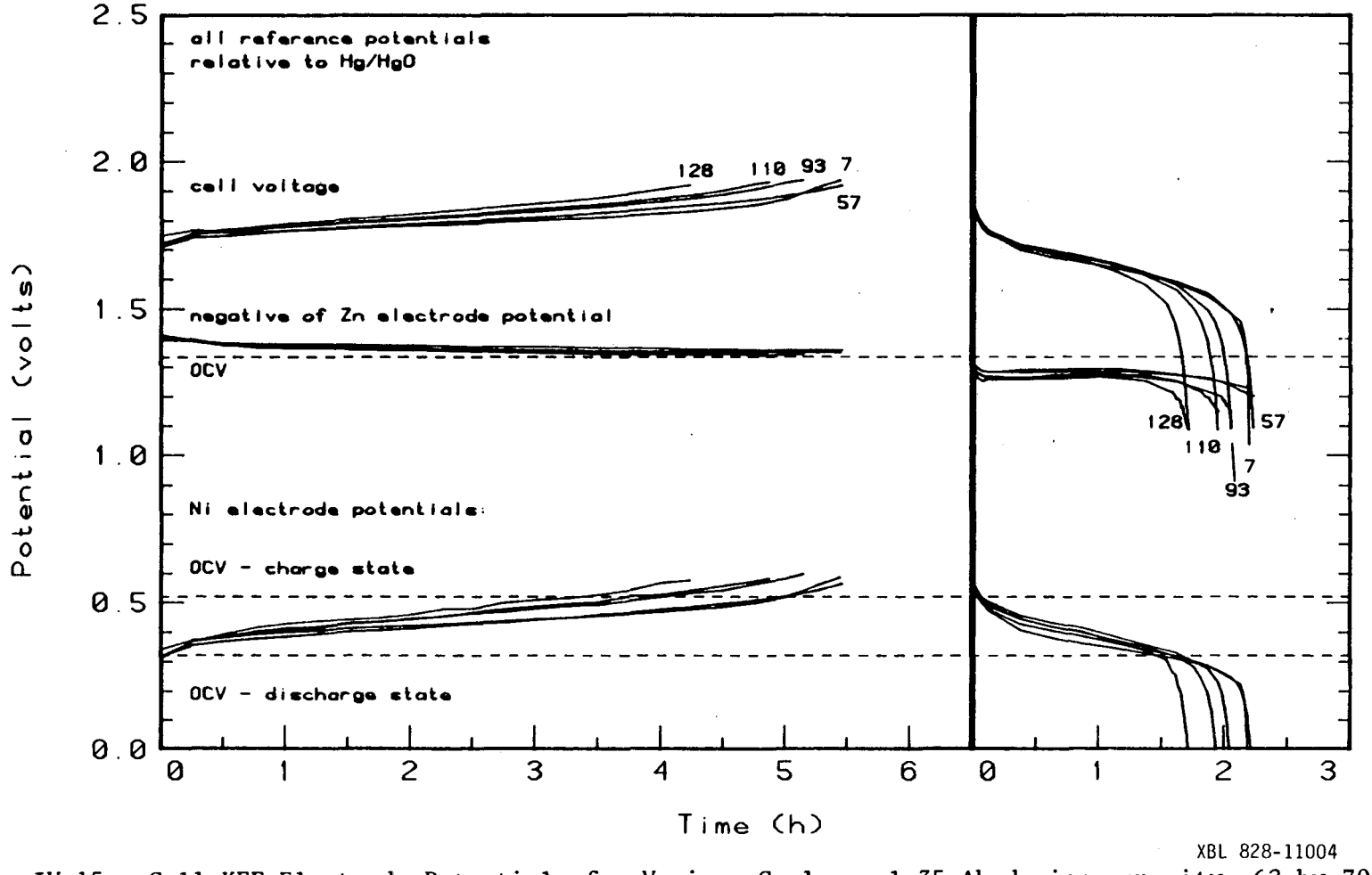

XBL 828-11004

Figure IV-15. Cell KFF Electrode Potentials for Various Cycles. 1.35 Ah design capacity, 62 by 70 mm Zn electrode with three times theoretical ZnO, cycled between two NiOOH counter electrodes in a 15.3% KOH-15% KF,Li-saturated,ZnO-saturated electrolyte. The 225 mA charge is shown at the left and the 540 mA discharge is shown at the right. The reference capillary was at the back side of the Ni electrode.

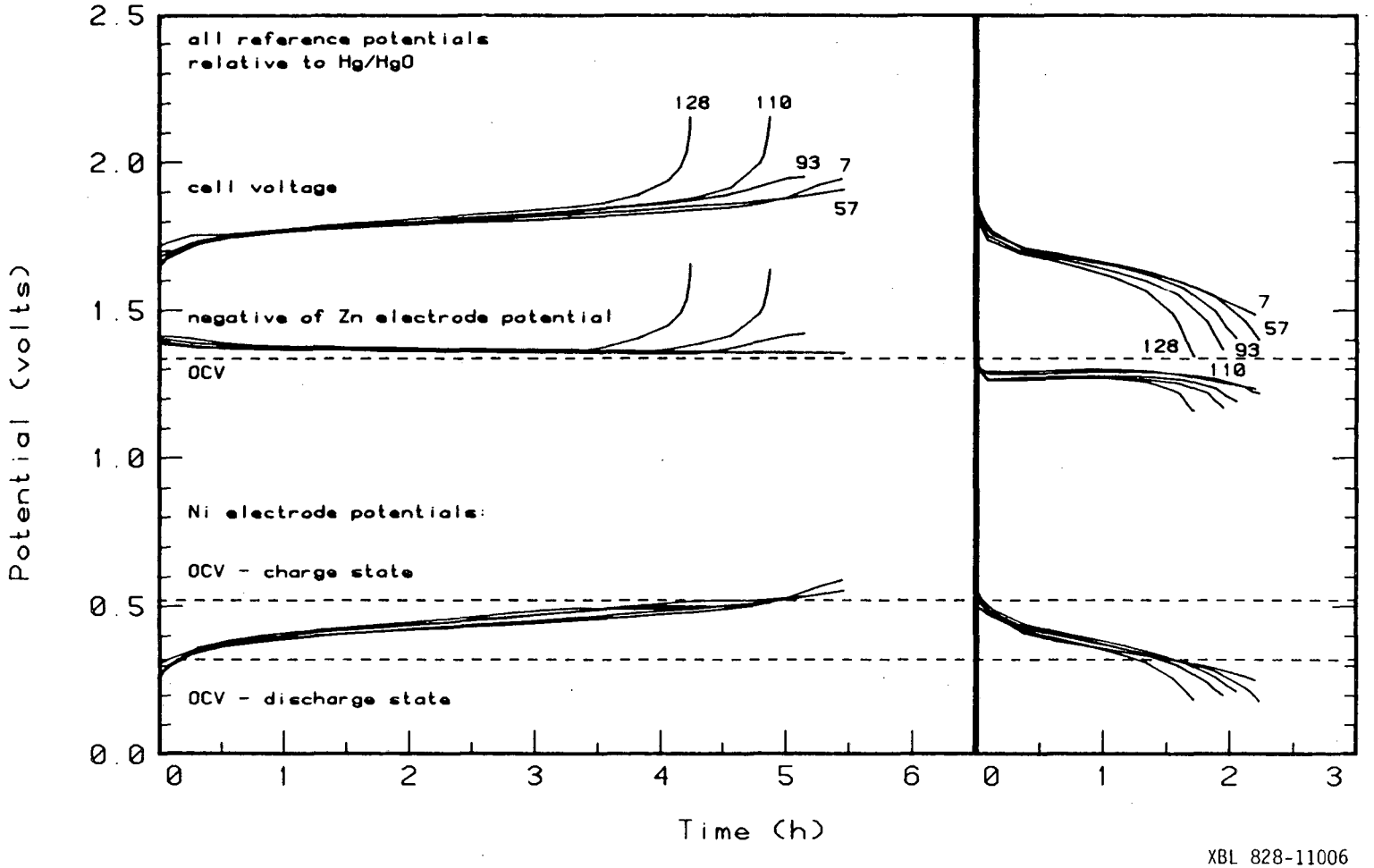

XBL 828-11006

Figure IV-16. Cell KFG Electrode Potentials for Various Cycles. 1.35 Ah design capacity, 62 by 70 mm Zn electrode with three times theoretical ZnO, cycled between two NiOOH counter electrodes in a 15.3% KOH-15% KF,Li-saturated, ZnO-saturated electrolyte. The 225 mA charge is shown at the left and the 540 mA discharge is shown at the right. On cycles 110 and 128 the charge was limited by a 2.15 V cell potential cutoff limit. The reference capillary was at the back side of the Ni electrode.

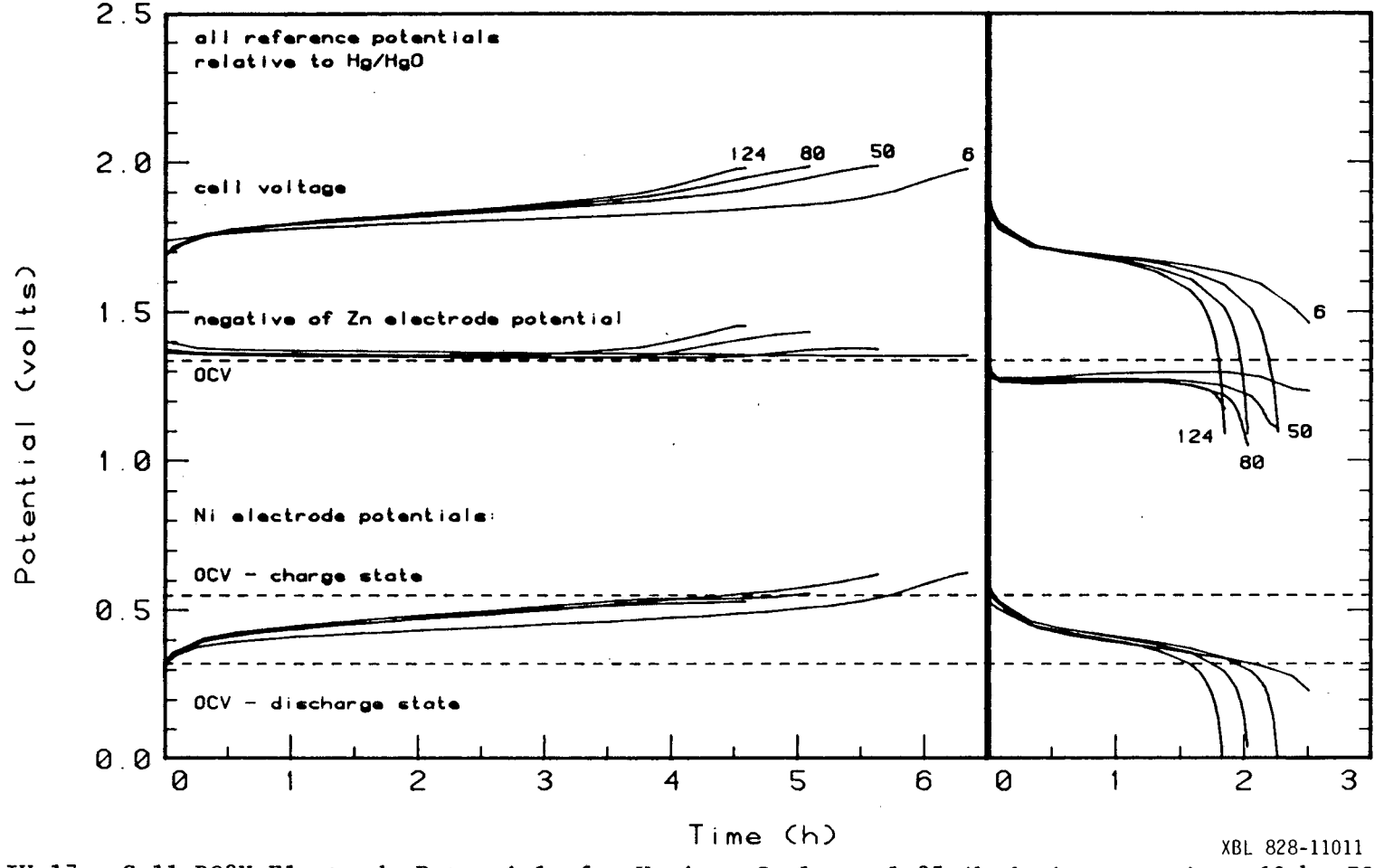

Figure IV-17. Cell BO3H Electrode Potentials for Various Cycles. 1.35 Ah design capacity, 62 by 70 mm Zn electrode with three times theoretical ZnO, cycled between two NiOOH counter electrodes in a 21.5% K_3BO_3-1.1% Li_3BO_3, ZnO-saturated electrolyte. The 225 mA charge is shown at the left and the 540 mA discharge is shown at the right. On cycle 6 the discharge was limited to 1.35 Ah. The reference capillary was at the back side of the Ni electrode.

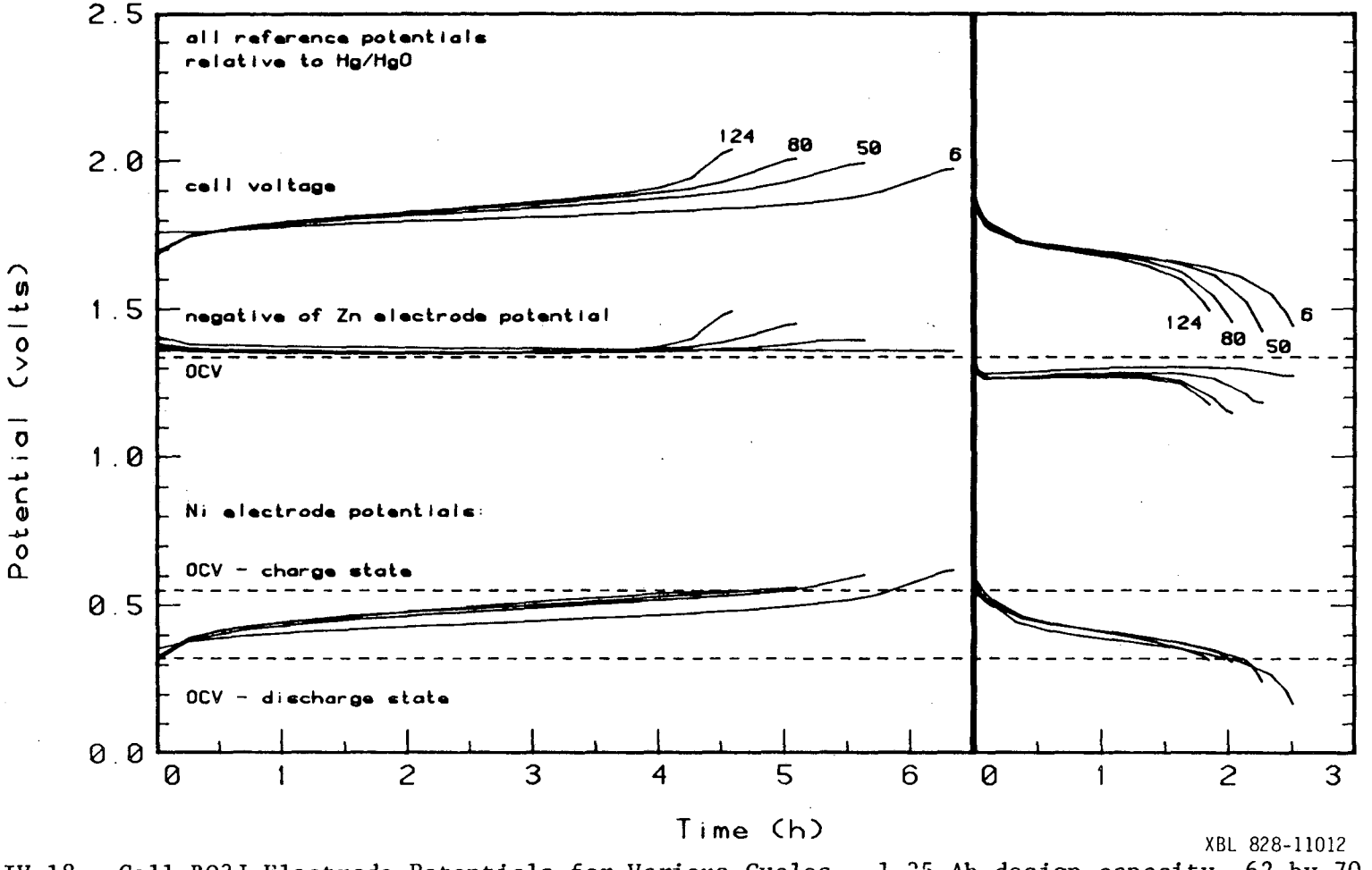

Figure IV-13. Cell BO3J Electrode Potentials for Various Cycles. 1.35 Ah design capacity, 62 by 70 mm Zn electrode with three times theoretical ZnO, cycled between two NiOOH counter electrodes in a 21.5% K_3BO_3-1.1% Li_3BO_3,ZnO-saturated electrolyte. The 225 mA charge is shown at the left and the 540 mA discharge is shown at the right. On cycle 6 the discharge was limited to 1.35 Ah. The reference capillary was at the back side of the Ni electrode.

potentials are plotted as the absolute value of the Zn vs. Hg/HgO potential for convenience in scaling the ordinate. For those cells in which open-circuit data were not obtained, the values from the cell with identical electrolyte are shown, except for cell HIGHB where 1.33 V was used for the Zn potential.

In general, Figures IV-11 to IV-18 show similar patterns. For example, cell HIGHD, Figure IV-12, shows a decline in charge and discharge time that corresponds to the decrease in capacity shown in Figure IV-1. At cycle 66 the capacity was higher than at cycle 4, and this shows as longer charge and discharge in Figure IV-12.

For all of the cells the discharge was limited by the nickel-oxide electrode not the Zn electrode. Its overpotential, seen as a deviation from the open circuit voltage, increases rapidly at the end of discharge, bringing the cell voltage to the 1.1 volt cutoff, unless the 1.35-Ah limit was reached first. For cell HIGHD the zinc electrode-potential shows unexplained dips near the end of discharge.

The nickel-oxide electrode's apparent loss in capacity, as cycling continues, is consistent with the idea that the zinc redistribution causes the loss in capacity. It has been proposed that less of the nickel-oxide electrode can be fully charged or discharged by the reduced-area Zn electrode. Upon discharge, the limited area supports the full discharge current, discharging the nickel-oxide electrode in less time than the full electrodes would be. Because of zinc's high exchange current density and the excess active material there is no noticeable increase in the Zn electrode overpotential.

At cycle 4 of cell HIGHD, the nickel-oxide electrode does not show a steep rise in overpotential at the end of discharge. This is because cell HIGHD was being cycled in series with cell HIGHB. In Figure IV-11 it can be seen that cell HIGHB's voltage reached the cutoff first. Cell HIGHB's voltage dropped below 1.1 volts prior to the end of discharge because the computer checks the voltage limits no more frequently than every 15 seconds.

Usually near the end of charge, the cell potential rises more steeply than in the middle of charging. This occurs because of the depletion of chargeable species in one electrode or the other. Generally the nickel-oxide electrodes became depleted in $Ni(OH)_2$ since these electrodes together contain only 1/3 as much active material as the zinc electrode. As the nickel-oxide electrodes become depleted, the overpotential rises until the next electrochemical reaction occurs. Near the end of charge the potential rises sufficiently for oxygen production to begin, causing a loss in coulombic efficiency. This inefficiency is compensated for by overcharging by about 4%.

The zinc electrode can also become depleted in chargeable material even though three times the necessary zinc material is present initially. This occurs, as explained in Chapter III, Section 1, because the zinc electrode charges more efficiently, eventually leading to depletion of ZnO. The depletion of zinc ($Zn(OH)_4^{=}$) in solution causes a higher overpotential (or a more negative electrode potential) sufficient to produce hydrogen at whatever rate is required by the current. It is not desirable to operate a cell in this condition because it has been reported that dendrite growth occurs at elevated overpotentials.[9] The

procedure used to prevent continued cell cycling under these conditions is explained in Chapter III, Section 1. It will be shown in the following section that the observed rise in overpotential of the zinc electrode probably does not occur with total depletion of the ZnO for some of the electrolytes tested.

A steep increase in overpotential is shown in Figure IV-16 for cell KFG cycles 110 and 128. Such a sharp rise in overpotential indicates total depletion of ZnO. The charge was limited in each of these cases by a 2.15 volt limit on the cell potential. The fact that the Zn electrode in cell KFG was limiting the amount of charge and the nickel electrodes in cell KFF were limiting the discharge reduced the capacity. The reduced cell capacity is reflected in the capacity versus area loss data in Table IV-5 where it is shown that the percent capacity loss exceeded the percent loss of area for the fluoride-containing electrolyte. The erratic nature of the capacity versus cycle number curve of Figure IV-2 was probably due to slight changes in charging efficiency with time that altered the relative state of charge of the Zn electrode of cell KFG and the nickel electrodes of cell KFF.

Cell KFF did not have such high charge overpotential, and in fact this cell appears to have had large overpotentials on the zinc electrode during discharge, indicating insufficient zinc metal was available. It is unknown how this apparent disparity in the state of charge of Zn electrodes KFG and KFF occurred, considering that they were cycled in series the entire time.

The interesting aspect of the high overpotential during charging of cell KFG is the lack of dendrite penetration through the separator. As noted in Section 2, the separator contained only one very small dark spot which may have been zinc.

Cells B03J and B03H show similar rises in charge overpotential though not as severe. In these cells the ZnO reserve could not be restored because the cell potential reached 0.0 volts shortly after reaching 1.1 volts due to a rapid rise of the zinc electrode overpotential indicating the zinc metal had been depleted. The possible existence of passivated or isolated zinc metal in these electrodes is discussed in the following section.

While the overpotential during charge of these two electrodes could not be avoided, no dendrite penetration was observed through the face of the separator, and the cell capacity was not reduced. In addition, the cell capacity was not reduced by high overpotentials on the zinc electrode during discharge of any of the eight cells. If passivated, isolated or densified zinc did exist, then it did not interfere in any way with the ability to charge or discharge any of the cells.

The least penetration of the separator was noted for the fluoride-containing electrolyte and the borate-containing electrolyte. The 3.5M OH^- electrolyte showed some penetration, and the maximum penetration was displayed by the cells which shorted, those containing the standard 7.4M OH^-. This same progression is observed in a listing of the average charge current densities near the end of each test shown in Table IV-8. The higher the current density, the greater the degree of penetration.

The higher average charge current density, coupled with the lower porosity and the probable decrease in available surface area, may lead to sufficiently high local current densities to increase dendrite growth rates. The observed zinc electrode overpotentials do not, however, correlate with the overpotentials observed to accompany zinc dendrite growth in alkaline electrolyte. Dendrite growth rates have been shown to occur at overpotentials greater than 75mV in 10% KOH electrolyte from low zincate concentrations to those nearly saturated with ZnO.[9]

Overpotentials of 60-70mV were observed during cycles prior to shorting but not during cycles where gross shorting was occurring. The 3.5 M OH^- electrolyte cells had overpotentials of 10mV, but some penetration of the separator was observed, whereas the fluoride and borate cells had >100mV overpotentials, at times, with no penetration.

Table IV-8
Average Charge Current Density at Completion of Cycling

Electrode	Average current density (mA/cm^2)
HIGHB	5.4
LOWE	4.2
BO3J	3.0
KFG	3.2

Projecting Diggle, Despic, and Bockris's[9] observed linear relationship between current density and zincate concentration at a 100mV overpotential, a saturated zincate concentration in a 7.4M OH^- electrolyte gives a current density of ~100 mA/cm^2. The average current densities

shown in Table IV-8 are considerably lower than this.* If zincate depletion were occurring in the electrolyte in the Zn electrode, the linear relationship indicates dendrite growth could occur at much lower current densities. But as noted, the cells that had penetration did not have overpotentials greater than 75mV, which has been determined to be the minimum overpotential for dendrite growth.

In conclusion, while the average current densities for the various cells may suggest a correlation with separator penetration, the observed Zn electrode overpotentials do not correlate with the penetration. The precise reason for penetration or absence of penetration in these eight cells cannot be explained. The absence of penetration in cells with the fluoride- and borate-containing electrolytes does make them attractive despite their reduced cell capacity and reduced capacity-retention-to-area-retention ratio.

5. Mass Balance, State of Charge and Electrochemically-Inactive Zinc

The quantity of passivated or isolated zinc was determined in the tab-containing half of the vertically bisected electrode using the method presented in Chapter III, Section 6. For some of the electrodes, air was present in the sealed system. Because the moles of gas in the measuring system decreased in several cases, indicating that the oxygen was reacting with the electrode, the air was purged from the system for the last four measurements. The measurements in the presence of air

* The current density on the Zn electrode is expected to be much lower than the average current density because of the high porosity and high surface area of the Zn electrode.

could be in error, since the oxygen could react with the zinc and hydrogen could be produced, giving a net increase or decrease in moles of gas. Where negative net gas quantities were measured, the quantity of zinc was calculated by assuming the lost gas was oxygen reacting with the zinc. The results are shown in Table IV-9 with those measurements made in air so indicated.

Table IV-9

Quantity of Electrochemically Inactive Zinc

Cell	Zinc (mg)
HIGHB	22[a,b]
HIGHD	42[a,b]
LOWA	2[a,c]
LOWE	3[a,c]
KFF	3±3[c]
KFG	0±3[c]
BO3H	13±3[c]
BO3J	42±3[c]

a) air in system, possible loss of gas volume by $Zn + 1/2\ O_2 = ZnO$; possible increase in gas volume by $Zn + 2H^+ = Zn^{2+} + H_2$
b) loss of gas; Zn calculated by assuming $Zn + 1/2\ O_2 = ZnO$
c) Zn calculated by $Zn + 2H^+ = H_2 + Zn^{2+}$

These quantities of zinc are small (<2%) compared to the initial 2.5g of zinc in the electrode half. It seems unlikely that the electrodes dissolved in the presence of air contained significant quantities of zinc, since the electrodes dissolved in the absence of oxygen contained so little zinc.

It can be concluded with some confidence that the electrodes cycled in the fluoride and borate electrolyte contained essentially no passivated or isolated zinc. The only qualifier on the conclusion for the fluoride- and borate-containing electrolytes is that the state of

passivation could have been altered by several days of storage in the electrolyte after the end of cycling. It is likely that the electrodes cycled in 7.4 M OH^- and 3.5 M OH^- electrolytes contained little passivated or isolated Zn either. Any error from uneven distribution of passivated zinc is also insignificant. An error as large as a factor of 2 would still result in an insignificant amount of electrochemically-inactive zinc.

Determining the state of charge can shed light on reasons for the observed electrode potentials. If the Zn were nearly depleted at the end of discharge then one would expect rising overpotentials at the end of discharge. If the ZnO were nearly depleted then one would expect rising overpotentials near the end of charge. These rising overpotentials at the end of charge were observed, and it would be useful to know the state of charge where the high overpotentials were observed. Zinc oxide loss from zinc electrodes has also been observed,[10] and it is of interest to know how much zinc was lost from the electrodes in these experiments.

Initially the electrodes were washed in a Buchner funnel. This caused an irrecoverable loss of material so electrodes HIGHD, KFF, KFG, B03J, and B03H were washed by allowing them to soak for roughly 6-8 hours in deionized water. The water was changed every few hours.

Table IV-10 shows the masses of the current collector, lead plate, initial electrode, final electrode halves, and the non-zinc material in each electrode half. There were losses of some PTFE and Pb from those electrodes washed in the Buchner funnel that would amount to at most an

error of 60 mg of non-zinc material from the total electrode. Table IV-11 contains all of the pertinent information regarding the mass balance of the four electrodes examined in the discharged state and Table IV-12 contains the charge-balance data. The post-test treatment of each of these electrodes is diagrammed in Figures III-1 and III-2. The zinc was considered to be in the form of ZnO following the discharge in excess electrolyte, washing and drying. This is not contradicted by the measurements of electrochemically-inactive zinc in the electrode.

Table IV-10

Mass of Electrode Components and Final Electrode Mass

Electrode	screen & tab[a] mass (g)	collector[b] mass after Pb plate (g)	initial electrode mass (g)	final mass[c] of tab half (g)	final mass[c] of non-tab half (g)	mass of[d] non-zinc portion of tab half (g)	mass of[d] non-zinc portion of non-tab half (g)
LOWA	2.106	2.514	9.126	4.125	2.672	2.20±0.05	0.71±0.05
HIGHD	2.102	2.363	8.870	4.584	2.679	2.10±0.05	0.64±0.05
KFF	2.126	2.676	9.178	4.626	3.596	2.31±0.05	0.76±0.05
B03H	2.114	2.484	8.972	4.725	3.163	2.17±0.05	0.69±0.05
LOWE	2.104	2.485	8.852	3.192	2.736	2.17±0.05	0.67±0.05
HIGHB	2.117	2.438	8.908	3.593	2.982	2.15±0.05	0.67±0.05
KFG	2.105	2.417	9.034	2.970	2.810	2.14±0.05	0.67±0.05
B03J	2.105	2.630	9.225	2.997	2.763	2.27±0.05	0.75±0.05

a) Screen mass 0.716±0.008g and tab mass 1.393±0.017g.
b) Surface area of screen ~3/4 of total and tab ~1/4 of total, even plating assumed.
c) Procedures used to prepare electrodes are described in Chapter 3, Section 6. The electrodes were bisected vertically into two equal halves within ±1/2mm.
d) Material lost from the electrode is assumed to be ZnO so all of the original current collector, Pb, PbO, and PTFE are shown in this column with PbO assumed to be Pb. The error is due to variation in the tab, screen, and Pb plate mass.

Table IV-11

Mass Balance for Discharged Electrodes

Electrode	Initial Zn metal basis	Final Zn and ZnO[a]	Final Zn[b] metal basis	Lost Zn metal basis
LOWA	4.993g 4.10Ah	3.89g	3.13g	1.86g
HIGHD	4.914g 4.03Ah	4.52g	3.63g	1.28g
KFF	4.910g 4.03Ah	5.15g	4.14g	0.77g
BO3H	4.900g 4.02Ah	5.05g	4.06g	0.84g

a) Pb, PTFE and current collector subtracted from final dry electrode mass.
b) Assuming mass in preceding column is 100% ZnO.

Table IV-12

Charge Balance for Discharged Electrodes

Electrode	Ah of Zn[a] in final electrode	Ah discharged on last cycle to 0.0V	Ah discharged after separator removed	Ah final cell capacity	Ah ZnO[b] in cell at full charge	Ah Zn[c] in cell at discharge
LOWA	2.57	1.37	0.019	0.84	>1.18	0.55
HIGHD	2.98	1.15	-	0.73	-	-
KFF	3.40	1.31	0.073	0.93	2.01	0.45
BO3H	3.33	1.56	0.017	1.0	1.75	0.58

a) From Table IV-11.
b) Ah Zn in final electrode minus Ah discharged on last cycle minus Ah discharged after separator removed.
c) Ah discharged on last cycle plus Ah discharged after separator removed minus Ah final cell capacity.

The cell LOWA electrode, after the final charge, contained about 1.39 Ah of metallic Zn, and the final capacity was 0.84 Ah which indicates the cell was being cycled between 1.39 Ah of Zn and 0.55 Ah of Zn. This fits well with the electrode potentials shown in Figure IV-13. The zinc electrode did not show any rise in overpotential on charge as would be expected if only 1.39 Ah of total Zn were present as metal in the electrode. At the end of discharge the 0.55 Ah of zinc present was apparently sufficient to prevent elevated overpotentials. The mass balance is poor, however. A loss of 1.86 g of zinc probably indicates how poor the washing procedure was more than any thing else.

Cell HIGHD is believed to have shorted so the state of charge during normal cycling cannot be determined. The mass balance is better; a loss of 1.28 g was determined. There was probably some mechanical loss due to the fragility of discharged electrodes. When attempting to discharge the zinc remaining in the electrode after removing the separator, the zinc electrode was accidentally shorted against the counter electrode for approximately 15 seconds. No additional zinc could be discharged so no value is reported in Table IV-12. This electrode has the highest quantity of electrochemically inactive zinc which may be due to the possibly high currents in the cell during shorting after cycle 118, causing passivation to occur.

Cell KFF contained 1.38 Ah of zinc at final charge and had a capacity of 0.93 Ah. The cell was thus cycled between 1.38 Ah and 0.45 Ah of zinc. This fits with the potential data shown in Figure IV-15. During charging the electrode showed no increase in overpotential as expected, and at the end of discharge the zinc electrode displayed a

sharp increase in overpotential indicating the 0.45 Ah of zinc was insufficient for good operation. The quantity electrochemically-inactive zinc was less than 3 mg, and the mass balance shows a loss of 0.77 g of Zn which is probably quite accurate because the washing method did not cause loss of material.

Cell BO3H contained 1.58 Ah of zinc metal at full charge with a final capacity of 1.0 Ah. A slight increase in overpotential at the end of discharge is shown in Figure IV-17 with a zinc content of 0.58 Ah, indicating this quantity of metal was insufficient. During the charge there was a definite increase in overpotential starting an hour before the end of charge. The charge balance indicates at least 1.75 Ah of ZnO should have been present in the zinc electrode at full charge. The overpotential may indicate a slow ZnO dissolution rate. Approximately 0.84 g of Zn was lost from the electrode, which is similar to that for cell KFF.

Table IV-13 contains data for each half of the electrodes removed from the cell in the charged state. For the electrode half dried and weighed in the charged state, the active mass is shown. For the electrode half discharged and then dried and weighed, the amount of discharge and the active-material mass are shown. The post-cycling procedures are described in Chapter III Section 6. Table IV-10 contains the raw data from which the active-material masses shown in Table IV-13 were derived.

For the discharged half of electrodes KFG and B03J, the Ah discharged correspond to a larger mass of zinc than was found in the electrode half after washing and drying. This loss of zinc (oxide) into the electrolyte was anticipated. (The X-ray images of redistribution were taken prior to discharging for this reason). The quantity of zinc in the electrolyte after discharging the electrode half was not determined. A similar type of material loss from the discharged half of electrodes LOWE and HIGHB is likely.

Table IV-13

Mass and Discharge Data for Charged Electrodes

Electrode half	Initial Zn	Final[a] Zn and ZnO	Zn discharged to 0.0V
LOWE[b]	2.404g 1.97Ah	2.07g	-
HIGHB[b]	2.443 2.00Ah	2.31g	-
KFG[b]	2.499g 2.05Ah	2.14g	-
BO3J[b]	2.490g 2.04Ah	2.01g	-
LOWE[c]	2.404g 1.97Ah	1.02g	0.547Ah 0.667g
HIGHB[c]	2.443g 2.00Ah	1.44g	0.109Ah 0.133g
KFG[c]	2.499g 2.05Ah	0.83g	1.445Ah 1.762g
BO3J[c]	2.490g 2.04Ah	0.73g	1.09Ah 1.329g

a) Pb, PTFE and current collector subtracted from final dry electrode mass.
b) Washed, dried and weighed in the charged state.
c) Discharged, dried and weighed.

The maximum amount of zinc (on a metal basis) that can be accounted for in these four electrodes is the sum of the discharged zinc and the active material in the undischarged half. Assuming the active material in the undischarged half is 100% Zn, a quantity of unaccounted-for zinc can be calculated and is shown in Table IV-14. Part of the unaccounted-for zinc would be the zinc initially in the form of ZnO in the discharged half of the electrode. The other part of unaccounted-for zinc is that lost from the zinc electrode during cycling. There may be less zinc in the undischarged half than assumed because the assumption

was made that the undischarged half was 100% Zn. The data presented in Table IV-14 is therefore a minimum value of unaccounted-for zinc.

Table IV-14 does not contain any useful information for electrodes LOWE and HIGHB. For electrodes KFG and B03J, some speculation is in order. Cell KFG showed a sharp rise in Zn electrode overpotential near the end of charge which indicates very little ZnO should have been left in the electrode. 1.10 grams of Zn are unaccounted-for; this is larger than the 0.77 gram lost from electrode KFF. Electrode KFG was in the charged state; mechanically, charged electrodes are much stronger. Material losses from handling electrode KFG should have been less than for electrode KFF. This seems to indicate that a few tenths of a gram of ZnO were still present in electrode KFG at the end of charge.

Cell B03J also had a rising zinc electrode overpotential near the end of charge. 1.64 grams of zinc are unaccounted-for. Such a large loss of zinc from the electrode is unlikely. Some ZnO probably remained in the electrode at the end of charge. Electrode B03H did have 1.7 Ah of ZnO at the end of charge and a 100 mV overpotential. This compares to a 130 mV overpotential for electrode B03J.

Only 0.547 Ah of zinc was discharged from half of electrode LOWE so a substantial amount of ZnO was probably present at full charge. A fair portion of the 2.07g of unaccounted-for zinc is probably unmeasured ZnO in the discharged half of the electrode.

Electrode HIGHB had very little Zn metal when half of the electrode was discharged. This cell had shorted so its state of charge was unknown but expected to be higher than the 0.11 Ah shown. Electrode HIGHB remained in the electrolyte for about 10 days with a less-than-perfect nitrogen blanket. The electrode apparently corroded significantly during this time.

Table IV-14

Minimum Unaccounted-for Zinc in Charged Electrodes[a]

Electrode	Zinc[b](g)
LOWE	2.07
HIGHB	2.44
KFG	1.10
BO3J	1.64

a) The maximum accountable zinc is the Ah of zinc discharged in one half of the electrode plus the mass of active material in the charged half of the electrode (assuming 100% Zn).

b) This quantity was present in the discharged half of the electrode as ZnO or was lost from the Zn electrode during cycling.

In Table IV-15 the estimated quantity of zinc and zinc oxide in each electrode are compared to the observed overpotentials at the end of discharge and charge, respectively. From this table, an idea of the relation between the quantity of ZnO at the end of charge and the overpotential on the Zn electrode at the end of charge can be obtained. Apparently a cell in the borate-containing electrolyte with 1.7 Ah of ZnO can have a substantial rise in Zn electrode overpotential at the end of charge. This rise in overpotential had been taken as an indication of depletion of ZnO, which is apparently not so. Cell KFG, with a 290 mV

rise in overpotential, may have had a few tenths of an Ah of ZnO and cell BO3J may have had a bit more ZnO based on the data shown in Table IV-14.

Electrodes KFG, BO3H and BO3J appear to have significant rises in discharge overpotential, but the electrodes apparently contained sufficient Zn metal at the end of discharge to allow complete discharge of the nickel-oxide electrodes.* Cell LOWA had no rise in discharge overpotential and 0.55 Ah of Zn metal at the end of discharge. Despite the rise in discharge overpotential, electrodes KFF, KFG, BO3H, and BO3J could be fully discharged to a cell potential of 0.0 V at the 10-hour rate, and no significant inactive zinc appeared to be present in the electrodes.

Table IV-15
Comparison of Zn Electrode Overpotentials
to Zn and ZnO Reserves

electrode	ZnO at end of charge, Ah	Zn overpotential at end of charge, mV	Zn at end of discharge, Ah	Zn overpotential at end of discharge, mV
LOWA	>1.2	<10	0.55	<10
LOWE	unknown	<10	unknown	<10
KFF	2.01	<10	0.45	150
KFG	unknown	290	unknown	80
BO3H	1.75	100	0.58	100
BO3J	unknown	130	unknown	100

* It has already been argued that electrode KFG and BO3J are mostly Zn at the end of charge, so at the end of discharge 1-2 Ah of Zn metal must remain.

In conclusion, at these charge rates, rises in overpotential indicative of soluble zinc depletion appear to occur even when 1.7 Ah of ZnO are present in Zn electrodes cycled in a K_3BO_3-Li_3BO_3 electrolyte. At the 2.5-hour discharge rate the zinc electrode appears to develop large overpotentials near the end of discharge for some electrolytes even when 1-2 Ah of Zn metal are present. The Zn metal is not inactive however, and can be discharged at the 10-hour rate.

The quantity of zinc in the electrolyte does not appear to be sufficient to account for the 0.75-1.25 g loss of zinc from the electrodes. The quantity of zinc in the electrolyte initially added to the cells is summarized in Table IV-16. These values are computed from the data in Tables IV-2 and IV-4. From the electrolyte samples obtained at the end of a discharge, the zinc in the electrolyte at the end of cycle life can be estimated. The data shown in Table IV-3 indicates the electrolyte was not significantly supersaturated. Only the electrolyte in the pores of the Zn electrode could be supersaturated.

Table IV-16
Quantity of Zinc in the Electrolyte
Initially Added to Cells

Cell	Zn (g)
LOWA	0.16
LOWE	0.15
HIGHB	0.46
HIGHD	0.44
KFF	0.11
KFG	0.11
BO3H	0.13
BO3J	0.13

Assuming a porosity of 76% in the electrode, as a worst-case analysis, 2.6 mL of electrolyte were in the Zn electrode. Using the supersaturated concentrations measured by Dirkse[3] of 10% for the 7.4M OH^- electrolyte and 5% for the 3.5M OH^- electrolyte, a possible Zn content can be estimated. For the 7.4M OH^- electrolyte this is 0.3 to 0.4 g, and 0.15 to 0.2 g for the 3.5M OH^- electrolytes. This is only a small part (25%) of the missing zinc and applies of course only to the four electrodes examined in the discharged state. It has been observed that zinc accumulates in Ni electrodes.[10] This may be where the 0.75-1.25 g of Zn has gone.

6. Morphological Studies Using SEM and Microanalysis Techniques

The morphology and structure of a porous battery electrode should be maintained such that the current density remains low and sufficient electrolyte is adjacent to the active material. The current density must remain low to prevent large overpotentials. As noted in Chapter I, Section 1, densification of the zinc has been observed and is suspected of reducing the ability of the zinc electrode to accept charge because of the low surface area.

To determine whether densified zinc was present or whether significant morphological changes had occurred, samples of the charged and discharged electrodes were examined using Scanning Electron Microscopy (SEM). Equipment and sample preparation procedures are described in Chapter III, Section 7. Densified zinc would be expected, because of its low surface area, to discharge less rapidly than porous zinc or to even passivate because of higher local current density and possible

electrolyte-starved conditions. If the densified zinc is not passivated and can be discharged in the excess electrolyte then this so-called densified zinc is totally functional and would not pose a problem in cell cycling. However, others have reported its existence and suspect that it is inactive and restricts the ability of the zinc electrode to be charged or discharged. If this densified zinc does then exist it should be found in the discharged electrodes. But based on the experiments presented in the previous section, the amount of zinc remaining as passivated, isolated, or densified is very small, in all cases less than 2%.

In addition to the attempt to observe densified zinc, the morphology of the charged electrodes was examined using the high-resolution SEM (see Section III-7) to determine whether the various electrolytes would cause a change in the structure of charged zinc. The elemental distribution in the electrodes was examined; however, due to the nature of the electrode topography and electrical characteristics, quantitative results were not obtainable using X-ray microanalysis. Meaningful results could not be obtained using Scanning Auger Microscopy (SAM) because the samples charged. The results of these three examinations are presented below.

6A. Morphological Comparison of Charged Electrodes in Various Electrolytes

The following SEM photographs were obtained using the high resolution ISI SEM (see Section III-7 for a description of the SEM equipment). The electrodes disassembled in the charged condition were LOWE, KFG and

B03J, but no photographs of charged electrodes from the standard 30% KOH-1% LiOH electrolyte were obtained since both cells HIGHB and HIGHD shorted. SEM micrographs of an electrode cycled in a similar electrolyte and appearing to contain zinc metal are shown in the following section, in which a comparison of zinc metal and zinc oxide morphology is made.

Electrode LOWE was examined in two locations on the electrode face. Figure IV-19a shows an unusual structure, and Figure IV-19b shows a more typical structure on the electrode 0.8mm away from the first area. The material shown in Figure IV-19a will be referred to as the compact structure, for obvious reasons. The porosity of this structure is very much less than the typical electrode material. The open area shown is a crack in the compact structure. Visually, the compact area had a dark grey appearance, similar to a finely divided metal, and a vitreous luster when wet, probably owing to its lack of large pore structure. It was most likely composed largely (if not entirely) of zinc metal judging by the color.

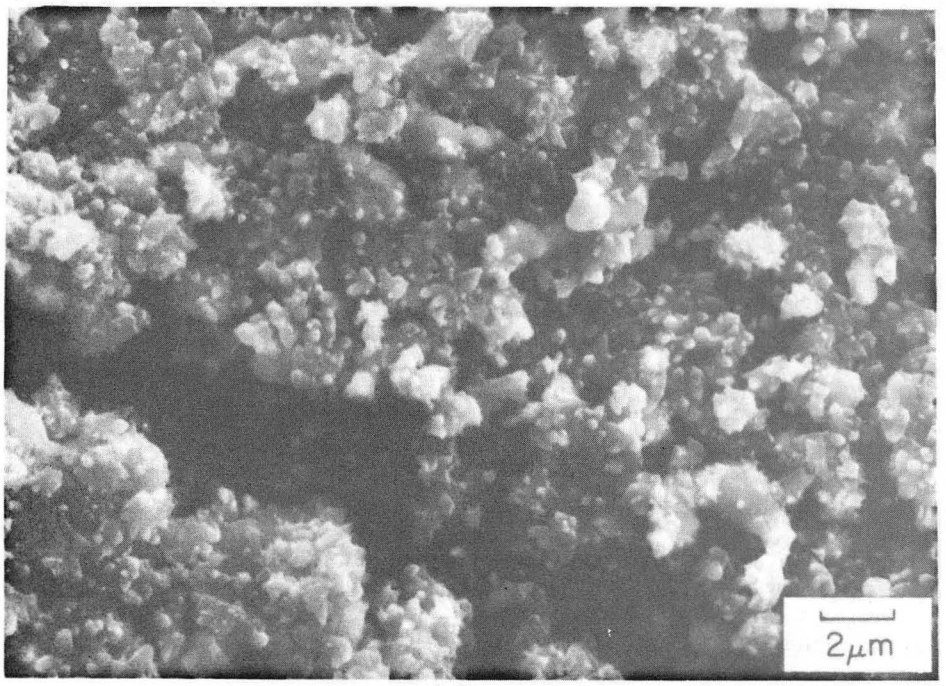

(a)

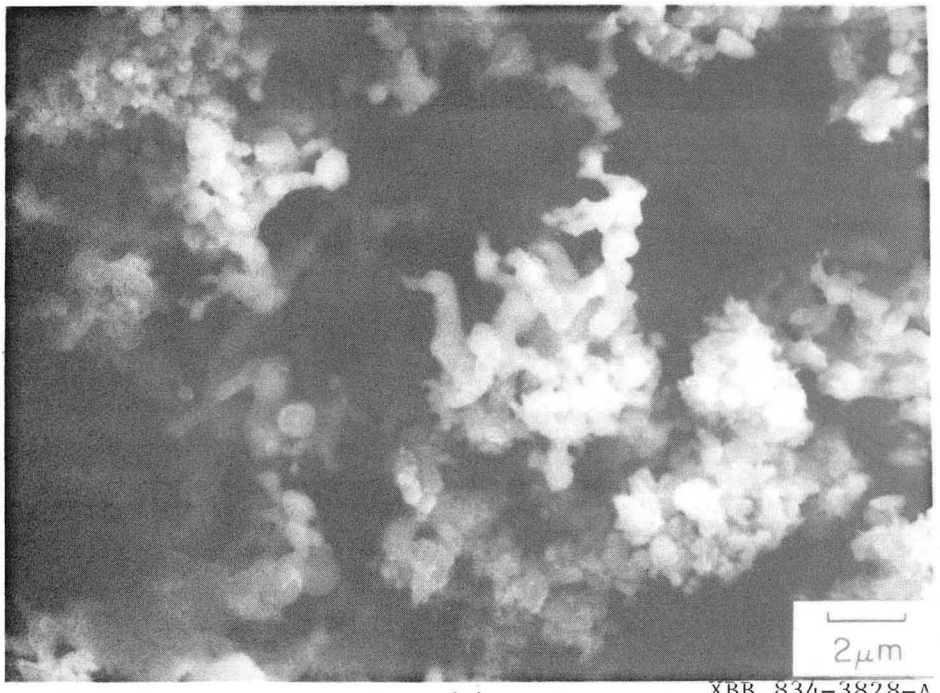

(b)

XBB 834-3828-A

Figure IV-19. Comparison of Morphology of Charged Electrode LOWE. Cycled in 14.4% KOH-1.1% LiOH electrolyte for 124 cycles between two NiOOH counter electrodes at an initial charge current density of 2.6 mA/cm^2. a) The location on the electrode is 0.8 mm below the location shown at the center of Figure IV-20. b) The location is shown at the center of Figure IV-20.

Figure IV-20 shows a portion of the compact area in a photograph centered on the area shown in Figure IV-19b. A portion of the compact area toward the right of center broke away when this face of the electrode was placed under tension. It can be seen that the compact area is not very thick; it does, however, coincide with the location of some of the most dense areas of the electrode as identified by X-rays as shown in Figure IV-4. The location is 38.0mm from the tab side of the electrode and 16.5mm from the top.

Densified zinc is characterized as non-porous having a metallic luster and does not describe the compact material observed here. The effect of this compact material on the operation of the cell is not known. The compact material did oxidize when the electrode was discharged in excess electrolyte, and the zinc electrode did not show any rise in overpotential during charge and essentially no rise in overpotential during discharge.

The face of the cell KFG zinc electrode contained no unusual features and in fact was extremely uniform in appearance. Figure IV-21 shows the SEM micrograph obtained of this electrode. The resolution is comparable to that of the other photographs at this magnification, but unlike electrode LOWE, a fine structure of 0.1μm particles either covers or makes up the larger 0.5μm structure, so the features appear less distinct.

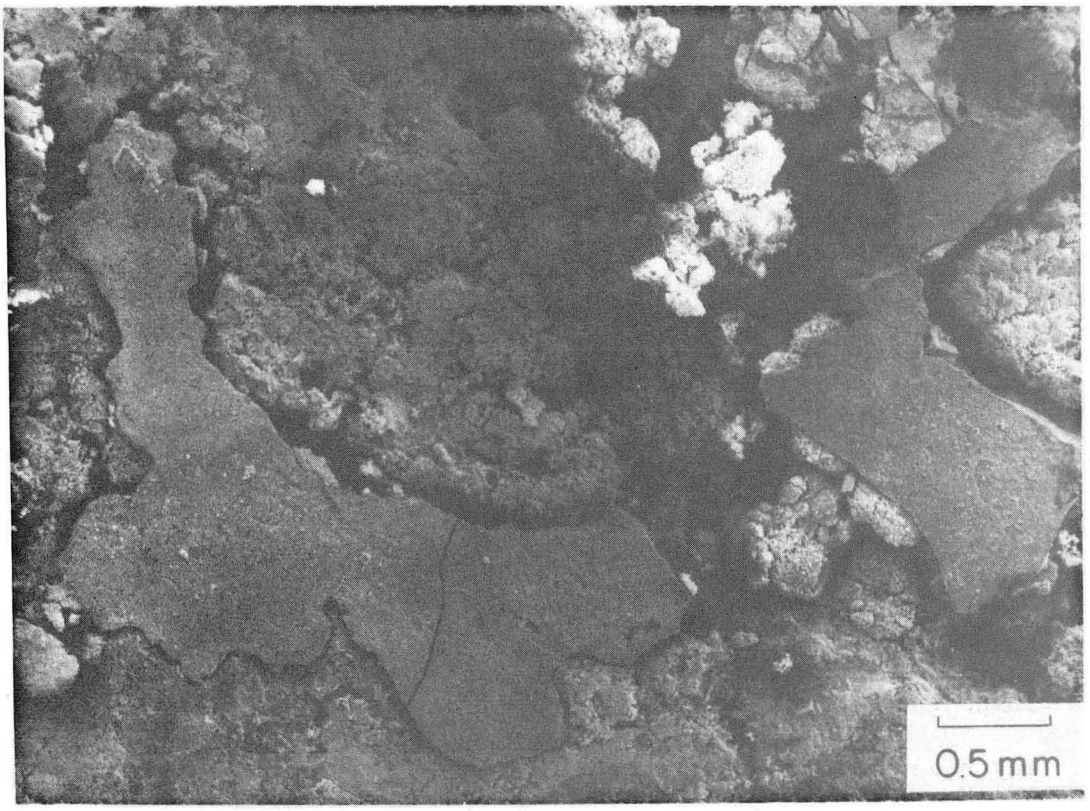

XBB 834-3829-A

Figure IV-20. Low Magnification SEM of Compact Area on Electrode LOWE. The electrode was cycled in 14.4% KOH-1.1% LiOH electrolyte for 124 cycles between two NiOOH counter electrodes. Upper right of photograph is toward the electrode top and the upper left is toward the tab side of the electrode.

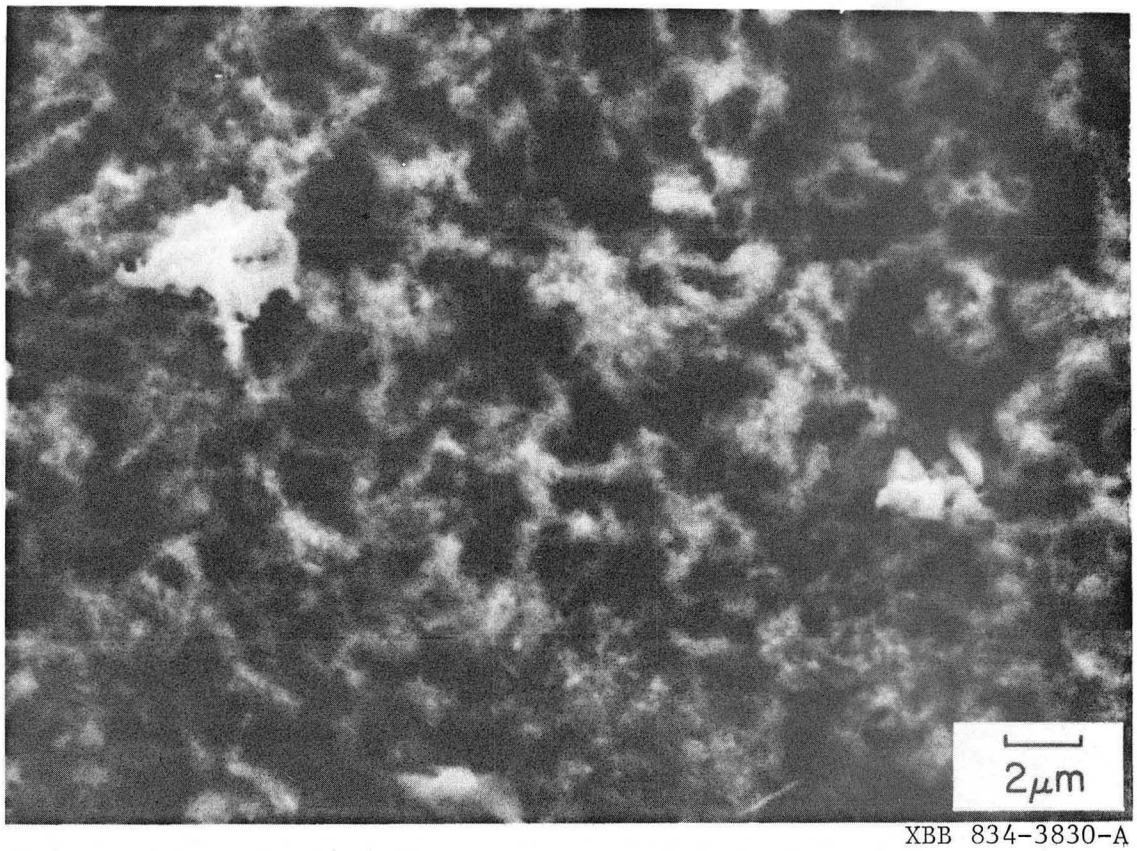

XBB 834-3830-A

Figure IV-21. Morphology of Charged Electrode KFG. The electrode was cycled in a 15.3% KOH-15.0% KF electrolyte for 130 cycles between two NiOOH counter electrodes at an initial current density of 2.6 mA/cm^2. The location on the electrode is 7 mm from the top edge and 49 mm from the tab side of the electrode.

The resolution of these SEM photographs is far below the capability of the machine. This SEM has good resolution to magnifications of 10^5; however, such resolution is achievable only in the absence of nonconducting materials in the chamber.[11] Teflon present in the electrodes appeared to charge or electrically isolate fractured portions of the electrode allowing them to charge, making it impossible to obtain high-resolution pictures of these electrodes. The charging on the discharged electrodes stripped of ZnO was so severe that pictures could be obtained only of electrode B03H (see Section 6c), even with a vapor deposited conductive carbon layer. The carbon coating was apparently ineffective at conducting away the charge because a continuous layer would not be deposited on the irregular topography. Gold-sputtered coatings appeared to be more effective on some samples not shown here. It is recommended that small (<0.5mm) samples be used to reduce isolation of fragments and that gold-sputtered layers be applied to obtain the best possible resolution.

Two micrographs of electrode B03J are shown in Figure IV-22a and b. Figure IV-22a shows a structure similar to that for cell KFG, a larger structure covered or composed of a finer-grain material. The second location in electrode B03J has a structure very similar to that seen in electrode LOWE.

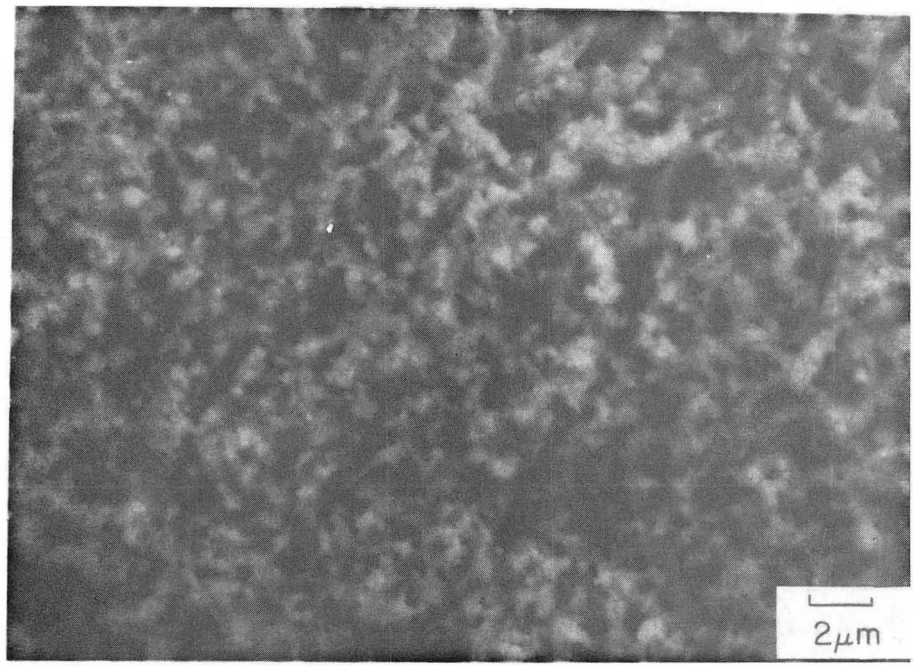

(a)

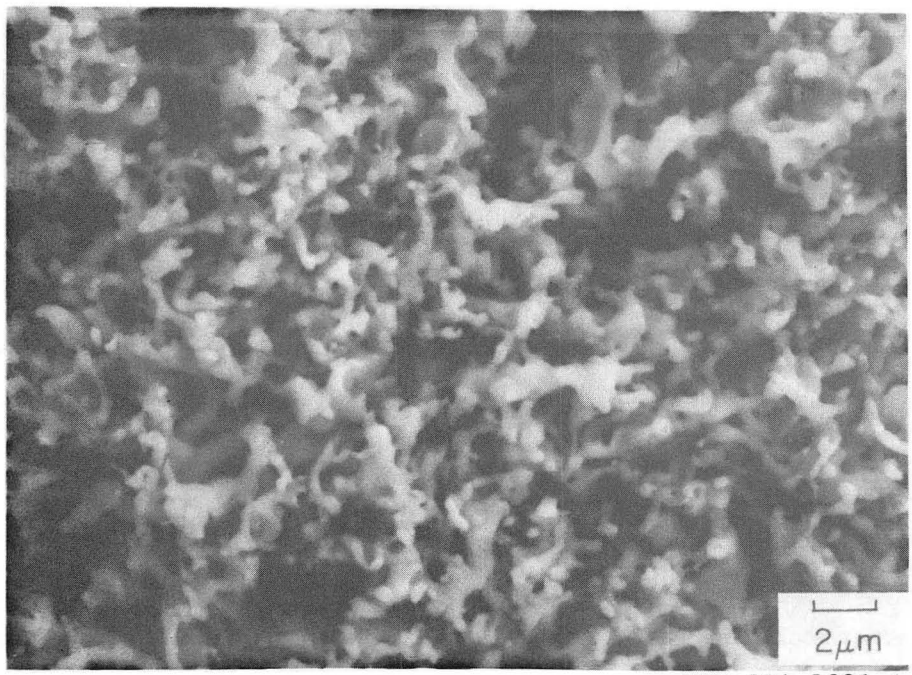

(b)

XBB 834-3831-A

Figure IV-22. Morphology of Charged Electrode B03J. The electrode was cycled in a 21.5% K_3BO_3-1.1% Li_3BO_3 electrolyte for 125 cycles between two NiOOH counter electrodes at an initial current density of 2.6 mA/cm^2. The locations on the electrode are a) 4 mm from the top edge and 36 mm from the tab side and b) 4 mm from the top edge and 35 mm from the tab side.

The basic structure of electrodes KFG, B03J and LOWE appear to be very similar with the exception of the compact areas of electrode LOWE. The basic structure is a network of approximately 0.5μm material. The electrodes cover a wide range of states of charge from ~1/3 zinc metal for electrode LOWE to greater than 75% zinc for electrode B03J to nearly 100% zinc for electrode KFG. In the following section, areas known to contain only Zn or only ZnO are shown, but in the pictures presented in this section it is difficult to distinguish ZnO from Zn. The darker material in the upper right of Figure IV-19b may be ZnO or PTFE. Electrodes B03J and KFG are largely zinc metal and look similar to the pictures of zinc metal shown in the next section. No areas obviously containing ZnO appear in micrographs of these two electrodes.

The micrograph of the porous portion of electrode LOWE (Figure IV-19b) contains particles with definite crystal faces; this is not observed in electrodes KFG and B03J. Cell LOWE was the only electrode exhibiting any degree of zinc penetration of the separator so these crystalline particles may be small dendrites, though this seems doubtful because the overpotentials were low and overpotentials for dendrite growth are >75 mV.[9] No large dendritic structures were observed in any of the many areas examined on electrode LOWE with either SEM. The fine structure of the B03J and KFG electrodes may be related to the higher overpotential these electrodes experienced near the end of charge.

In general the three electrodes had a very porous structure, none of it typical of what is commonly referred to as densified zinc. The micrographs presented here are not special or unusual structures, and are typical of other regions of the electrodes.

6B. Morphological Comparison of Zinc and Zinc Oxide

During the preliminary cell cycling experiments designed to test the cell, electrode construction, cell-cycling hardware and computer programs, several cells were tested and SEM micrographs were obtained. These micrographs were obtained by using the lower-magnification AMR SEM. Fortunately, due to good electrode conductivity, micrographs with good resolution were obtained up to 6k magnification.

The zinc oxide SEMs were obtained from a zinc electrode cycled in a 31% KOH-1% LiOH electrolyte for 55 cycles The cell was allowed to stand vented to the atmosphere for several months. During this time the zinc corroded and the current collector partially corroded. For the current collector to corrode, no protective metallic zinc could have been present, so it is likely that all of the zinc present was in an oxidized form. The general structure shown in Figure IV-23 does not resemble any of the micrographs shown above in Section A, though 0.3μm particles of ZnO may be embedded (and unobserved) in the structure. The Teflon particles are approximately the same size, but the particles in Figure IV-23 are certainly ZnO because the entire electrode appeared this way.

Another electrode was cycled 54 cycles in a similar electrolyte. The cell had shorted on cycle 52 but appeared to contain significant amounts of zinc metal. An area probably containing ZnO (based on the micrograph of Figure IV-23) is shown in Figure IV-24. Another area of the same electrode with a different structure is shown in Figure IV-25. If Figure IV-23 and IV-24 are ZnO-containing areas then Figure IV-25 must be either a different crystal structure or primarily zinc metal.

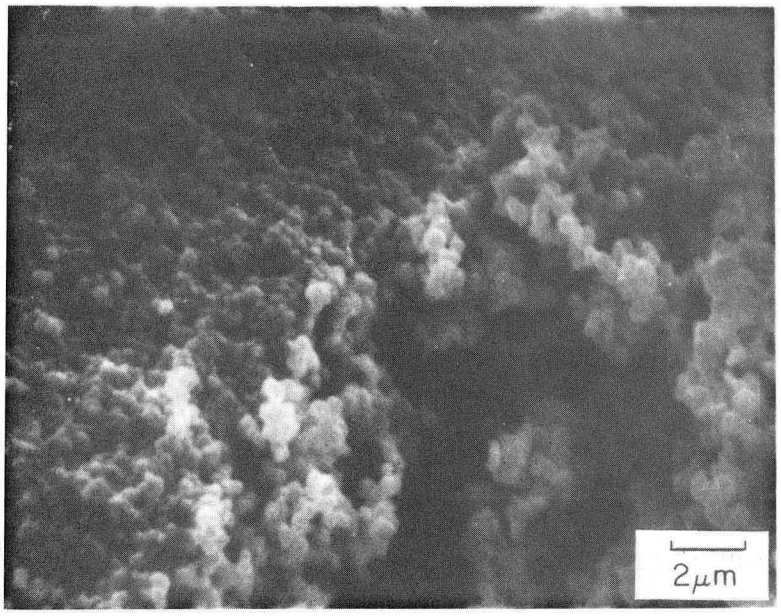

Figure IV-23. Morphology of Oxidized Zinc. Corrosion product of porous Zn electrode after 4 months in 31% KOH-1% LiOH electrolyte.

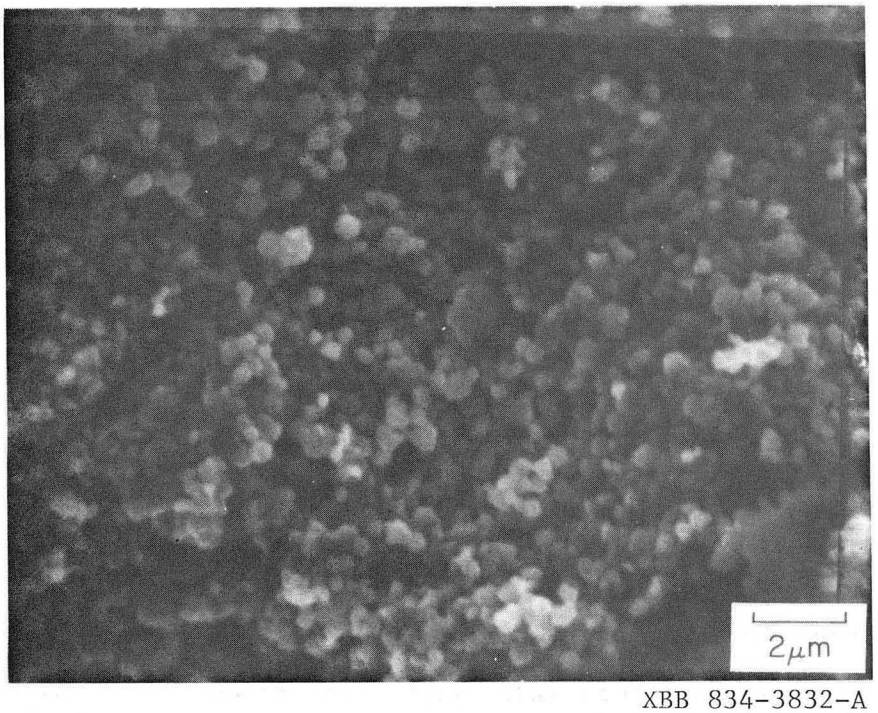

XBB 834-3832-A

Figure IV-24. Morphology of Partially-Charged Zn Electrode. Electrode after 55 cycles in 31% KOH-1% LiOH electrolyte shown in partially-charged state after internal shorting.

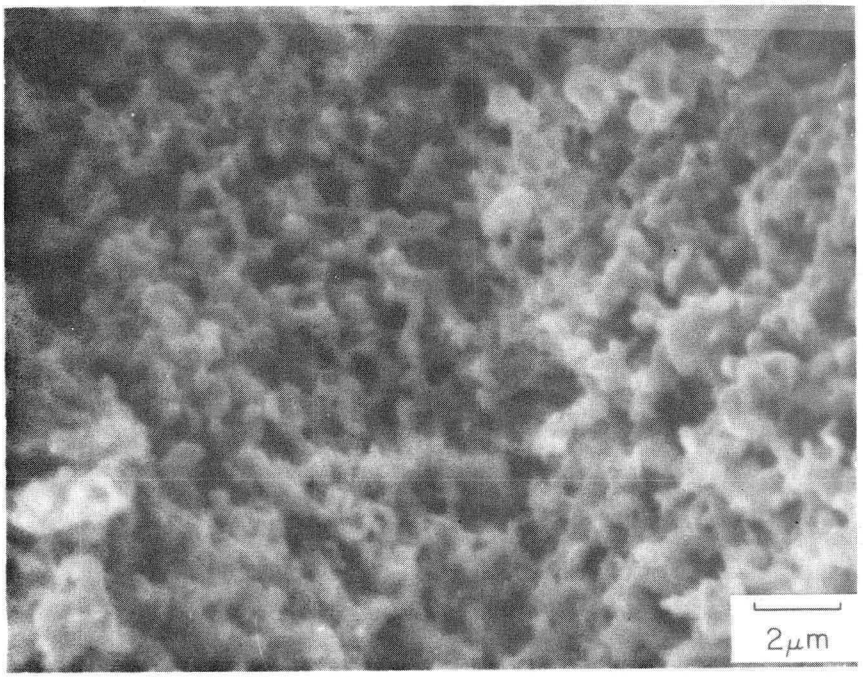

Figure IV-25. Morphology of Partially-Charged Zn Electrode. Electrode after 55 cycles in 31% KOH-1% LiOH electrolyte shown in charged state after internal shorting.

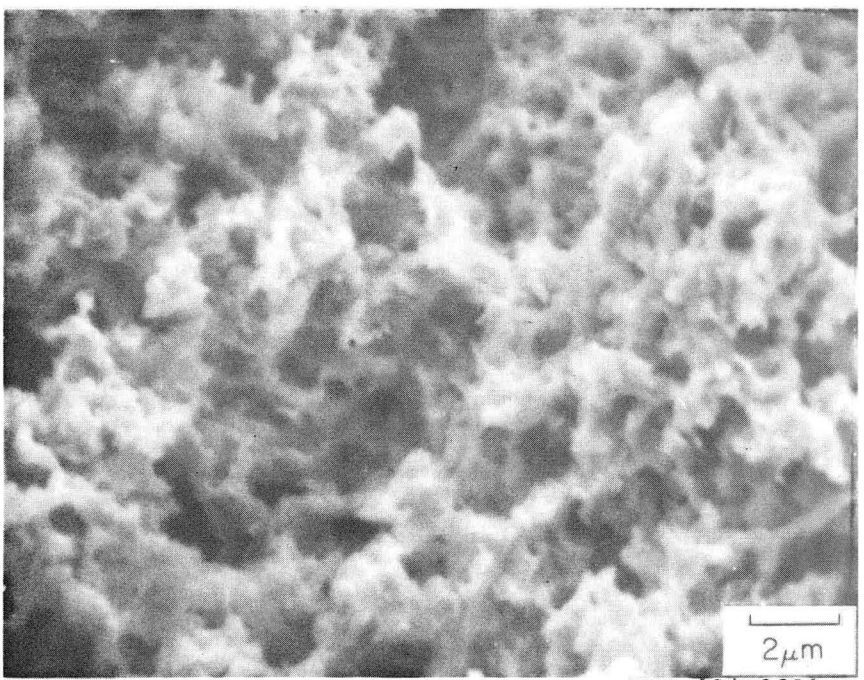

XBB 834-3833-A

Figure IV-26. Morphology of Zn Metal in Porous Zn Electrode. Electrode shown after oxidized Zn dissolved with 10M NH_4OH-1M NH_4Cl. Same Zn electrode as shown in Figures IV-24 and IV-25.

Using a method similar to that proposed by McBreen[12] the ZnO was dissolved in a 10M NH_4OH-1M NH_4Cl solution and the sample was then washed with water and methanol and vacuum dried. A SEM micrograph of the ZnO-free sample was then obtained and is shown in Figure IV-26. The zinc morphology is very similar to the structure shown in Figure IV-25 which must be mostly metallic zinc as well.

On the average, electrode LOWE was composed of 50% to 30% ZnO, and electrode B03J contained up to 25% ZnO. The micrographs of these electrodes appear similar to that of Figures IV-25 and IV-26, except for some areas of electrode LOWE as shown in Figure IV-19b. Apparently structures composed of mixtures of Zn metal and ZnO appear similar to structures composed mostly of Zn metal. The only conclusive test to determine whether or not a specific area contained Zn or ZnO would be to examine an area before and after dissolving the ZnO with the NH_4OH-NH_4Cl solution.

6C. Morphology of Zinc in a Discharged Electrode

It was noted earlier that the examination of a discharged zinc electrode was of interest to determine the morphology of electrochemically-inactive zinc. Hopefully the morphology of passivated zinc, whether densified or not, would yield a clue on the effect of various electrolytes on the electrode morphology and the quantity of passivated zinc. In Section 5, Table IV-9, the quantity of electrochemically-inactive zinc in 1/2 of the electrode was shown to be less than 2% of the total zinc in all cases. The quantity of passivated or isolated zinc is therefore insignificant.

Zinc electrode B03H contained the largest amount of apparently inactive zinc. The zinc in this electrode appeared to be, judging by the grey color, limited to a thin (~3mm) ring bordering the thinned central portion of the electrode shown in the X-ray image of Figure IV-7. After dissolving the ZnO with the NH_4OH-NH_4Cl solution, SEM micrographs were obtained. One is shown in Figure IV-27, and has a morphology similar to that shown in Figure IV-22b for electrode B03J. The zinc is not densified and appears to have similar porosity and structure to that of the charged electrode. It is therefore not likely to be passivated zinc but possibly disconnected (isolated). Another explanation is that the narrow 3mm wide band appearing to contain the remaining zinc had such a low area that the overpotential of the zinc (or opposing Ni metal, or both), was sufficiently high that the cell potential reached 0.0 volts before the zinc could completely discharge.

For the other discharged zinc electrodes, LOWA, KFF and HIGHD, the electrode appeared to contain little zinc; none would be expected based on the measurements of electrochemically-inactive zinc shown in Table IV-8. As noted in the preceding paragraphs SEM photographs of these electrodes could not be obtained, even with a carbon coating, due to severe charging effects.

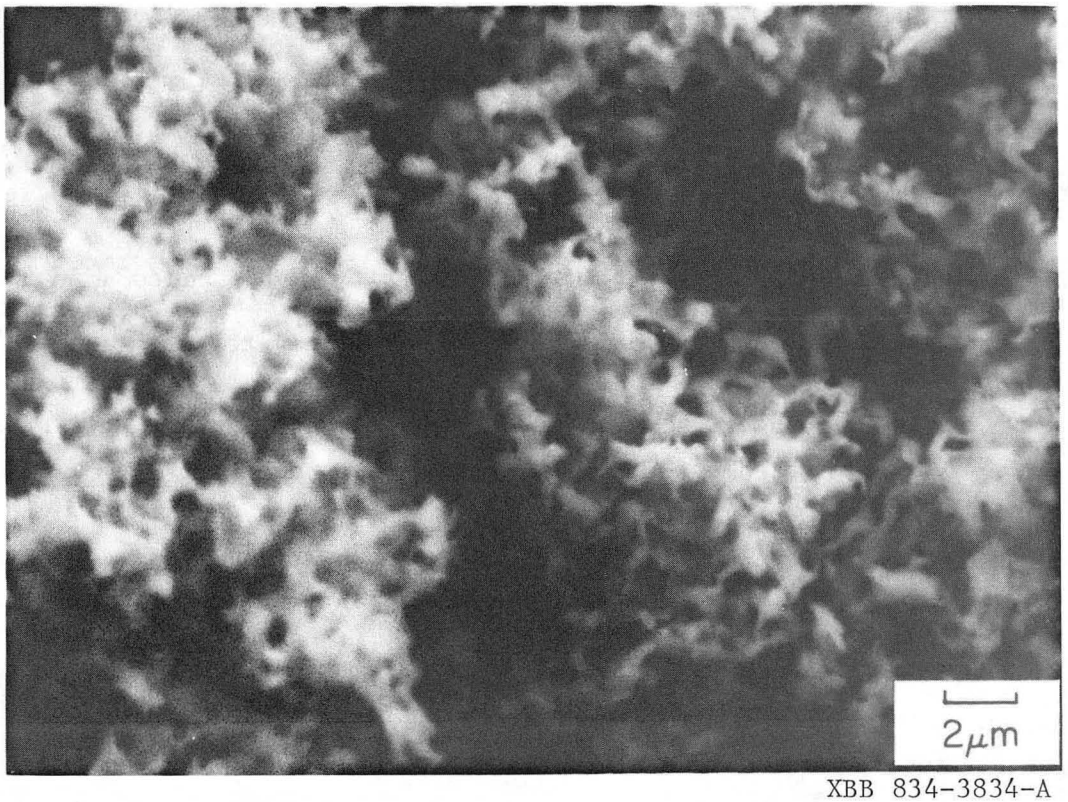

XBB 834-3834-A

Figure IV-27. Morphology of Zn metal in Discharged Electrode BO3H. The electrode was cycled in a 21.5% K_3BO_3-1.1% Li_3BO_3 electrolyte for 125 cycles. It was then discharged at 6.2 mA/cm^2 to 1.1V cell potential and at 1.6 mA/cm^2 to 0.0V in cell, then at 1.6 mA/cm^2 to 0.0V in excess electrolyte with separator removed. Oxidized Zn dissolved in 10M NH_4OH-1M NH_4Cl. The location is 39 mm from the top of the electrode and 37 mm from the tab side of the electrode.

6D. X-ray Microanalysis

When sufficiently high-energy electrons strike an atom, core electrons can be ejected from the atom. Electrons in the atom at higher energy levels can then release X-rays of specific energy as they fall to the lower energy levels. Methods to detect these X-rays have been developed for quantitative analysis and elemental mapping. The technique is known by several names: Electron Microprobe (EMP), Analytical Electron Microscope (AEM) and Electron Probe Microanalysis (EPMA).

Two methods of X-ray discrimination are used, one by energy and the other by wavelength. The Energy Dispersive Spectrometer (EDS) is usually a silicon crystal from which an electronic pulse is obtained as the energy of each X-ray is dissipated in the crystal. The wavelength-dispersive spectrometer makes use of the Bragg planes in a crystal to deflect a particular wavelength X-ray into a detector similar to a Geiger-Muller tube.[11] The EDS detection method is inherently noisy, spreading the characteristic X-ray energy over a band wider than that obtained with a wavelength-dispersive detector. A typical detection limit for a wavelength-dispersive detector is 0.05 atom %. Using EDS, the detection limit is several times higher. Because of the window present on most EDS detectors the analysis is limited to fluorine and elements with atomic numbers greater than 9, although windowless detectors are available that can detect oxygen. The wavelength- dispersive detector does not have such a limitation and detection of elements with atomic numbers as low as Be is possible by using the proper crystal.

At Lawrence Berkeley Laboratory's Materials and Molecular Research Division (MMRD), an SEM with an EDS detector and a computer system capable of elemental mapping and standardless quantitative analysis is available. This system was used to obtain the SEM pictures and elemental maps presented in this section. Another machine using a wavelength-dispersive detector is in use at MMRD for point analysis. Standards are required for quantitative analysis. The wavelength-dispersal device is a single channel device -- that is only one wavelength is measured at a time. A spectrum is possible but is difficult to obtain, so this machine is normally used only to make a quantitative analysis of samples for which the elemental composition is known.

An example of an elemental map for Pb is shown in Figure IV-28a. The SEM secondary-electron image of the same area of zinc electrode KFG is shown in Figure IV-28b. The lead lies at the location of the current collector and is of course due to the lead that is electroplated onto the current collector to suppress hydrogen evolution. The electrode's active material initially contained approximately 0.75 atom percent lead which could account for some of the dots in the other areas; however, the lead peak is located at the maximum of the Bremstrahlung background radiation so most of the dots are due to this background radiation. A map of the zinc distribution is shown for comparison in Figure IV-29.

Two X-ray spectra were obtained from areas shown in Figure IV-28b. A spectrum from the far right of Figure IV-28b is shown in Figure IV-30a and one from the upper center (about 0.17 mm from the current collector) is shown in Figure IV-30b. A slight amount of lead was detected in the area at the right of Figure IV-28b but none in the upper center. A

standardless analysis was made by the computer using the ZAF method,[11] and a concentration of 0.5 atom percent lead was calculated. It can be noted that the detection limit for lead is on the order of 0.2 atom percent using the EDS detector.

In computing a composition using the ZAF method, the sample is assumed to be flat and homogeneous to calculate the electron beam penetration, which varies with atomic number, and to calculate the absorbence of X-rays from each element. The fluorescence factors for each element are also used in the calculation. A good theoretical method is not available to calculate compositions of rough or non-homogeneous samples, because there are too many unknown variables to account for in such materials.

The effect of absorbence from rough topography can easily be seen in the zinc map shown in Figure IV-29. Compared to Figure IV-28a and b, the zinc should appear at equal intensity everywhere except where there is lead on the current collector; however, the topography blocks the emitted X-rays en route to the detector, which is located at a shallow angle with respect to the sample surface. This affects the quantitative analysis because the lower energy X-rays are more strongly absorbed. As shown in the spectrum of Figure IV-30a the Pb peak is located at an X-ray energy of 2.36 keV and the zinc peak used for analytical calculation at an energy of 8.03 keV. Thus the X-rays from lead are preferentially

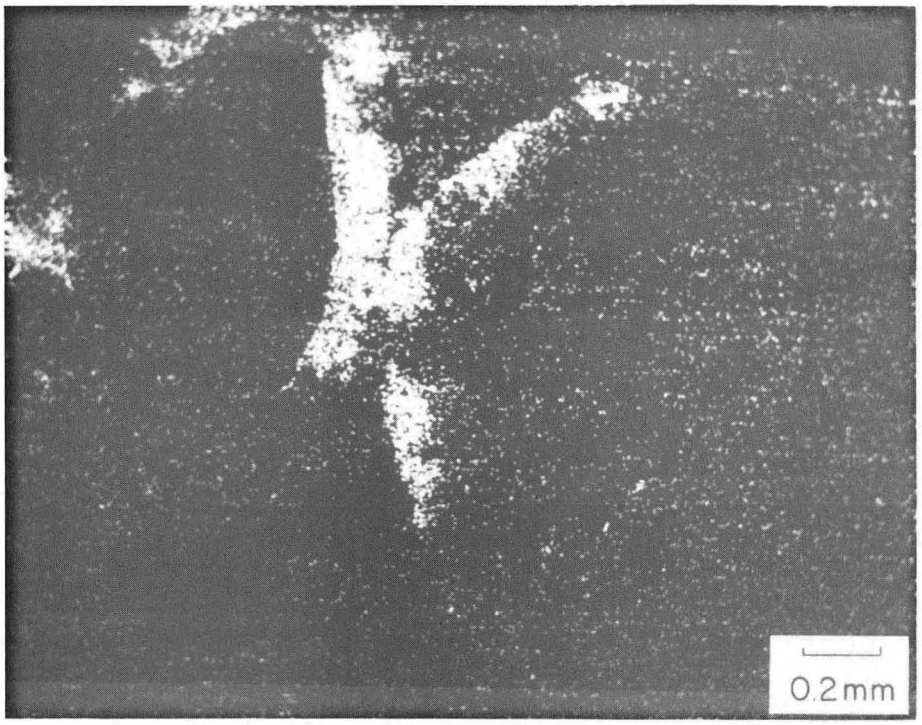

(a)

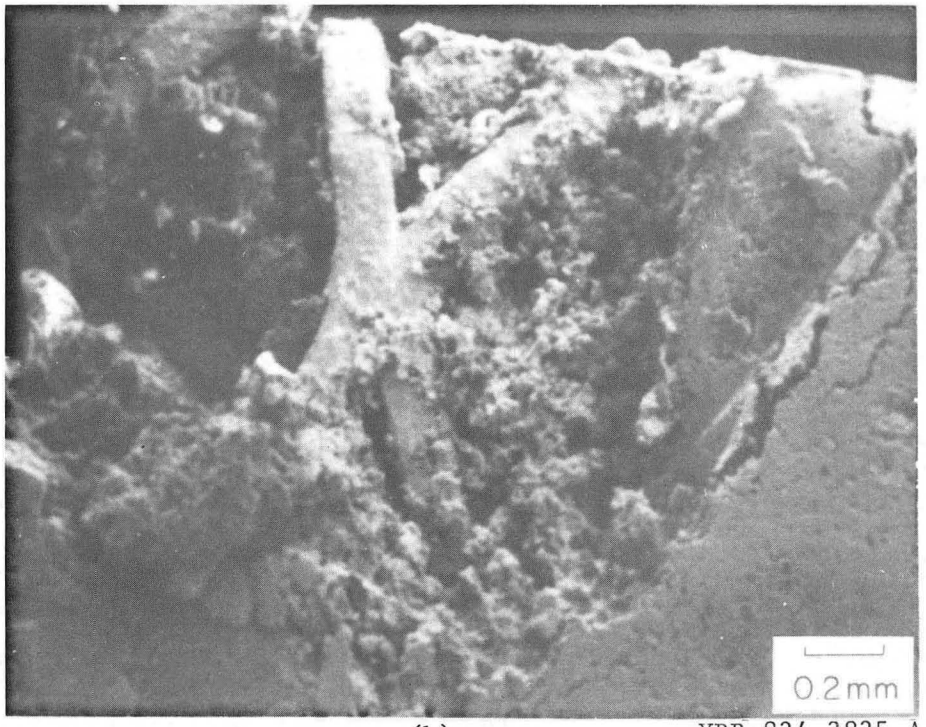

(b)

XBB 834-3835-A

Figure IV-28. Lead Map of Zn Electrode KFG. a) Pb map of area and b) secondary electron image of area showing exposed current collector.

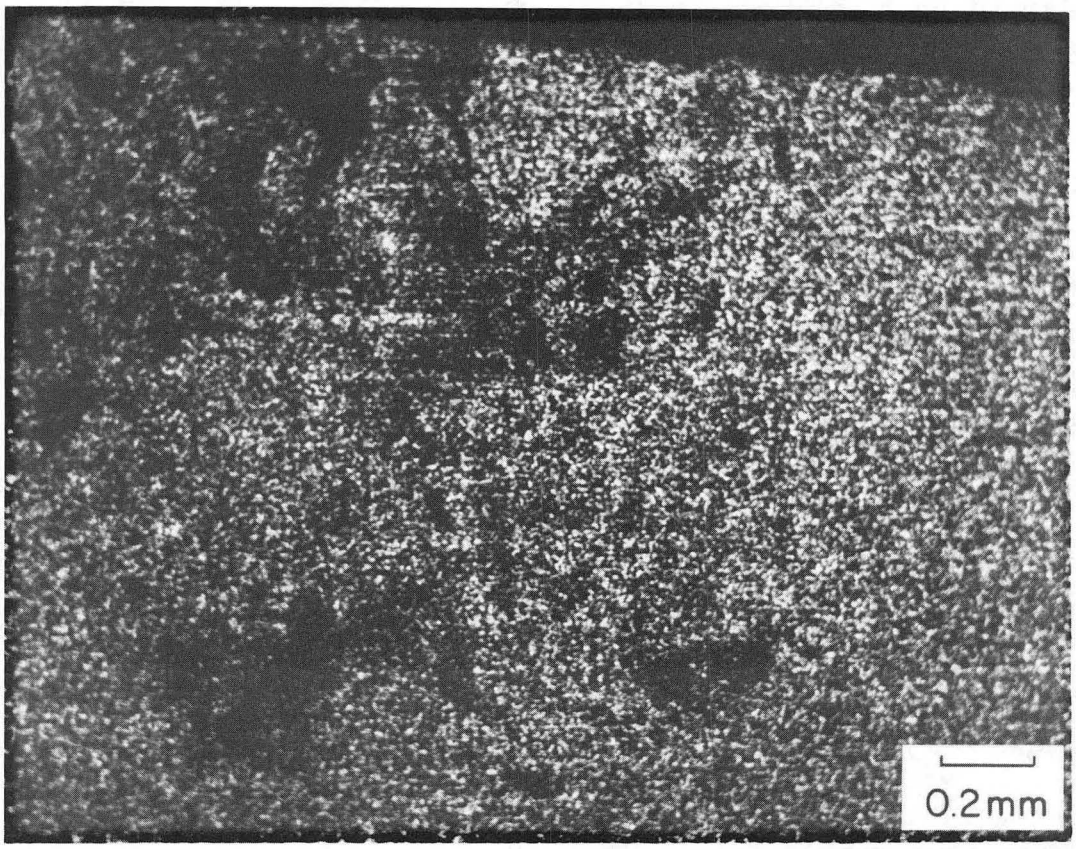

XBB 834-3836-A

Figure IV-29. Zinc Map of Zn Electrode KFG. The map is of same area shown in Figure IV-28b.

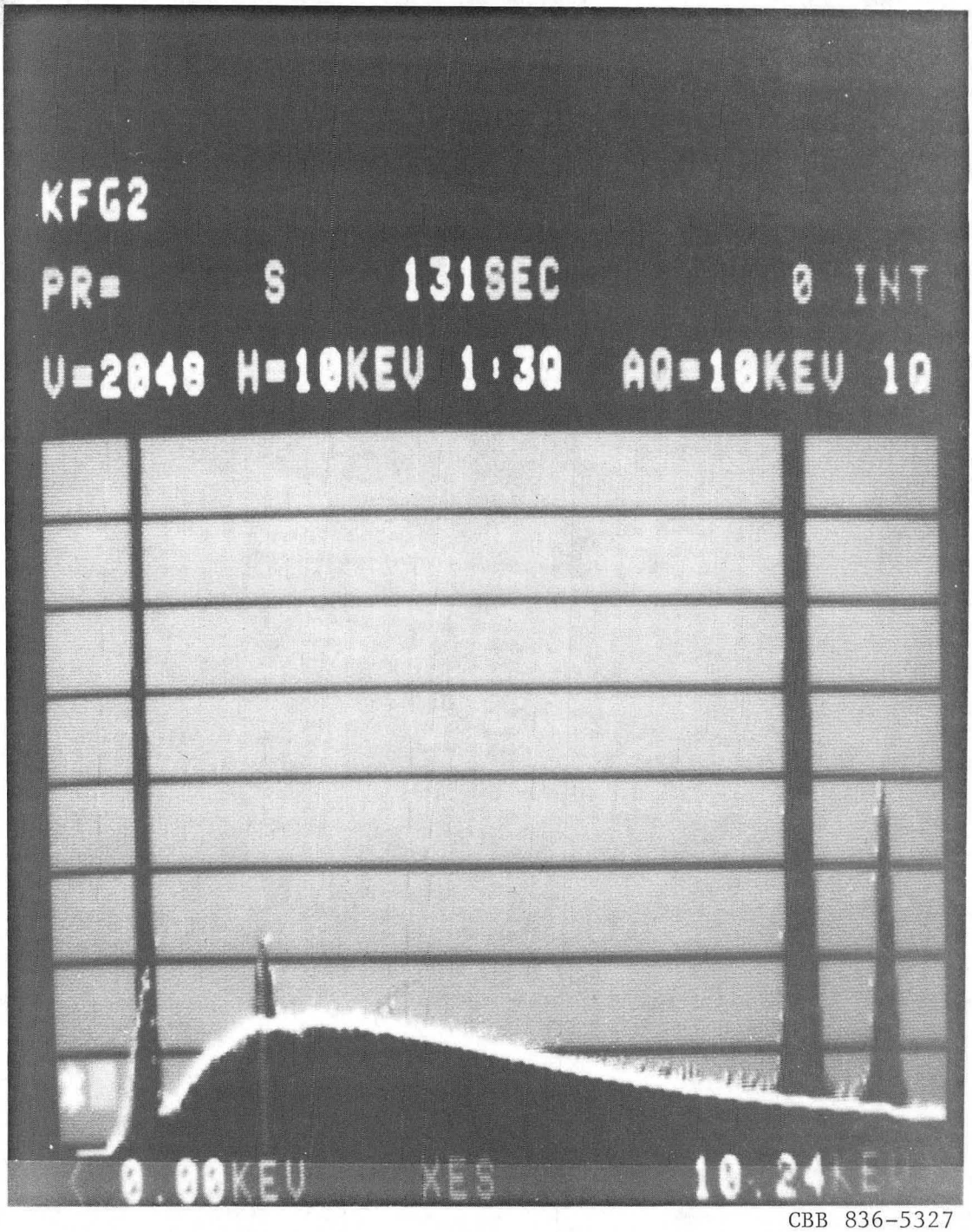

CBB 836-5327

Figure IV-30a. X-ray Spectrum of Electrode KFG. X-ray spectrum from 20 KeV electrons, detected by 77°K Si crystal energy dispersive detector. Spectrum from area shown at far right of Figure IV-28b.

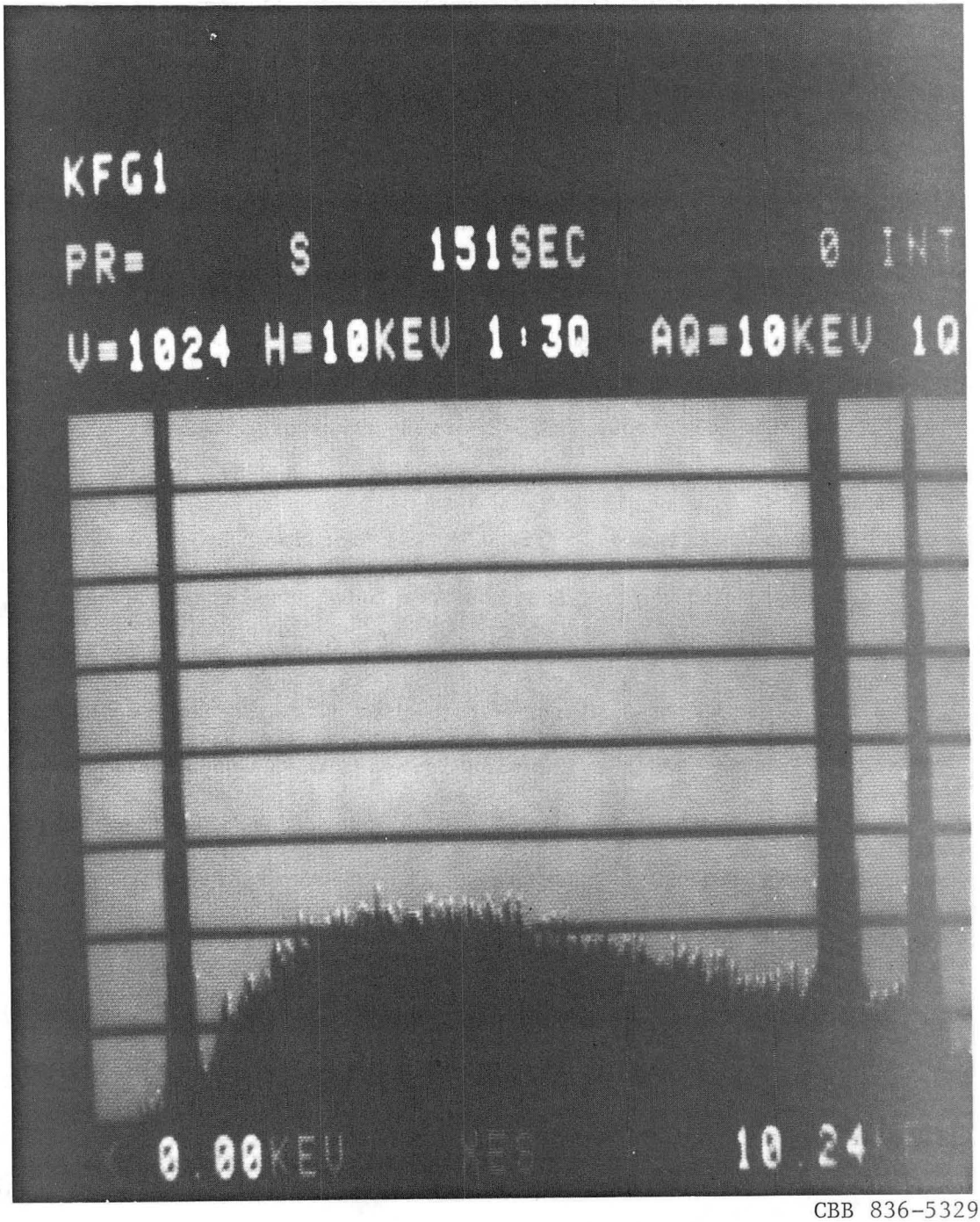

CBB 836-5329

Figure IV-30b. X-ray Spectrum of Electrode KFG. X-ray spectrum from 20 KeV electrons, detected by 77°K Si crystal energy dispersive detector. Spectrum from area shown at upper center of Figure IV-28b.

absorbed which is accounted for in the ZAF method for flat samples but can lead to errors of a factor of 3 or more in samples of rough topography. Furthermore, this error will not be constant, varying from location to location. Because of this large error in quantitative analysis, the quantity of lead will be presented here as: (a) not detected, (b) minor component, or (c) major component (for lead concentrations apparently greater than 5%).

Unlike zinc electrode KFG, charged zinc electrode LOWE contained areas with significant lead concentration. A spectrum from the compact area is shown in Figure IV-31. It was obtained by scanning an area approximately 0.1mm on a side that included the area shown in Figure IV-19a. The spectrum also contains copper; however, this is most likely due to the presence of a copper strip (used to hold the sample) 1mm from the area scanned. This conclusion is based on a copper map of the area which showed a random distribution of copper. Variation expected from topography was not present in the map, whereas variations in the distribution of lead and zinc were present in their respective maps.

The compact area was not the only area with a high concentration of lead. A lead map of the compact area and surrounding areas is shown in Figure IV-32a with the corresponding secondary-electron image shown in Figure IV-32b. Other areas appear to contain similar amounts of lead; most of the variation appears to be due to the uneven topography of the electrode.

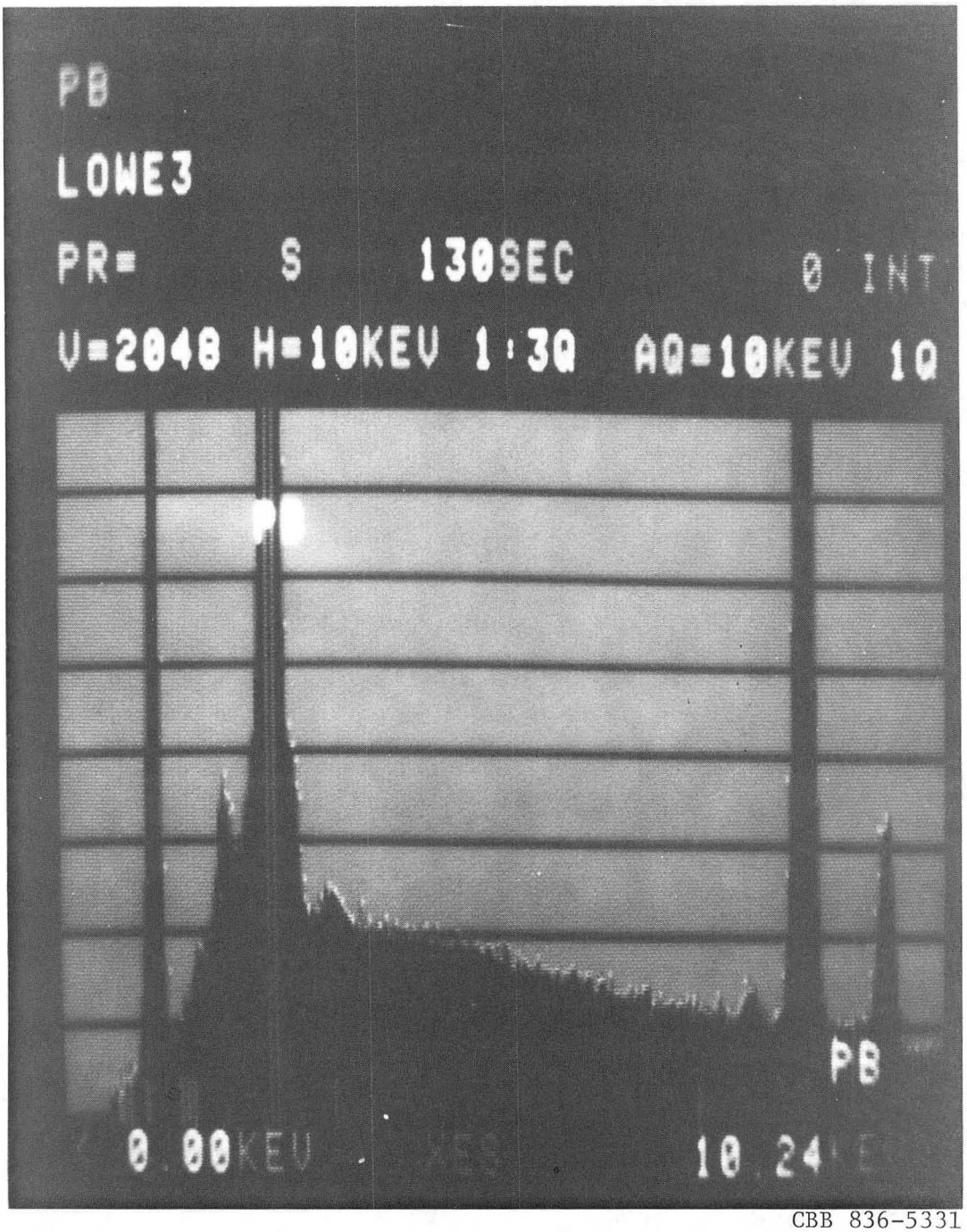

CBB 836-5331

Figure IV-31. X-ray Spectrum of Surface of Zinc Electrode LOWE. X-ray spectrum obtained with 20 KeV electrons and a 77°K Si, energy dispersive detector. Scanned area located in compact area at bottom right of Figure IV-32b.

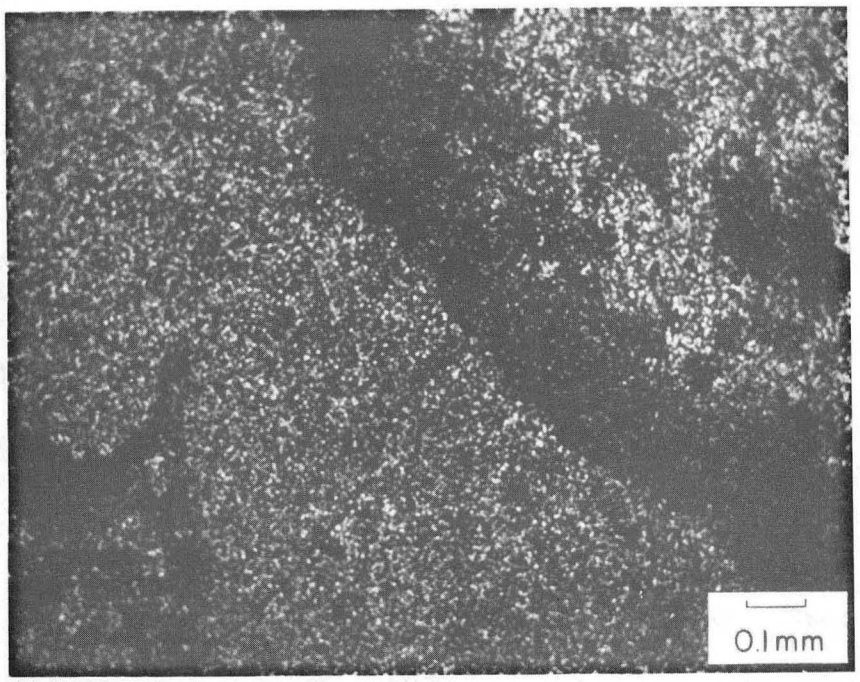

(a)

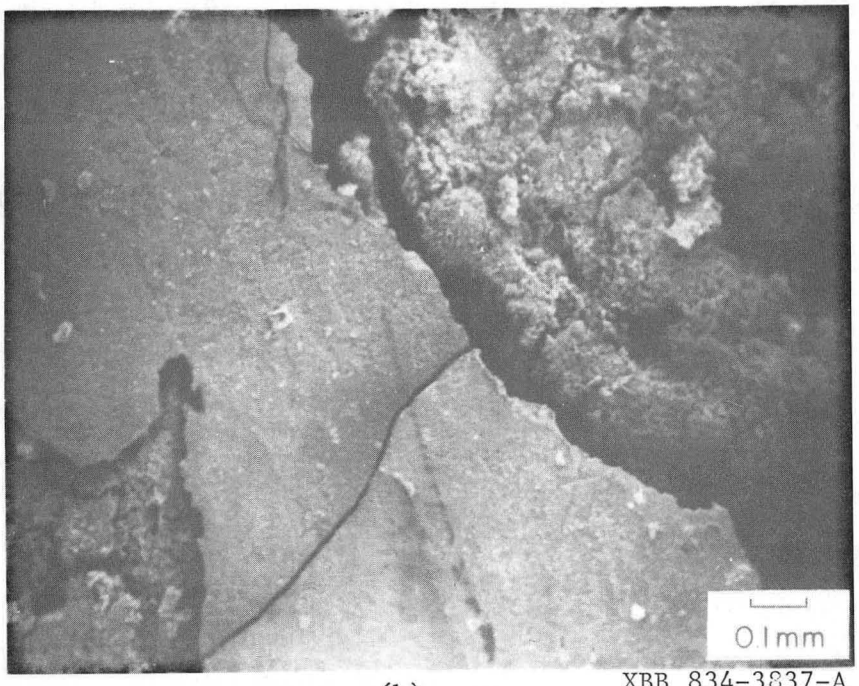

(b)

XBB 834-3837-A

Figure IV-32. Lead Map of Compact and Surrounding Areas of Zinc Electrode LOWE. a) Lead map of area shown in b) secondary electron image. Electrode LOWE cycled 124 times in a 14.4% KOH-1.1% LiOH electrolyte between two NiOOH counter electrodes using a polypropylene microporous separator (Celgard 3401).

Obviously the entire electrode cannot contain such a large amount of lead, but the thickness of this lead-containing layer is not known. In another spectrum obtained in an area of this electrode in which half of the electrode had been chipped away to expose the current collector, the spectrum showed a minor amount of lead. That particular area was located 50μm from a strand of current collector.

Samples of charged electrodes in the standard electrolyte are not available because both cells in this experimental series shorted. But some electrodes from preliminary cells examined with X-ray microanalysis did show similar concentrations of lead at the surface and others did not. The significance or cause of this concentration of lead in the portion of electrode against the separator is not known. No other variations in elemental distribution were observed. The microstructure could not be examined with X-ray microanalysis because the depth of X-ray emission is ten times the dimension of the zinc and zinc oxide particles and possibly 40 times the depth, due to the porosity of the electrode.

Because of the composition of the window material on the EDS detector used for X-ray analysis, oxygen could not be determined; however, even if oxygen could be detected, individual zinc or zinc oxide particles could not be identified because of the large volume of X-ray emission area compared to the particle size. General areas could possibly be mapped for oxygen using the proper detector. The mapping would, however, be very sensitive to topography, even more so than that for lead because of the low oxygen X-ray energy and thus strong absorption of the X-rays.

6E. Scanning Auger Microscopy

Another microanalytical technique is Scanning Auger Microscopy (SAM), in which the quantity of Auger electrons is measured. The Auger electrons are created when an electron falls into a vacant lower level giving its energy to another electron which becomes the Auger electron. The lower level is vacated by collisions with high energy electrons directed toward the sample. Of course in some cases, the falling electron emits an X-ray. The X-ray fluorescence process is more probable for the heavy elements and the Auger process is more probable for the light elements.

Auger-electron detectors are single-channel devices so a spectrum is obtained one channel at a time. This greatly reduces the time available to collect a signal for each channel. To keep the signal-to-noise ratio sufficiently high, large beam currents are necessary. This means that large electron-beam diameters are used, which limits magnification.

Only general features the size of tens of micrometers can be mapped. The only features of such size in these zinc electrodes are the current collector mesh and the compact areas on electrode LOWE. The particle sizes in the zinc electrodes are on the order of 0.5μm as shown in the figures of the previous sections. This is about 1/2 the size of the SAM electron beam. Zinc oxide or zinc particle discrimination is thus not possible nor is mapping of lead in zinc particles. The detection limit for lead is about 1 atom percent, so one would not expect in any case to see lead unless it was unusually concentrated at the surface.

An attempt was made to obtain an analysis of zinc electrode LOWE. The charging problems that occurred when using the SEM's turned out to be much more severe in the SAM, probably because of the much higher current. The first area examined did not produce a good spectrum even after removing approximately 200nm of the ZnO that was suspected to exacerbate the charging problem. A spectrum was obtained of the compact area. Lead was possibly present, but its concentration was too low to obtain quantitative results. Chlorine was present at a concentration of about 6% and was still present at a concentration of 1-2% after removing 200 to 300 nm of material by Ar-ion sputtering. Some carbon was also present at the initial surface.

The X-ray microanalysis showed significant levels of lead, but significant levels were not detected by SAM. Apparently the lead was deeper than 200 to 300 nm. The chlorine may have been present in the X-ray spectrum, but the width of the lead peak would have obscured it. Carbon contamination was expected from drying the sample in the vacuum oven which was not equipped with a cold trap. The source of the chlorine contamination is not known.

Mapping large areas for zinc and oxygen to determine the relative abundance of zinc and zinc oxide is possible; however, the surface composition may not reflect the bulk composition of the area. In the electrolyte, zinc corrodes to form hydrogen and zinc oxide. Because the electrode remained in the electrolyte for 1 to 3 days, all zinc in these samples would be expected to have a surface layer of zinc oxide to some unknown depth. This layer could be removed by Ar-ion sputtering, but the character and composition of the original surface would be lost.

SAM does not appear to be a good technique to use on these electrodes because of severe charging and the small size of the structures in the electrode. Identification of regions of zinc metal and zinc oxide is not possible because zinc metal is probably covered with a layer of zinc oxide to an unknown depth. The distribution of the lead cannot be mapped either because of poor sensitivity to this element unless unusually high concentrations are present. Interpretation of any such distribution would be difficult to make because the current density is not well characterized within a porous electrode.

7. Summary

One of the more interesting and important observations from this series of experiments was that a cell containing the fluoride electrolyte did not have any zinc penetration of the separator with 290 mV of overpotential on the charging Zn electrode. Cells containing the borate electrolyte were similarly remarkable in that an overpotential of 130 mV in one cell and 100 mV in another cell during charge did not result in zinc penetration through the face of the separator. The cells cycled in the 3.5 M OH^- electrolyte without any additional salts had some penetration of the separator, and both of the cells using the 7.4 M OH^- electrolyte shorted with overpotentials less than 100 mV, one in 27 cycles, the other in 118 cycles. An explanation for the differing extents of penetration is not apparent.

There has been some speculation that reducing the zinc concentration in the electrolyte would reduce the dendrite penetration of the separator and shorting in cells. The extent of penetration observed in these cells does not, however, correlate with the ZnO saturation limit. The ZnO saturation limit for the fluoride- and borate- containing cells and the 3.5 M OH^- electrolyte-containing cells was nearly the same, but the cells containing the 3.5 M OH^- electrolyte had some separator penetration whereas the fluoride- and borate-containing cells had no separator penetration. The supersaturation limit may be the important factor but it was not measured for the fluoride- and borate-containing electrolytes. It is possible that the additional ions in the fluoride- and borate-containing electrolytes reduced the supersaturation limit below that of the electrolyte with the 3.5 M OH^- concentration and no additional anions.

The initial capacities of each of the four sets of cells were different. From highest to lowest the order was: 7.4 M OH^- electrolyte, borate-containing electrolyte, 3.5 M OH^- electrolyte, and fluoride-containing electrolyte. To determine whether or not the differences are due to the electrolyte or chance variations in NiOOH electrode construction, one can compare the variation in capacity between the pairs of cells cycled in identical electrolytes and the variation in capacity among the different electrolytes.

Some differences in capacity did exist between the two cells cycled together in series. The differences appear to have been a few percent for the borate-containing cells and the cells containing the 3.5 M OH^- electrolyte. The difference is slightly larger, about 5%, for the

fluoride-containing cells. The two cells cycled in the 7.4 M OH^- electrolyte had a large difference in initial capacity, about 25% based on extrapolating the capacity loss for cell HIGHD from cycle 34 back to cycle 1.

Because the other three pairs of cells had much smaller differences in capacity, one can assume there was some error in NiOOH electrode loading, electrolyte filling and soaking, or alignment that reduced the capacity and led to the rapid redistribution of zinc material in cell HIGHB. This lower capacity and rapid degradation of performance of cell HIGHB was probably atypical. The performance of cell HIGHD was probably representative of the 7.4 M OH^- electrolyte.

All of the conclusions regarding the 7.4 M OH^- electrolyte are derived from the performance of one cell and all of the risks involved in drawing conclusions from one data point are evident. The data for cell HIGHB has been included to support some of the data for cell HIGHD. The tendency toward shorting and the atypical zinc redistribution toward the edges and bottom were common between cells HIGHD and HIGHB.

Since the capacity differences between cells in identical electrolytes were smaller than the differences among cells with different electrolytes, one can conclude that the lower initial capacities were a true reflection of the effects of the electrolyte on NiOOH electrode capacity and not due to chance variation in NiOOH electrode construction. The effect of the different electrolytes on capacity was probably due to the different hydroxide activity and electrolyte conductivity. The fluoride-containing electrolyte had a small concentration of Li which

probably also contributed to the lower capacity of the NiOOH electrodes in these cells compared to the others containing about 0.5 M Li.

By examining Table IV-5, one can see the redistribution of zinc material across the electrode was almost identical for each pair of electrodes. The redistribution was the least for the electrode cycled in the borate-containing electrolyte and only slightly higher for the electrodes in the fluoride-containing electrolyte. This redistribution was much less than that of the electrodes in the 7.4 M OH^- electrolyte, nearly a factor of four less area loss.

The reduced redistribution rate was the anticipated and desired effect of using an electrolyte with a reduced ZnO solubility. The major purpose of these experiments was to demonstrate this effect in addition to examining the effect of the electrolytes on overall cell performance to determine whether or not these electrolytes are viable alternatives to the standard 7.4 M OH^- electrolyte. The 3.5 M OH^- electrolyte without any additional salts reduced the redistribution rate 35% below that of the standard 7.4 M OH^- electrolyte. The reason for the difference in redistribution rates between this electrolyte and the fluoride- and borate-containing electrolytes with similar ZnO solubility is not known.

The electrodes cycled in the 3.5 M OH^- electrolyte were packed 6% looser than in the other six cells. This may have had an effect on the redistribution rate but it could not have been a large effect because this packing difference was not much larger than the 2% variation in thickness present in each electrode. Another possible cause for the

difference in redistribution rate could be the difference in the ZnO supersaturation limit of the electrolyte. This limit was not measured, but if the supersaturation limit for the fluoride- and borate-containing electrolyte is lower than in the 3.5 M OH^- electrolyte, because of a salting out effect from the additional ions, then a plausible explanation for the differences would be in the potentially smaller concentration gradients present with a lower Zn concentration.

While the cell cycled in the 7.4 M OH^- electrolyte had the most severe zinc redistribution, it had the highest capacity prior to shorting. This higher capacity is partly due to the higher initial capacity but with the extensive redistribution of the Zn electrode (56% area loss), a higher capacity loss would be expected. A comparison of the capacity retained to the area retained (Table IV-6) indicates that there is nearly 1:1 correspondence between the cell capacity and the area for the six cells cycled in the electrolytes with a low hydroxide concentration. The cell cycled in the 7.4 M OH^- electrolyte had a capacity-retention-to-area-retention ratio of 1.5. The capacity was 50% higher than would be expected from the remaining Zn electrode area.

It is not expected that significant redistribution occurred during the four cycles after cell HIGHD shorted. The lower performance for those cells in a low hydroxide electrolyte cannot be explained by decreased performance of the Zn electrode. No excessive overpotentials were observed (except for cell KFG) and passivated or densified zinc was not present. It is possible that the metallic Zn and ZnO were not uniformly distributed.

If sufficient ZnO were not present in a portion of the electrode then the opposing NiOOH electrode may not charge, or if sufficient metallic Zn were not present then a full discharge may not be possible. High Zn electrode overpotentials would not appear because Zn has a high exchange current density compared to the NiOOH electrode material and because the Zn electrode was cycled in such a way as to have excess Zn and ZnO in the electrode. The limitation on cell performance would appear on the NiOOH electrode in the form of higher overpotentials and diminished capacity since smaller regions of the NiOOH electrode would become involved in the charge transfer process.

A large enough difference in ZnO and Zn distribution to affect cell performance does not seem likely. To accept the idea of a variance in the Zn-ZnO distribution one would have to propose that this did not happen in the highly redistributed electrode in the 7.4 M OH^- electrolyte but did happen in the slightly redistributed electrodes in the fluoride- and borate-containing electrolytes. A reasonable explanation for the reduced ability of the low hydroxide-containing cells to retain capacity relative to the Zn electrode area is that the lower hydroxide activity and lower conductivity directly reduced the NiOOH electrode performance. The amount of permanent capacity loss from degradation of the NiOOH electrode was not determined after the cells were disassembled.

The zinc concentration in the electrolyte was measured following the last discharge to a cell potential of 1.1V at the 2.5-hour rate. The purpose of the measurement was to determine the extent of supersaturation of the electrolyte. Extensive supersaturation was not found, in fact, the zinc concentration was close to the saturation value. All but

one of the electrolyte samples came from the NiOOH electrode compartment. The one sample from the Zn electrode compartment was obtained from a region several centimeters away from zinc material and was supersaturated by about 25%. The electrolyte in the pores of the Zn electrode could not be sampled, but a maximum amount of dissolved ZnO can be determined by assuming all of the electrolyte in the pores was supersaturated to the highest level observed by other investigators. The zinc content could, at most, have been 0.4g in the 7.4 M OH^- electrolyte and 0.2g in the 3.5 M OH^- electrolyte above the saturation level. From the mass balance made on four of the cells, 0.75 to 1.25g of zinc was missing from the Zn electrodes. Only a portion of this lost zinc can be accounted for by assuming the electrolyte in the Zn electrode was supersaturated. Presumably most of the missing zinc migrated into the NiOOH electrodes but the NiOOH electrodes were not analyzed to verify this.

Depth of discharge (DOD) of a zinc electrode is known to affect the redistribution rate. The four sets of cells each had a different average depth of discharge as shown in Table IV-7. The cells with the lowest DOD had the second most shape change, not the least shape change. The difference in the DOD between cells HIGHD and BO3H was about 4% while the difference in redistribution was more than 30%. No correlation between the DOD and redistribution is evident. One must conclude that the DOD had a minor effect on the redistribution.

The quantity of passivated or electrically isolated zinc was measured in one-half of the Zn electrode from the four borate- and fluoride-containing cells and found to be less than 2% of the Zn in the initial electrode. The amount of such zinc in the other four cells

could have been more than 2% because of an experimental error in the analysis, but less than 2% was measured. To the eye, the discharged half of these four electrodes did not appear to contain metallic zinc.

Based on a mass and charge balance on the Zn electrodes, a few observations can be made concerning the relationships between the state of charge and the Zn electrode potentials. It appears that the zinc oxide dissolution rate may have been slow during charge of electrode B03H. With 1.75 Ah of ZnO in the electrode at the end of the last charge, an overpotential of 100 mV existed. For the four cells cycled in the fluoride- and borate-containing electrolytes significant overpotentials existed (80-150 mV) at the 2.5-hour discharge rate. With as much as 1-2 Ah of metallic zinc present in the electrode, overpotentials of 80 and 100 mV were present for a fluoride- and a borate-containing cell, respectively. This zinc was not passivated or isolated, however. It could be discharged at the 10-hour rate. These overpotentials did not significantly reduce the discharge time since the NiOOH electrode overpotential rose rapidly at the end of discharge, abruptly bringing the cell potential down to the 1.1 volt limit.

A zinc electrode cycled in the 3.5 M OH^- electrolyte had 0.55 Ah of metallic zinc left at the end of discharge and less than a 10 mV overpotential. One of the electrodes cycled in the borate-containing electrolyte had a 100 mV overpotential with 0.58 Ah of metallic zinc left at the end of discharge and one of the electrodes cycled in the fluoride-containing electrolyte had a 150 mV overpotential with 0.45 Ah of metallic zinc left in the electrode. While it was noted above that Zn electrodes discharged in the fluoride- and borate-containing electrolytes

had significant overpotentials with even more metallic zinc present, the overpotential for the electrode with 0.45 Ah of Zn was 50 mV higher than any of the other three, indicating that 0.45 Ah of metallic zinc is marginal for proper cell operation. About 0.5 Ah of metallic zinc is probably the minimum for good cell operation with a 1.35 Ah Zn electrode.

The structures of the Zn electrodes were examined using several techniques: Scanning Electron Microscopy (SEM), X-ray microanalysis, and Scanning Auger Microscopy (SAM). The SAM analysis was not useful because the electrode samples were not sufficiently conductive (they charged when struck by the electron beams). Examination of the Zn electrodes in their charged state (B03J, KFG, LOWE) with SEM revealed a structure composed of approximately 0.5 μm particles; dendrites were not observed. No significant differences in structure were noted among the three electrodes with the exception of regions of electrode LOWE. Some portions of this electrode had a thin compact material on the face of the electrode. The compact material contained roughly 0.5 μm particles but was not as porous as other regions of the electrode. This compact material discharged completely at the 10-hour rate so it was not inactive.

Densified zinc was not observed (using SEM) in any of the electrodes in the charged state. No densified zinc was visible to the eye in any of the discharged electrodes after dissolving the ZnO in an NH_4OH-NH_4Cl solution. The exposed Teflon charged and made it impossible to examine the discharged electrodes with SEM, except for a portion of electrode B03H. Using SEM this portion of electrode B03H appeared identical to zinc material in the charged electrodes and may have been isolated zinc.

The quantity of Zn and ZnO in a particular region could not be determined with SEM. The structure of electrodes known to contain mixtures of Zn and ZnO (LOWE and BO3J) appeared similar to the structure of Zn electrodes stripped of ZnO with the NH_4OH-NH_4Cl solution. The structure of corroded Zn electrodes containing 100% ZnO was not like the structure of Zn and ZnO mixtures or structures of mixtures stripped of ZnO. The ZnO structure was composed of nearly spherical 0.5 μm particles and was easily distinguishable from the Zn-ZnO mixtures and metallic Zn.

X-ray microanalysis was used to examine the electrodes in the charged state for any unusual concentrations of elements. Lead was found to exist in high concentrations at the face of the electrode cycled in the 3.5 M OH^- electrolyte (LOWE). Such concentrations had been observed in some electrodes used in preliminary studies not reported here, but was not observed in the electrode cycled in the fluoride-containing electrolyte (KFG). An X-ray map of a portion of electrode LOWE several mm square showed that the lead was present across this entire portion of the electrode. The lead did not appear to be related to any topographical features on the electrode. Lead was detectable in some portions of the electrode cycled in the fluoride-containing electrolyte in minor amounts and undetectable in other locations. No X-ray microanalysis was performed on the electrode cycled in the borate-containing electrolyte.

The X-ray microanalysis technique has several limitations. The particles in the electrodes were too small to be elementally mapped because the X-ray emission zone has a radius 10-40 times larger than the radius of a particle. Oxygen could not be mapped because the detector was not sensitive to these lower energy X-rays; detectors are available for oxygen, however. Quantitative elemental analysis was not possible because of the rough topography. Rough topography leads to variation in electron penetration depth and variations in absorbance of emitted X-rays. Variations in absorbance of X-rays from Zn and oxygen would be even larger than that of Pb and Zn, leading to even more difficulty in interpreting X-ray emissions when studying Zn and oxygen.

8. References for Chapter IV

1. E.J. Cairns and J. McBreen, in "Advances in Electrochemistry and Electrochemical Engineering," Volume 11, H. Gerischer and C.W. Tobias, Eds., John Wiley and Sons, (1978).

2. S.U. Falk and A.J. Salkind, "Alkaline Storage Batteries," John Wiley and Sons, New York, (1969).

3. T.P. Dirkse, in "Power Sources 3, Proceedings of 7th International Symposium," D.H. Collins, Ed., Oriel Press, Newcastle-Upon-Tyne, England, (1970).

4. T.P. Dirkse, J. Electrochem. Soc. 128, 1412 (1981).

5. G.A. Dalin in "Zinc Silver Oxide Batteries," A. Fleischer and J.J. Lander, Eds., John Wiley and Sons, New York, p. 87-95 (1971).

6. J. McBreen, J. Electrochem. Soc. 119, 1620 (1972).

7. J. J. Lander, in "Zinc Silver Oxide Batteries," A. Fleischer and J.J. Lander, Eds., John Wiley and Sons, New York, p. 457-469 (1971).

8. H.N. Seiger, 154th Meeting Electrochem. Soc., October 1978, Abstract 87.

9. J.W. Diggle, A.R. Despic and J. O'M. Bockris, J. Electrochem. Soc. 116, 1503 (1969).

10. H.N. Seiger, Proc. of 16th Intersoc. Energy Conv. Eng. Conf., Vol. 1, p. 102, Amer. Soc. of Mech. Eng., New York, (1981).

11. O.C. Wells, A. Boyde, E. Lifshin and A. Rezanowich, "Scanning Electron Microscopy," McGraw-Hill Book Co., New York (1974).

12. J. McBreen, personal communication, May 1981.

Chapter V

Conclusions and Recommendations

The capacity decline of rechargeable alkaline cells containing zinc electrodes was determined by several researchers to result largely from the redistribution of the zinc material to a smaller area of the electrode, usually toward the center and lower portion of the electrode. Choi, Bennion and Newman have proposed a convection model and McBreen has proposed a diffusion model. Both models are based on a driving force dependent on a zinc concentration gradient. Reducing the zinc solubility should therefore reduce the redistribution rate and thus the rate of capacity loss.

The dilute-solution solubility product of Zn salts can be used with dilute-solution complex-formation constants of Zn^{2+} by OH^- to predict solubilities of Zn salts in strong alkali to within an order of magnitude. The sparingly-soluble salt $Zn_3(PO_4)_2$ can be shown to be very soluble in strong alkali, as has been observed, and the sulfide salt appears to be less soluble than ZnO. Neglecting the effects of other complexes, the equilibrium concentration of $Zn(OH)_4^=$ is predicted to be 0.074 M for a $S^=$ concentration of 0.074 M in a 7 M OH^- solution. Sulfide is not, however, an attractive anion to add to the electrolyte because it will oxidize at the potential of the commonly-used counter electrodes. A search for Zn salts of stable organics or metal-oxide anions with solubility products similar to that for ZnS was not attempted, but is strongly recommended.

The effect of electrolytes exhibiting reduced ZnO solubility on the zinc electrode redistribution rates was determined using electrolytes with 1/2 the normal hydroxide concentration and KF or $K_xH_{3-x}BO_3$ added to improve conductivity. The borate- and fluoride-containing electrolytes reduced the rate of loss of zinc area from 0.46% per cycle to only 0.09 to 0.14% per cycle, compared to the standard 30% KOH-1% LiOH electrolyte for 1.35 Ah (94% ZnO, 4% PTFE and 2% PbO) Zn electrodes with 3 times stoichiometric Zn. The cells were cycled 125 times to a discharge cut-off of 1.1 volts at the 2.5-hour rate and charged at the 6-hour rate between two NiOOH counter electrodes with a combined nominal capacity of 1.35 Ah. Zn electrodes cycled in the low-concentration KOH electrolyte, without additional potassium salts and with a 6% looser packing, had a reduced area-loss rate of 0.3% per cycle.

The nickel oxyhydroxide electrode appeared to be better able to accept charge when cycled in the standard electrolyte than when cycled in the other electrolytes used here. Cells cycled with a lower hydroxide concentration had lower initial capacities, apparently due to either lower conductivities or lower hydroxide activity. But in addition, the capacity retention of the standard electrolyte cell was greater than the capacity retention of low-hydroxide electrolyte cells, by 50%, per unit Zn electrode area. While the low-hydroxide cells have a percent capacity retention equal to or less than the percent area retention, the standard-electrolyte cell had an estimated 66% capacity retention for a 44% area retention. This lower performance of the low-hydroxide electrolyte cells is probably also related to the lower electrolyte conductivity and/or hydroxide activity. Lithium is insoluble in fluoride

electrolytes such as that tested here, and this may lower the $Ni(OH)_2$ utilization compared to an electrolyte containing lithium and a similar hydroxide concentration. The lower depth of discharge does not appear to have been a significant factor in the better capacity retention of cells with the fluoride electrolyte.

The borate and fluoride additions greatly reduced the rate of zinc penetration through the separator. The cell with the standard electrolyte shorted through the separator face after 118 cycles, and a similar cell in only 27 cycles. Overpotentials of 60-70 mV were present on the Zn electrode during cycles prior to shorting. The cells with low-hydroxide electrolyte without additional potassium salts had some zinc penetration through the separator with overpotentials of less than 10 mV. The conditions leading to the observed penetration are not known. No zinc penetration was observed through the face of the separators of any of the four borate- or fluoride-containing cells, even with Zn electrode overpotentials during charge of 290 mV in a caustic-fluoride-electrolyte cell, and 100 and 130 mV in caustic-borate-electrolyte cells.

Apparently the zinc oxide dissolution rate limits the rate of charging the Zn electrode in the borate electrolyte. High overpotentials of 100 mV were observed for an electrode with 1.7 Ah of ZnO. Another caustic-borate-electrolyte cell had charge overpotentials of 130 mV with up to 0.8 Ah of ZnO in the electrode. Similar measurements of the state of charge versus Zn-electrode overpotential are recommended for the standard and low-hydroxide electrolyte without additional potassium salts to determine whether ZnO inaccessibility is typical or limited to

the borate electrolyte.

Apparently 0.75-1.25 g of Zn migrates away from Zn electrodes irrespective of the type of electrolyte. Supersaturation of the electrolyte in the Zn electrode pores is insufficient to account for this Zn loss and significant supersaturation of the bulk electrolyte does not occur.

Less than 2% inactive zinc is present in cells cycled under the conditions used here. SEM examinations showed no densified zinc in any electrodes and no zinc dendrites in three charged electrodes examined, those from fluoride, borate and 3.5M OH^- electrolyte cells. The measurement of the quantity of inactive zinc was made after a complete discharge at the 10-hour rate. This lack of inactive zinc complements the observation that none of the zinc electrodes had excessive overpotentials during discharge.

Appendix A

Derivation of Solubility Expression for Zinc in Aqueous Alkaline Electrolyte

1. Zinc hydroxide solubility

The purpose of this section is to develop an expression to predict zinc hydroxide solubility from the solubility product and hydroxyl ion complex-formation equilibrium expressions. The effect of the changing density will be ignored as will the activity coefficients, though the latter will be maintained for the sake of completeness. In the following expressions, parenthesis, ( ), will be used to denote activity and brackets, [ ], for concentration.

The solubility-product expression for zinc hydroxide is:[1]

$$Ksp = [Zn^{2+}][OH^{-}]^2 \qquad [A-1]$$

A value of $3.5 \cdot 10^{-17}$ is used here for Ksp (see section II-3). At the low concentrations where Ksp is determined, the activity coefficients are nearly unity so Ksp is the thermodynamic equilibrium constant and equation [A-1] can be expressed as

$$Ksp = (Zn^{2+})\ (OH^{-})^2 \qquad [A-2]$$

The Zn^{2+} ion is complexed by hydroxyl groups[2,3] (as well as water molecules[2]) in alkaline solution. The four equilibrium expressions and the reactions are:

$$K_1 = \frac{(Zn(OH)^+)}{(Zn^{2+})(OH^-)} \qquad [A\text{-}3A]$$

$$Zn^{2+} + OH^- \rightleftarrows Zn(OH)^- \qquad [A\text{-}3B]$$

$$K_2 = \frac{(Zn(OH)_{2(aq)})}{(Zn(OH)^+)(OH^-)} \qquad [A\text{-}4A]$$

$$Zn(OH)^+ + OH^- \rightleftarrows Zn(OH)_{2(aq)} \qquad [A\text{-}4B]$$

$$K_3 = \frac{Zn(OH)_3^-}{(Zn(OH_2)_{(aq)})\ (OH^-)} \qquad [A\text{-}5A]$$

$$Zn(OH)_{2(aq)} + OH^- \rightleftarrows Zn(OH)_3^- \qquad [A\text{-}5B]$$

$$K_4 = \frac{(Zn(OH)_4^=)}{(Zn(OH)_3^-)\ (OH^-)} \qquad [A\text{-}6A]$$

$$Zn(OH)_3^- + OH^- \rightleftarrows Zn(OH)_4^= \qquad [A\text{-}6B]$$

The expressions [A-3A] through [A-6A] can be combined to give the overall complex formation reaction

$$\beta_4 = \frac{(Zn(OH)_4^=)}{(Zn^{2+})(OH^-)^4} \qquad [A\text{-}7]$$

A value of $2.7 \cdot 10^{15}$ will be used here for β_4 (see section II-3).

Because of the magnitudes of K_1, K_2, K_3, and K_4 the predominant species at hydroxyl ion concentrations >1M is $Zn(OH)_4^=$. Neglecting activity coefficients, the ratio $[Zn(OH)_4^=]/[Zn(OH)_3^-]$ is ~32 for $[OH^-]$ = 1M. The valid range for the derivations to follow is then for hydroxyl ion concentrations greater than 1M.

The intermediate hydroxyl complexes will be ignored in the following derivation because their concentrations are small relative to the zinc tetrahydroxyl complex. Ignoring all but the tetrahydroxyl species enables one to combine equations [A-2] and [A-7] to eliminate (Zn^{2+}), the result is

$$(Zn(OH)_4^=) = \beta_4 Ksp\ (OH^-)^2 \qquad [A\text{-}8]$$

Since $Zn(OH)_2$ is highly soluble in strong base, any estimate of the solubility must take into account the fact that hydroxyl ions are used to complex the $Zn(OH)_2$. This can be accounted for by the use of a

charge balance which is an equation containing concentration terms

$$[M^+] = [OH^-] + 2[Zn(OH)_4^=] \qquad [A-9]$$

where $[M^+]$ is the alkali metal concentration. The other species are not included because of their small concentrations.

The concentration of hydroxyl ions is eliminated by combining equation [A-9] with equation [A-8] rewritten with activities expressed in terms of activity coefficients and concentrations. When the resulting quadratic is solved for the $Zn(OH)_4^=$ concentration the following expression is obtained:

$$[Zn(OH)_4^=] = \frac{M}{2} + \frac{X}{8} - \frac{1}{2}\sqrt{\frac{X^2}{16} + \frac{MX}{2}} \qquad [A-10],$$

where $M = [M^+]$ = alkali metal concentration

$$X = \frac{\gamma_{Zn(OH)_4^=}}{(\gamma_{OH^-})^2} \quad \frac{1}{\beta_4 Ksp}$$

The radical is preceeded by a negative sign to obtain agreement between equation [A-8] and [A-10] in the limit as the MOH concentration goes to zero.

2. Zinc phosphate solubility

In this section the equations used in section II-5 will be derived. The dissolution of zinc phosphate proceeds by the following reaction

$$Zn_3(PO_4)_{2(s)} \overset{\rightarrow}{\leftarrow} 3Zn^{2+} + 2PO_4^{\equiv} \qquad [A\text{-}11]$$

With the equilibrium expression

$$Ksp_{PO_4} = (Zn^{2+})^3 (PO_4)^2 \qquad [A\text{-}12]$$

Ksp_{PO_4} is reported as the solubility product;[1] however it is presented above as the thermodynamic equilibrium constant since the concentrations are low at the measurement conditions, so the activity coefficients are near unity.

To determine the zinc solubility in the presence of hydroxyl and phosphate ions, consider that the major zinc species in concentrated hydroxyl ion solution is $Zn(OH)_4^{=}$ and its concentration is proportional to the Zn^{2+} concentration as shown in equation [A-7]. Equation [A-12] can be substituted for (Zn^{2+}) in equation [A-7], and after rearranging the following is obtained:

$$(Zn(OH)_4^{=}) = \beta_4 (Ksp_{PO_4})^{1/3} (OH^-)^4 (PO_4^{3-})^{-2/3} \qquad [A\text{-}13]$$

Because the hydroxyl ions are used to complex the Zn^{2+} ions, the decrease in $[OH^-]$ must be accounted for if $[Zn(OH)_4^{=}]$ is large. This can be done by using a charge balance.

$$[M^+] = [OH^-] + 3[PO_4^{3-}] + 2[Zn(OH_4^{=})] \qquad [A-14]$$

Where $[M^+]$ is the alkali metal concentration.

Equation [A-14] can be solved for $[OH^-]$ and substituted into [A-13] to give

$$\gamma_{Zn(OH)_4^{=}}[Zn(OH)_4^{=}] = \beta_4 Ksp_{PO_4}^{1/3}[PO_4^{3-}]^{-2/3} (\gamma_{PO_4^{3-}})^{-2/3} x$$

$$\gamma_{OH^-}^4([M^+] - 3[PO_4^{3-}] - 2[Zn(OH)_4^{=}])^4 \qquad [A-15]$$

For the special case of dissolving zinc phosphate in an MOH solution the total zinc is equal to three-halves of the phosphate concentration. The appropriate equation is:

$$[Zn(OH)_4^{=}] + [Zn^{2+}] = \frac{3}{2}[PO_4^{3-}] \qquad [A-16]$$

But since $[Zn^{2+}]$ is small equation [A-16] becomes

$$[Zn(OH)_4^{=}] = \frac{3}{2}[PO_4^{3-}] \qquad [A-17]$$

Substitution of equation [A-17] into equation [A-15] for the phosphate concentration gives an implicit expression for the zinc phosphate solubility in an MOH solution.

$$[Zn(OH)_4^=]^5 = (\tfrac{9}{4})\beta_4^3 Ksp_{PO_4} ([M^+]-4[Zn(OH)_4^=])^{12} \frac{(\gamma_{OH^-})^{12}}{\gamma_{PO_4}^2 \gamma_{Zn(OH)_4^=}^3} \quad [A-18]$$

3. Zinc sulfide solubility

In this section the derivation of equation [2-7], the ZnS solubility in alkaline solution, will be detailed. Zinc sulfide dissolves by the following reaction

$$ZnS_{(s)} \overset{\rightarrow}{\leftarrow} Zn^{2+} + S^= \quad [A-19]$$

with the equilibrium expression

$$Ksp_S = (Zn^{2+})(S^=) \quad [A-20]$$

Again Ksp_S is used as the thermodynamic equilibrium because the solubility product is determined at low concentrations.

Assuming the zinc tetrahydroxyl ion is the major species, the Zn^{2+} activity in equation [A-7] can be replaced by the Zn^{2+} activity obtained by rearranging equation [A-20]. The result is:

$$(Zn(OH)_4^{=}) = Ksp_S \beta_4 \frac{(OH^-)^4}{(S^=)} \qquad [A-21]$$

Because of the possibly-high zinc tetrahydroxyl concentration, a charge balance must be included,

$$[M^+] = [OH^-] + 2[Zn(OH)_4^{=}] + 2[S^=] \qquad [A-22]$$

Equation [A-22] can be solved for $[OH^-]$ and substituted into equation [A-21] to give the following expression:

$$[Zn(OH)_4^{=}] = \frac{Ksp_S \beta_4 (\gamma_{OH^-})^4}{(\gamma_{Zn(OH)_4^{=}})(\gamma_{S^=})[S^=]} ([M^+]-2[Zn(OH)_4^{=}]-2[S^=])^4 \qquad [A-23]$$

This equation applies at equilibrium whether the solution is produced by dissolution of ZnS in KOH or zinc hydroxide or oxide in a K_2S/KOH electrolyte. For ZnS dissolution in MOH, one sulfide ion is produced for each zinc tetrahydroxyl ion. With this substitution for $[S^=]$, equation [A-23] becomes

$$[Zn(OH)_4^{=}] = \sqrt{\frac{Ksp_S \beta_4 (\gamma_{OH^-})^4}{\gamma_{Zn(OH)_4^{=}} \gamma_{S^=}}} ([M^+]-4[Zn(OH)_4^{=}])^2 \qquad [A-24]$$

which can be solved explicitly for the zinc tetrahydroxyl ion concentra-

tion.

$$[Zn(OH)_4^{=}] = \frac{8[M^+] + \frac{1}{\sqrt{\frac{I}{A}}} - \frac{16[M^+]}{\sqrt{\frac{I}{A}}} + \sqrt{\frac{I}{A}}}{32} \qquad [A\text{-}25a]$$

$$A = \frac{Ksp_S \beta_4 (\gamma_{OH^-})^4}{\gamma_{Zn(OH)_4^{=}} \gamma_{S^{=}}} \qquad [A\text{-}25b]$$

where $[M^+]$ is the alkali metal concentration. The negative sign is chosen on the radical to obtain agreement between equation [A-25] and [A-21] as the MOH concentration goes to 0.

The sulfide-bisulfide ratio is determined from the disassociation expression[1]

$$SH^- \underset{\leftarrow}{\rightarrow} H^+ + S^{=} \qquad [A\text{-}26a]$$

$$K_1 = \frac{(H^+)(S^{=})}{(HS^-)} \qquad [A\text{-}26b]$$

where $K_1 = 1.2 \cdot 10^{-15}$ and the disassociation constant for water is:

$$Kw = (H^+)(OH^-) \qquad [A\text{-}27]$$

Solving [A-27] for the hydronium activity and substituting into equation [A-26b] gives

$$\frac{K_1 (OH^-)}{Kw} = \frac{(S^=)}{(HS^-)} \qquad [A-28]$$

The mean molar activity of KOH (a_{KOH}) has been reported.[4] If the activity of K^+ and OH^- are taken to be equal, then the hydroxyl ion activity is 20 in 7M KOH. Substituting this activity and K_1 and Kw into equation [A-28] gives the $(S^=)/(HS^-)$ ratio as 2.4.

4. References

1. R.B. Fisher and D.G. Peters, "Chemical Equilibria," W.B. Saunders, Pub., Philadelphia (1970).

2. T.P. Dirkse, J. Electrochem. Soc. 128, 1412 (1981).

3. R.A. Reichle, K.G. McCurdy and L.G. Hepler, Can. J. Chem. 53, 3841 (1975).

4. N.A. Hampson, G.A. Herdman and R. Taylor, J. Electroanal. Chem. 25, 9 (1970).

Appendix B

Zinc Electrode Manufacture

The ZnO electrodes were made by the use of a "filter table" method in which a slurry of the ZnO powder and other constituents is vacuum-filtered and the resultant filter cake pressed to the desired thickness. The electrode was made from a lead-plated current collector pressed between two wet filter cakes. The lead was added to reduce the rate of hydrogen evolution. A. Tobias built most of the filter table as well as the mold used to press the electrodes to their final thickness.

The chemicals used were reagent-grade or similar quality with the exception of the commercial-grade solvents used to degrease the copper. A description of the various materials used to make the electrode is presented below and is followed by a summary of the procedures used. The individual pieces of equipment and their use are described at the end of this appendix.

1. Materials Specifications

Degreasing Solvents:
water, isopropanol, and hexane followed by isopropanol and water again

Pickling solution prior to spot welding:
5:1 water to 70% nitric acid

Current Collector:
Exmet* expanded metal mesh 3 Cu 6-4/0

---

* Exmet Corp., Bridgeport, Connecticut.

Tab:

0.25-mm copper sheet cut to 1 cm width
(0.2 mV IR drop at 540 mA discharge current)

Lead Plate:

13μm-thick deposits obtained from vigorously-stirred lead fluoroborate solution at 33 mA/cm^2 current density

Solution to remove copper oxides prior to plating:

warm 9 M NH_4OH solution for 1-2 hours, use immediately before plating Pb

ZnO:

Mallinckrodt Inc.,* lot EEA
99.9% ZnO
0.005% Pb
0.001% Fe
meets ACS reagent-grade specifications
Cd analyzed at 0.0004%

PbO:

Mallinckrodt Inc.,* lot KMXE PbO yellow, low silver
99.9% PbO
0.0002% Cu
0.0012% Fe
0.001% Ag

Binder:

Teflon Type 30** dispersion of submicron particles with 5.5% wetting agent

Filter Table Support Media:

Feltmetal*** 400 series stainless steel filaments in 3.2-mm sheet, originally 90% porosity crushed to 85% porosity

---

* Mallinckrodt Inc., Paris, Kentucky.

** E.I. Dupont de Nemours and Co., Wilmington, Delaware.

*** Brunswick Corp., DeLand, Florida.

2. Construction Procedures

a) Prepare Current Collector

The current collector was prepared by cutting the mesh to the exact dimensions of the mold to insure adequate support for the ZnO. The tab and screen were degreased and pickled in nitric acid for a few seconds. The degreasing was necessary before spot welding because oils will carbonize during spot welding. This residue cannot be subsequently removed and an incomplete lead plate will be obtained. The nitric acid removes most of the oxide and leaves a fresh metal surface for spot welding. The separate tab and screen were then weighed.

The spot welds were made at 16 locations on a 1 cm^2 portion of the tab using tungsten-tipped electrodes. The screen and tab were aligned with a holder machined from a 1/4-inch acrylic sheet to match the screen dimensions and tapped for and fitted with a screw to hold the tab in the proper location. Access to the tab/screen junction was made through a slot machined in the side of the holder. After spot welding, the tabs were stamped (preferably near the screen) to aid in identification of electrode X-ray images.

b) Pb Plating

The current collector was degreased again to insure a continuous layer of Pb could be deposited, and it was completely deoxidized at this point. An NH_4OH solution was used because it selectively removes the oxides without dissolving the metal. Nitric acid will dissolve a

significant portion of the metal before all of the oxide is removed. The current collector was plated immediately after deoxidizing and rinsing because copper tarnishes quickly. The lead plate was formed as specified in the materials specifications. The plated collector should be rinsed and dried immediately to reduce corrosion from oxygen. The completed current collector should then be weighed again.

c) ZnO and PbO Preparation

The ZnO and PbO were dried at 200-250°C for more than two hours and stored in a water-free atmosphere until used. After weighing the material for 1/2 electrode, (with sufficient extra material to make up for anticipated losses) it was not kept in a water-free atmosphere.

d) PTFE Preparation

The particles in a Type-30 dispersion can be coagulated by adding isopropanol to the dispersion. It was found to be advantageous to wash the surfactant from the coagulated suspension to prevent foaming while blending. Washing and decanting the Teflon four times with 8-10 mL of isopropanol was found to be sufficient.

e) Mixing

A Sears Roebuck Co. seven-speed blender, at a setting of 5, was used to mix the ZnO and PbO in 200 mL of water. Five minutes was allowed for mixing the oxides and five minutes for mixing the coagulated PTFE with the oxides.

f) Electrode Assembly

The filter table was fitted with a gasket and cover plate with an opening 1mm smaller than the current collector and sized to cover and seal the unused portion of the table. A sheet of wetted Whatman "50" filter paper, onto which the slurry was poured, was placed under the gasket. After the filter cakes for both halves of the electrode had been made, the filter paper on one half of the electrode was trimmed 0.5-mm larger than the filter cake on each side and the current collector was placed on the other half. The current collector was worked into the paste with a spatula. The other half was then placed on the current collector and lightly pressed down with the spatula. The filter cake was made 1mm smaller than the mold to insure that the entire electrode would fit in the mold. The filter paper on one half of the electrode was trimmed to fit into the mold. During pressing the ZnO paste flows to fill the mold.

g) Pressing

The layout of the electrode in the mold is described later in section 4. The wet electrode was not dried before pressing because material of such porosity cracks during drying. During pressing, blotter paper was placed under the mold ring and against one face of the electrode to absorb the water and was replaced as necessary to insure that the water flowed in a direction perpendicular to the plane of the electrode. Water flow in any other direction can carry ZnO with it, leaving voids in the electrode. The final press was to 13.4 kN without

blotter paper and with shims in place. The force needed to press most of the water into the blotter paper before the final press was determined by trial and error. Overpressing the electrode with the blotter paper in place will squeeze the electrode to become thinner than intended.

h) Drying

Before drying the electrode, the excess filter paper on the bottom edge was carefully trimmed. The electrode was vacuum dried while hanging vertically with the bottom of the electrode resting on a solid surface. This prevented excessive stress and torque on portions of the electrodes as the filter paper dried and shrank.

3. Filter Table Design

The filter table was designed to produce a filter cake of the electrode materials by vacuum filtering a ZnO, PbO and binder slurry. The table consists of a porous support medium to support the filter cake as it forms, an acrylic frame to support the porous support medium, and a gasket and cover arrangement to seal the unused portion of the porous support medium.

A set of two sheets of 12-mm aluminum plate were used to compress the gasket. A low-modulus gasket material, natural rubber, was used to seal the uneven surface with a minimum of compression force. The porous support medium is fragile and can easily be crushed, so care must be

taken when tightening the clamps. A sketch of the filter table is shown in Figure B-1.

4. Mold Design and Use

The four parts of the aluminum mold are shown in Figure B-2. All faces of the mold were machined flat and parallel to within 25μm. When using the mold, the platens of the press must be parallel to insure the electrode thickness will vary by less than 25μm. Two strips of rubber, thicker than the stack of shims, were placed along the shims to insure that the mold ring was tight against the lower plate. If not, the ZnO paste could ooze through out the gap. After pressing to final thickness, a check was made that none of the electrode had interfered with the necessary tight fit of the mold ring and lower plate. If any part of the electrode had interfered with the fit, the electrode would not have the proper thickness. When such material was found, it was trimmed away and the electrode repressed. This examination was best made by lifting the mold ring away from the mold piston, electrode and lower plate, cleaning the mold ring, and if necessary, trimming the interfering material from the electrode. The mold piston was not moved because doing so would make it difficult to fit the electrode back into the mold ring without damaging the electrode.

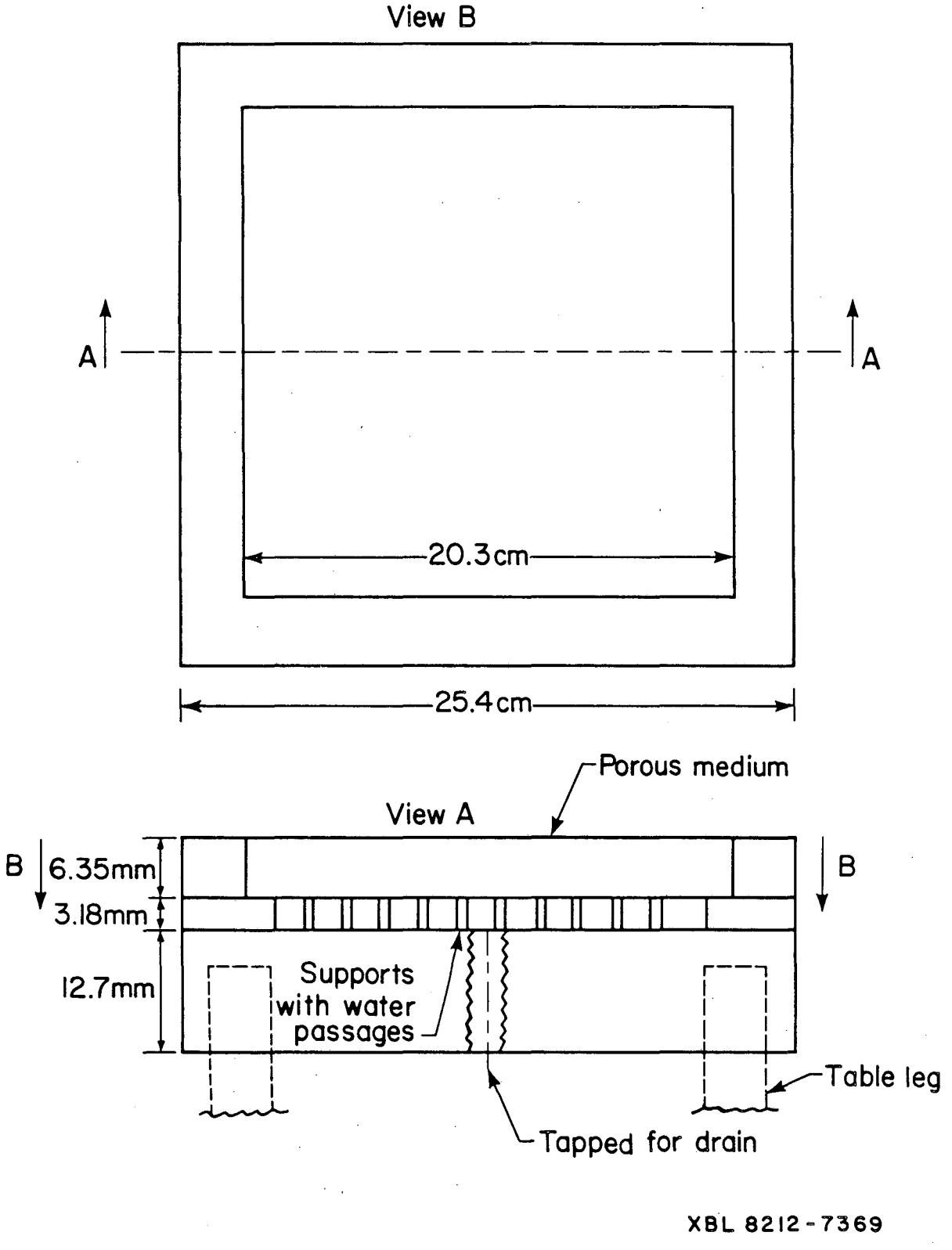

Figure B-1. Filter Table.

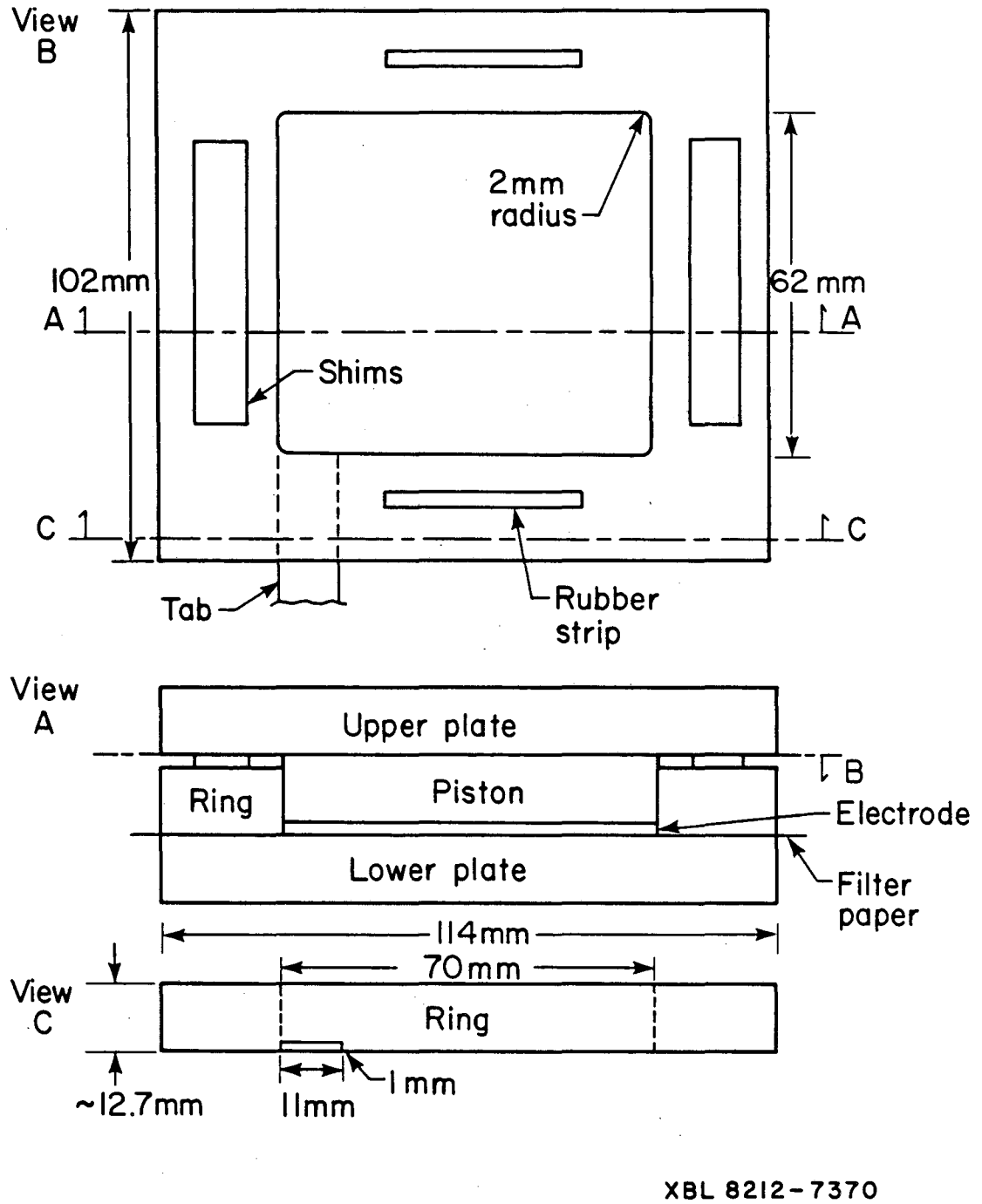

Figure B-2. Electrode Mold.

Appendix C

Cell Case Design

1. Design Considerations

The electrodes were arbitrarily sized to 62-mm tall by 70-mm wide and the cell case designed around these dimensions. A gap of 1.5mm was allowed around the side edges and the bottom. Ideally the cell case would be sized to fit tightly against the edges of the electrode to reduce the higher current density at the edges caused by the primary current distribution,[1] but adequate space must be allowed for the separator seal. The height of the cell case was designed to keep the terminals sufficiently high above the electrolyte level to minimize the leak rate of electrolyte through any potential defects in the terminal seal.

It has been reported that zinc redistribution rates are accelerated by misalignment of the electrodes in a cell stack.[2] For this reason the Zn electrodes were produced with a variation in thickness of 25μm or less (see Appendix B), and the cell cases were machined to a similar tolerance. The inside faces of the cell cases were machined flat to 25μm, and the spacer, which holds the front and rear faces apart, was machined flat and parallel to within 50μm. The spacer was designed to be 6.6-mm thick to accommodate a 1/8-inch (3-mm) tube and leave sufficient room that the drill bit would not break through the side. Any

excess space in the cell had to be filled with a packing material so the thickness of this piece had to be kept to a minimum.

Acrylic was chosen for the cell case because of its stiffness, clarity and resistance to alkali. It was felt that the ability to see into the cell to observe operation could be necessary at times. Though resistant to alkali, care must be taken when cleaning acrylic. Short exposure to acids or hydrocarbon solvents will damage the acrylic and lead to crazing. For the metal parts, nickel is the material of choice since it is not affected by these electrolytes in a strongly oxidizing atmosphere. Due to the high cost of nickel, the tubing and screws were stainless steel. The screws were nickel plated to reduce the leach rate of iron. The tubing was not expected to be frequently contacted by the electrolyte.

The nickel terminals and stainless steel tubing were epoxied in place using a long-chain amine-epoxy resin. This resin was found to have reasonably good resistance to KOH. An `O'-ring seal was not used on the terminals because that would have required that the nickel terminals be threaded to keep the terminal in place. The cost to machine threads along the length of the terminal was prohibitively high. Insufficient room was available to seal the fill and vent tubes with an `O'-ring.

An Hg/HgO reference electrode was chosen because of its stability[3] and ease of construction. Ideally, a reference electrode should be placed between the counter and working electrodes, but consideration of

the reported serious effects of flaws and misalignment on zinc redistribution[2] dictated against the placement of any foreign objects between the electrodes. Attempts to construct a reference electrode that would fit in the electrolyte reservoir at the top of the electrode were not successful. Unstable reference values were obtained, probably because of mixed-electrode potentials involving oxygen. In addition, the mercury from the reference electrode could not be conveniently excluded from the electrolyte with certainty.

With the above considerations in mind, a reference electrode was placed behind the nickel electrode. The reference electrode was connected to the electrolyte at the backside of the nickel electrode through a capillary designed to restrict the quantity of Hg diffusing to the bulk electrolyte. The capillary was packed with acrylic fiber to prevent bubbles from filling the capillary. It was found that those capillaries not tightly packed had some bubble blockage of the capillary. To prevent a mixed-electrode potential, the platinum wire used to make electrical contact with the mercury was epoxied into the bottom of the reference cell compartment and the exposed wire was entirely covered by mercury.

A zinc reference electrode would not be expected to have a mixed-potential problem because the exchange current density of zinc is considerably higher than that for mercury. The zinc reference electrodes were found to corrode too quickly, however, and "recharging" these reference electrodes was inconvenient. The potential of a zinc reference electrode would change as the concentration of zinc changed. Such

added complications in interpreting reference electrode potential data were undesirable.

2. Cell Case Design

The dimensional specifications for the cell case are shown in Figures C-1 and C-2. A suggested modification to use `O´-ring seals on the terminals is shown in Figure C-3. This modification may be necessary if the epoxy seals at the terminals leak significantly. The cases were manufactured with English-unit machine tools, so the corresponding dimensions are given in English units.

3. Rate of Mercury Diffusion Through Reference Cell Capillary

The capillary for the reference cell was designed as noted above to prevent significant diffusion of Hg into the cell. As a worst case, it was assumed that steady state diffusion was occurring in the capillary and that the mercury concentration in the cell electrolyte was zero. From Fick´s Law

$$\text{flux} = -D \frac{\partial c}{\partial x} \qquad [C\text{-}1]$$

or for steady state

$$\text{flux} = -D \frac{(0-C)}{L} \qquad [C\text{-}2]$$

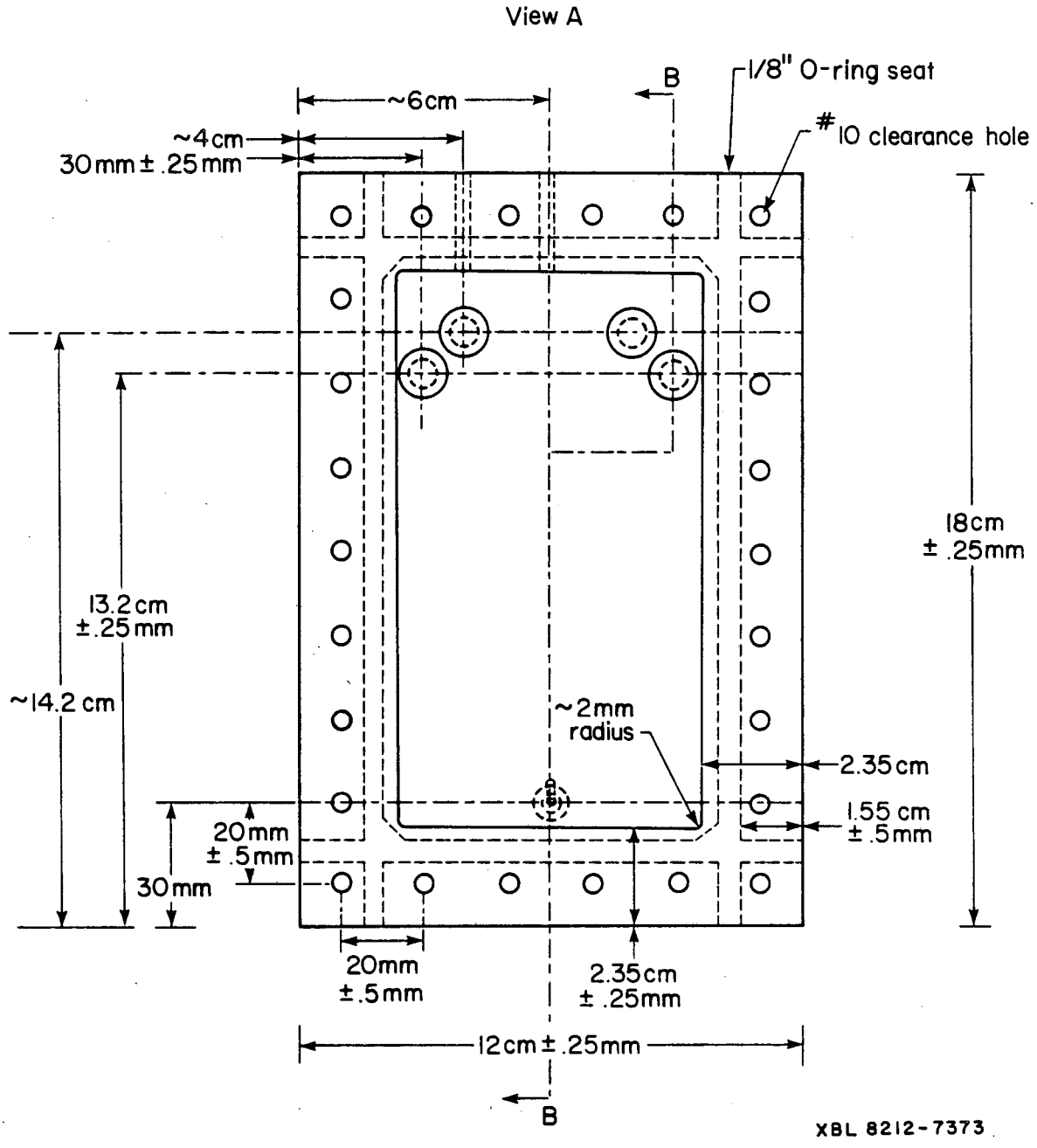

Figure C-1. Cell Case Frontal View.

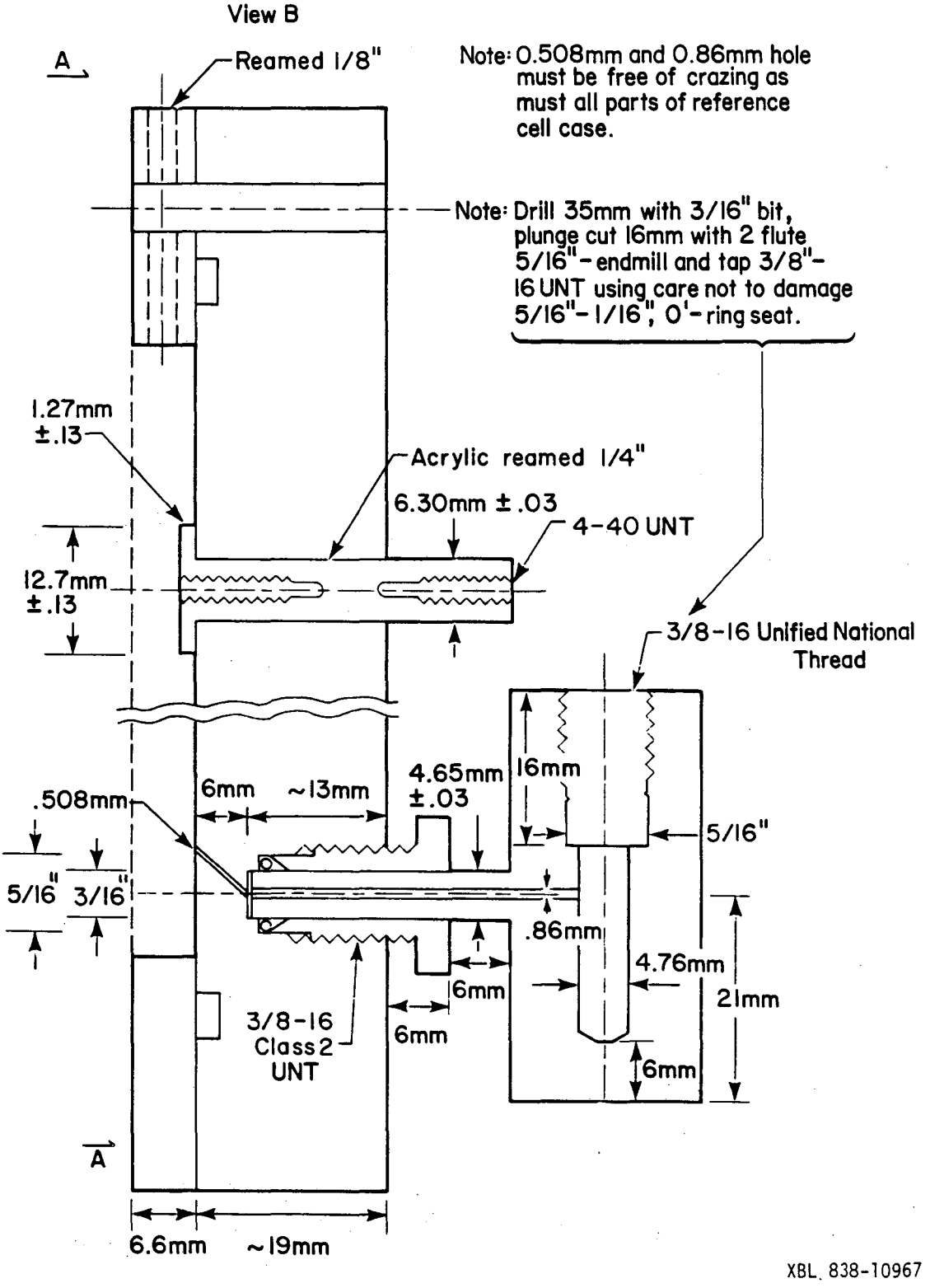

Figure C-2. Cell Case, Terminal, Vent Tubes, and Reference Electrode Compartment Detail.

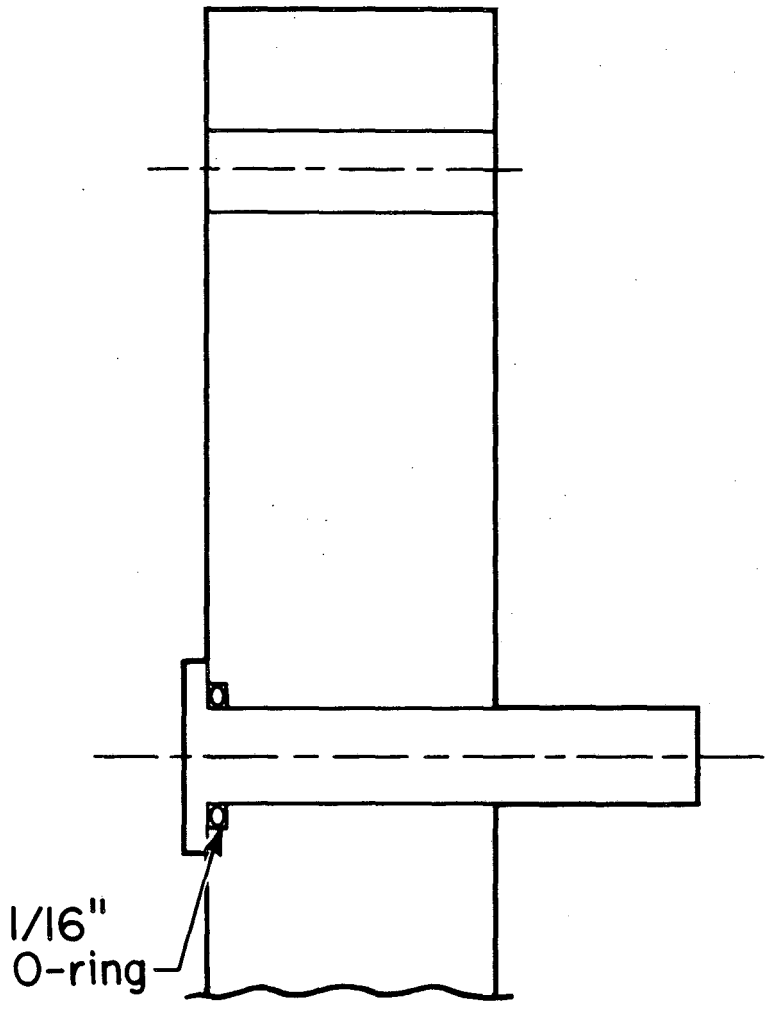

XBL 8212-7371

Figure C-3. Cell Case, Terminal Modification Detail.

where

C = concentration of Hg^{+2} in reference cell

L = length of capillary

D = diffusion coefficient

An estimated value for the diffusion coefficient[4] is $1.6 \cdot 10^{-5}$ cm^2/s.

The rate of mass transfer is the flux of Equation [C-2] times the area. The total Hg diffusing into the cell is:

$$mgHg = \frac{ADTC}{L} \qquad [C-3]$$

The concentration of Hg^{2+} for yellow HgO dissolved in sodium hydroxide has been reported[5] and ranges from $2.55 \cdot 10^{-4}$ molal in 0.6 molal NaOH to $3.11 \cdot 10^{-4}$ molal in 5.952 molal NaOH. For this calculation a value of $2.5 \cdot 10^{-4}$ moles/L should be sufficiently accurate. This gives the total Hg diffusing into the cell in 40 days as $6 \cdot 10^{-3}$ mg, which is $1 \cdot 10^{-4}$% of the Zn electrode mass and is therefore expected to be insignificant.

4. Reference Electrode Compartment

The reference electrode compartment was machined from an acrylic rod to the dimensions shown in Figure C-2.

5. Pictorial Views of Cell Case

An exploded view of a cell, showing the layout of the electrodes is presented in Figure C-4. A fully-assembled cell is shown in Figure C-5. The platinum wire contacting the mercury was introduced through the bottom of the reference cell case for the experiments described in this thesis, rather than as shown in Figure C-5.

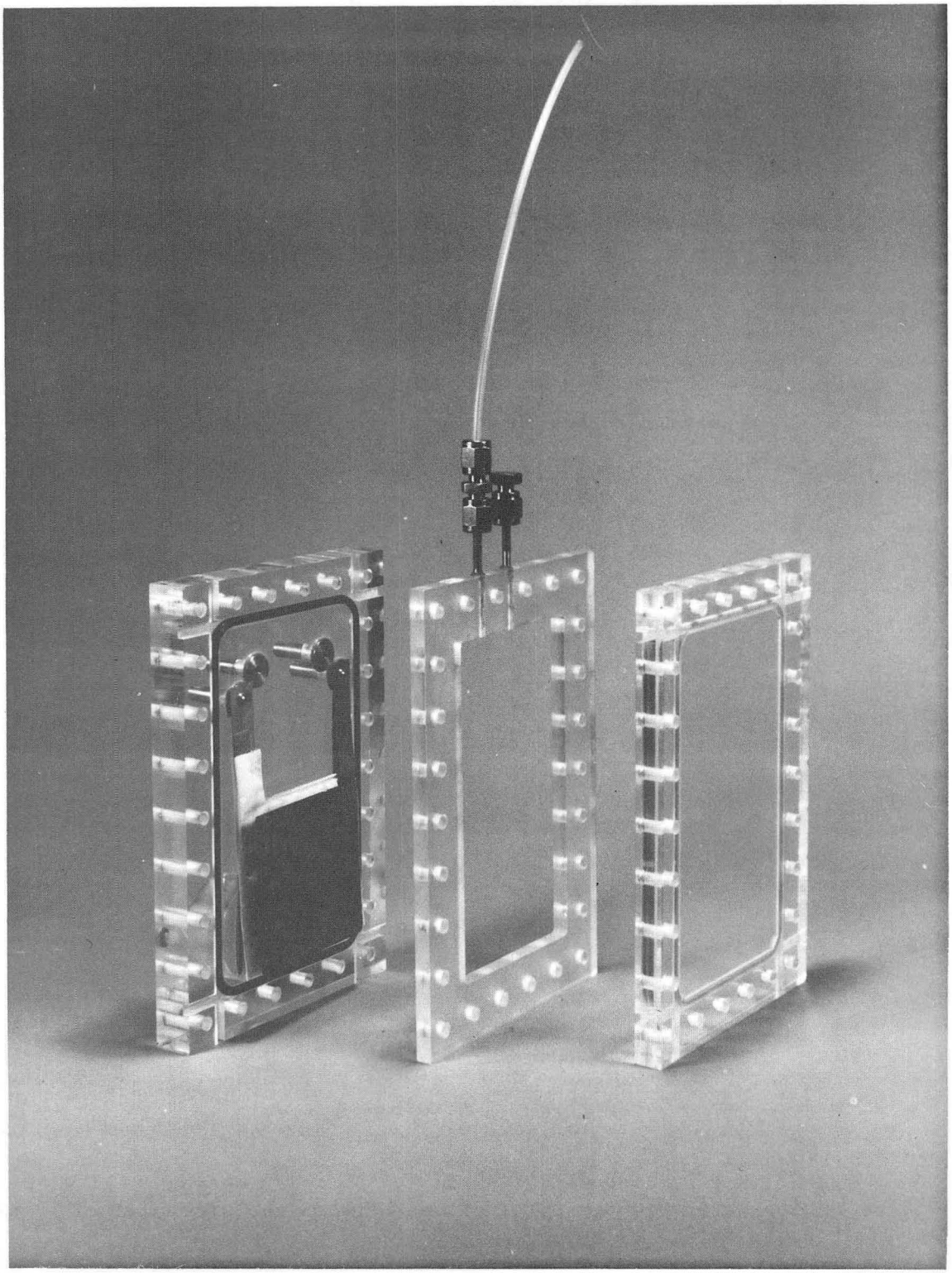

CBB 825-4772

Figure C-4. Exploded View of Cell Case. Shown with tri-electrode 1.5 Ah cell with separator-wrapped Zn electrode between two NiOOH electrodes.

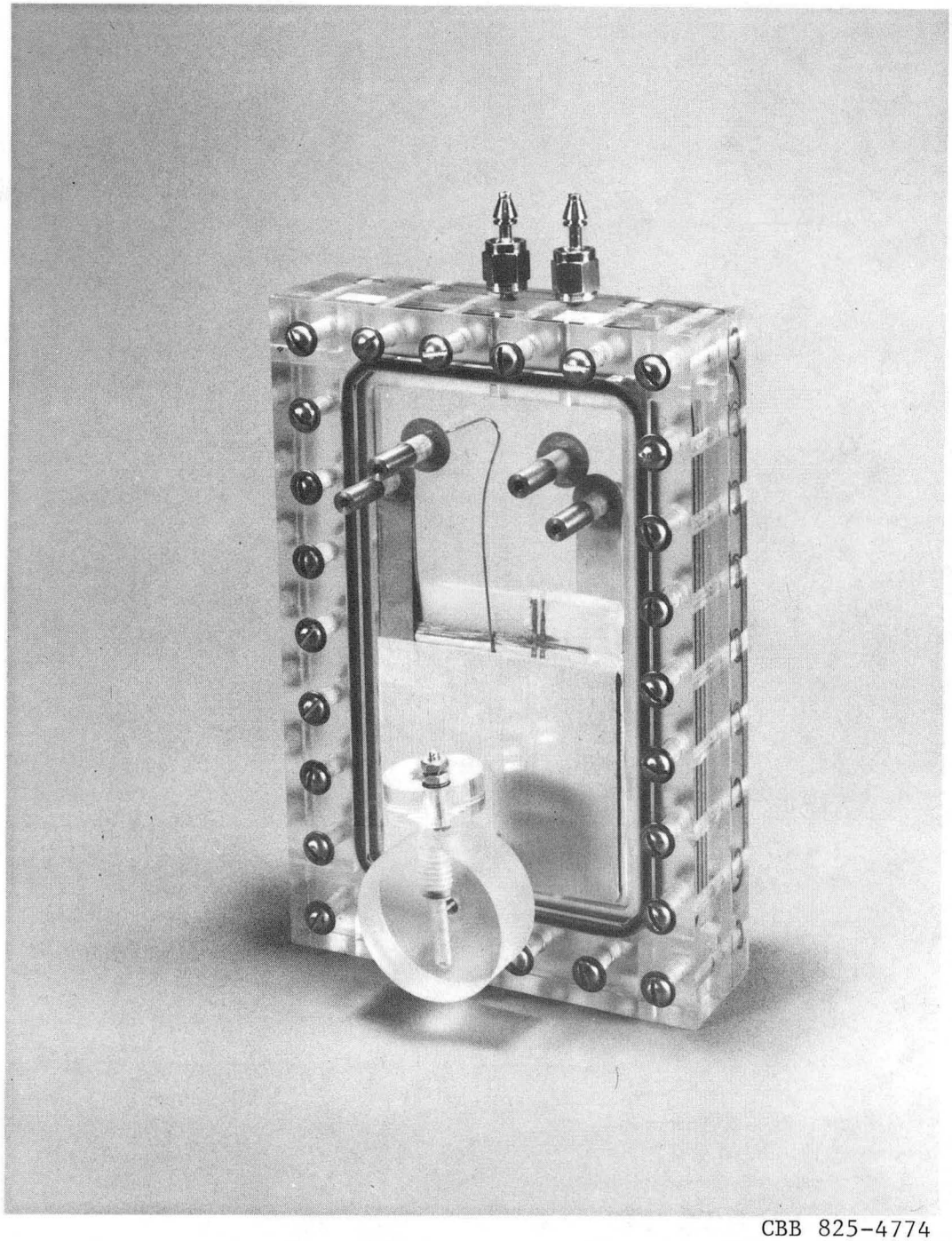

CBB 825-4774

Figure C-5. Fully Assembled Cell. Shows 1.5 Ah tri-electrode cell with separator wrapped Zn electrode between two wick wrapped NiOOH electrodes.

6. References

1. J. McBreen, J. Electrochem. Soc. 119, 1620 (1972).

2. E.J. Cairns and J. McBreen, in "Advances in Electrochemistry and Electrochemical Engineering," Vol. 11,p. 321, H. Gerischer and C.W. Tobias, Eds., John Wiley and Sons (1978).

3. S.U. Falk and A.J. Salkind, "Alkaline Storage Batteries," John Wiley and Sons, New York (1969).

4. R.H. Perry and C.H. Chilton, "Chem. Eng. Handbook," 5th edition, eqn. 3-34, McGraw-Hill Book Co., New York (1973).

5. W.F. Linke, "Solubilities, Inorganic and Metal-Organic Compounds," Vol. 1, 4th ed., p. 1248, D. Van Nostrand Company, Inc., Princeton, N.J. (1958).

Appendix D

Carbonate Analytical Methods

1. Introduction

Carbon dioxide dissolves in alkali solutions to produce $CO_3^=$ ions, which form sparingly-soluble salts with zinc.[1] It is believed by some investigators that precipitation of zinc carbonate in the pores of the nickel oxyhydroxide electrode accounts for some of the observed capacity loss of cells containing the nickel oxyhydroxide electrode.[2] Whether or not carbonate causes capacity loss, it is desirable to minimize the concentration of carbonate in the electrolyte to at least obtain reproducible and consistent results.

Carbonate analysis in the absence of competing equilibria can be accomplished using acid-base titration techniques. With sufficient care, analysis to hundredths of a percent carbonate can be made, as will be shown in Section 3 below. In the presence of other acid-base reactions with endpoints between pH 8.3 and pH 4, the use of acid-base titration is usually not practical. A technique has been developed, however, for carbonate analysis in the presence of dissolved zinc oxide in concentrated alkali solution using EDTA.[3] The technique is not practical at low concentrations of carbonate (<1%), and the reported 0.1% standard deviation is difficult to reproduce. The 95% confidence intervals are very wide, considering the number of 0.5-g samples that can be

obtained from a small cell such as those used in these experiments. The results from this analytical technique are presented in the following section.

Alternate methods of carbonate analysis are available which involve acidifying the alkali solution containing the carbonate and collecting the resultant CO_2 in another alkali solution (or solution capable of complexing CO_2) without the interfering elements or radicals. This alkali solution can then be analyzed for carbonate using acid-base titration. Such a technique does not work, however, for the fluoride-containing electrolyte because HF will be evolved and absorbed by the alkali scrubbing solution as well.

The acidification and CO_2-scrubbing method was not attempted on any of the electrolytes, and because of the poor sensitivity of the method using EDTA none of the hydroxide-containing electrolytes were analyzed for carbonate after cycling had been completed. The initial hydroxide-containing electrolytes (7.4M and 3.5M) were analyzed for carbonate, before saturation with ZnO, using the acid-base titration method. Based on the low carbonate contamination obtained with the electrolyte make-up procedures, the other electrolytes were assumed to have a similarly low carbonate concentration, about 0.05%. To prevent absorption of carbon dioxide by the cell electrolyte, the cells were connected to a manifold purged with air scrubbed with a 1 M NaOH solution. A thymolphthalien indicator was added to the NaOH solution to indicate depletion of hydroxide. The indicator endpoint is in the range of pH 9 to pH 10.

2. Carbonate Analysis Using Ba-EDTA

A method of carbonate analysis in the presence of dissolved Zn^{2+} species has been developed using EDTA.[3] The concentration of zinc in the solution for which the author reported results was, however, less than 1/4 that produced by saturation of the solution with ZnO, and, in additon, carbonate concentrations were very high (about 9%). Attempts to measure carbonate at concentrations of 0.04% in 45% KOH using a modification of the method were unsuccessful.[4] Additional measurements of carbonate at the 0.5% level were recommended, a likely concentration for a cell vented to the atmosphere for a month, and are reported here.

The method involves use of EDTA to complex the zinc and Ba to precipitate the carbonate while titrating the hydroxide to pH 8.3 (phenolphthalein endpoint). If a second titration without Ba or EDTA is made to pH 4, then all the hydroxide will be neutralized, including that complexing the zinc, and all carbonate will be converted to carbonic acid (or CO_2 and water). The difference in titrant added to the two samples of electrolyte, on a unit sample basis, is due to the conversion of carbonate to carbonic acid. For a 31% KOH electrolyte containing 0.5% K_2CO_3, the requirement is to detect a difference of 1 part in 100 between the two titrations.

Argon can be used to prevent air from contacting the sample and increasing the amount of carbonate, but the quantity of argon in the flask will fluctuate from titration to titration. Such fluctuation in mass was found to be intolerable because it masked the small difference

in quantity of titrant between the two samples. A possible method to eliminate the problem of finding a difference between two large numbers would be to neutralize most of the hydroxide and then take two portions of the neutralized sample and titrate one to pH 8.3 with Ba-EDTA and the other to pH 4. The moles of titrant would be smaller and the difference would be a larger percentage of the total titrant. The problem with such a method is that the zinc oxide will precipitate. Identical samples of the partially-neutralized electrolyte will not be obtained because the slurry cannot be completely homogenized.

The procedure for the analysis reported here was identical to Otterson's[3] with the exception that a correction was made to the results of the titration to pH 4. This titration neutralizes all of the free hydroxide, hydroxide-complexing Zn, and carbonate, but in addition some HCl is required to bring the solution to pH 4 (10^{-7} mole per mL or 10^{-5} mole for a typical 100 mL solution). This quantity of acid is equivalent to approximately 0.1 wt% K_2CO_3 for the solutions analyzed.

It is important for such a titration, where a small difference between large numbers is desired, to be certain that the indicator and Ba-EDTA are at the endpoint before adding to the sample. For the pH 4 titration the methyl orange indicator was added to 50 mL of water and adjusted to the endpoint using 0.1M HCl and 0.1M KOH. Careful addition to the sample in the flask is also necessary because loss of even a fraction of a drop of the sample will cause an error larger than 0.5 wt% carbonate.

Unlike the Ba-EDTA makeup procedure suggested by Otterson, the Ba and EDTA were mixed immediately before use because precipitates of EDTA salts were a problem. In fact if any precipitates formed before the Ba-EDTA solution was brought to pH 8.3, the solution was discarded because the precipitation is accompanied by a change in the number of protons associated with the EDTA ion and the precipitate was stable at pH 8.3.

The presence of precipitates during titration greatly complicated the titration because it was desirable not to exceed the endpoint where $BaCO_3$ may dissolve and CO_2 be lost from the solution. The dissolution of the precipitate occurred near the endpoint requiring careful and thus hour-long titrations. The Ba-EDTA solution was made up to a composition of 0.05 M Na_2H_2Y and 0.5 M $BaCl_2$. A total of 50 mL of this solution was added to each 0.8-0.9g sample. The full theory and calculations are described by Otterson.[3]

After the final procedure was worked out, a sample containing 1.00% K_2CO_3, in addition to 0.04% K_2CO_3 from the KOH make up solution, was analyzed. Three samples were titrated to pH 4 (methyl orange endpoint) and three to pH 8.3 (phenolphthalein endpoint) after addition of 50 mL of the Ba-EDTA solution. The correction of the pH 4 titration yields the data shown in Table D-1 after adjustment to a unit-gram basis.

Table D-1

Equivalents Titrant per gram for 1.0% K_2CO_3 Solution

pH 4 endpoint	pH 8.3 endpoint
$9.08 \cdot 10^{-3}$	$8.989 \cdot 10^{-3}$
$9.15 \cdot 10^{-3}$	$9.042 \cdot 10^{-3}$
$9.105 \cdot 10^{-3}$	$9.041 \cdot 10^{-3}$

As noted above the difference in titrant between the pH 4 and pH 8.3 titration is equivalent to twice the moles of carbonate. Otterson apparently combined his pH 4 and pH 8.3 titrations in pairs to calculate the carbonate content and calculated the average and estimate of variance from these pairs. The individual titrations to pH 4 and pH 8.3 should be statistically treated directly. These measurements are expected to be normally and independently distributed. The variations are taken to be independent of the quantity of carbonate titrated. This is not exactly true, because the observations reported in Table D-1 are adjusted to a per gram basis, but since the samples are nearly the same size (only a 4% difference), the variation is expected to be nearly independent of the magnitude of the observation. (Another way of describing this is to say the correlation between the observation and the deviation from the actual value is zero).

If the variation in the measurements for the pH 4 and pH 8.3 titrations is due to identical reasons then the measurements can be pooled to calculate the estimate of the variance. In this case the estimate of variance of the difference will be the weighted average of the estimate of the variance of the pH 4 and pH 8.3 titrations. If the variance is

not identical for the two types of titrations then the variance of the difference is the sum of the variance calculated for each type of titration. It appeared that this was the situation for these titrations. The titrations to pH 8.3 were more variable, probably because of a slow equilibrium involving the EDTA.

The estimates of the variance of the two sets of data shown in Table D-1 do not differ substantially so one might be tempted to pool the data to calculate the variance. In light of some of the titration data not presented here and the data presented below, it is doubtful that a pooled estimate of the variance is justified.

Without pooling, however, the 95% confidence interval is very wide. The estimate of the variance of the pH 4 titrations is $1.26 \cdot 10^{-9}$ $moles^2/g^2$ and for the pH 8.3 titrations $9.2 \cdot 10^{-10}$ $mole^2/g^2$. These are calculated from the formula:[5]

$$s^2 = \frac{\Sigma(y)^2 - (\Sigma y)^2/n}{n - 1} \qquad [D-1]$$

where s^2 is the estimate of the variance

n is the number of samples and

y is the individual observation

The pooled estimate of the variance[5] is:

$$s^2_{pooled} = \frac{(n_1-1)s_1^2 + (n_2-1)s_2^2}{n_1 + n_2 - 2} \qquad [D-2]$$

which yields $1.09 \cdot 10^{-9}$ $mole^2/g^2$ for the data.

The 95% confidence interval is then

$$0.61 \text{ wt\%} \pm 0.52 \text{ wt\%} \quad K_2CO_3 \qquad [D-3]$$

If the data are not pooled to obtain the estimate of the variance then the 95% confidence interval is:

$$0.61\% \pm 1.13\% \quad K_2CO_3 \qquad [D-4]$$

For the latter result the 95% confidence interval is so large that the result is useless. Even though the known 1.0% K_2CO_3 composition is within the interval, so is zero. The pooled estimate of the variance gives only a slightly more satisfactory result, at least zero is not in the interval. One standard deviation is 0.23 wt%, which is three times larger than that reported by Otterson. Otterson's electrolyte, however, contained 1/3 as much zinc as the electrolyte whose data are shown in Table D-1. Considering that more difficulty was experienced with precipitates than Otterson indicated, the poorer results could be expected.

Prior to adding the carbonate to the previously-described solution the solution was analyzed for carbonate. The composition was 43.7% KOH and 5.66% ZnO. The results of four titrations are shown in Table D-2.

Table D-2

Equivalents of Titrant for a Low Carbonate Solution

pH 4	pH 8.3
$9.0887 \cdot 10^{-3}$	$9.231 \cdot 10^{-3}$
	$9.088 \cdot 10^{-3}$
	$9.075 \cdot 10^{-3}$

One data point is far from the other two for the pH 8.3 titration. This is believed to be due to partial protonation of the EDTA. Because the variation of the pH 8.3 data was so large, additional samples were not titrated to pH 4 since their variation was expected to be smaller than that of the pH 8.3 titration.

A variance calculated from the data in Table D-2 and equation D-1 gives a 95% confidence interval of:

$$-0.3\% \pm 1.5\% \quad K_2CO_3 \qquad [D-5]$$

with a standard deviation of 0.6%. This is three times larger than the standard deviation calculated for the sample containing 1% carbonate. If the outlying point is excluded, the difference between the titrations is equivalent to 0.05 wt% K_2CO_3 which is close to the composition expected. The statistics do not justify excluding this point however.

Electrolyte from a cell vented to the atmosphere for several months was analyzed by this procedure. Four titrations, two to each pH, were obtained. The data are shown in Table D-3. The variance was determined from a pooled estimate giving a result of 2.6 wt% ± 1.0 wt% K_2CO_3.

Table D-3

Equivalents of Titrant for an Electrolyte from a Zn/NiOOH Cell

pH 4	pH 8.3
$6.0924 \cdot 10^{-3}$ mole	$5.736 \cdot 10^{-3}$ mole
$6.1601 \cdot 10^{-3}$ mole	$5.754 \cdot 10^{-3}$ mole

Even though the variation in the moles of titrant is small, the 95% confidence interval is large because only four samples were obtained. Normally only two samples could be obtained because the amount of available electrolyte is small.

Based on these results the Ba-EDTA method appears to be unsatisfactory for measurement of carbonate in alkaline Zn containing electrolyte in the range of 0.5 wt% K_2CO_3. A carbonate content of less than 0.1 wt% is desirable to obtain cell-cycling data free of the possible compounding effects of carbonate. The strategy employed in the cell cycling experiments described in this thesis was to make low-carbonate electrolyte and prevent carbon dioxide absorption by venting the cells into a manifold purged with CO_2-free air.* All of the electrolytes were assumed to contain low carbonate based on the carbonate analysis of the KOH-LiOH electrolyte before ZnO addition. The other electrolytes were made up using the same procedure and low carbonate reagents.

3. Carbonate Titration Between the Phenolphthalein and Methyl Orange Endpoints.

Titration of an alkaline $OH^- - CO_3^=$ solution between pH 8.3 and pH 4 will yield the quantity of carbonate.[6] At pH 8.3, the phenolphthalein endpoint, the hydroxide is neutralized and the carbonate is converted to bicarbonate. During the titration from pH 8.3 to the methyl orange endpoint at pH 4, the bicarbonate is converted to carbonic acid and the water is raised to 10^{-4} M hydronium ion concentration.

By measuring the quantity of titrant necessary to reach the pH 8.3 endpoint and the pH 4 endpoint, both the hydroxide and carbonate content can be determined. The quantity of carbonate is equivalent to the moles of titrant between pH 8.3 and pH 4, minus the moles of hydronium ions in the final solution. The hydroxide content is equal to the quantity of titrant needed to reach pH 8.3 minus the quantity of carbonate.

The method was tested on a 46.3% KOH solution containing <0.04 wt% K_2CO_3 (according to the manufacturer) to which K_2CO_3 was added to make ~0.5% K_2CO_3 and ~1% K_2CO_3 solutions. The data are shown in Figure D-1 as added carbonate versus measured carbonate.

The 95% confidence interval[5] over the 0.5 to 1% range is less than 0.25%, which is better than the data shown in Table D-1 by a factor of 2 for only 4 samples. The samples were not analyzed further because more precise measurements were desired than this particular choice of sample size and technique could produce. The sample size was about 1 gram and an argon blanket was used, which made it difficult to obtain accurate

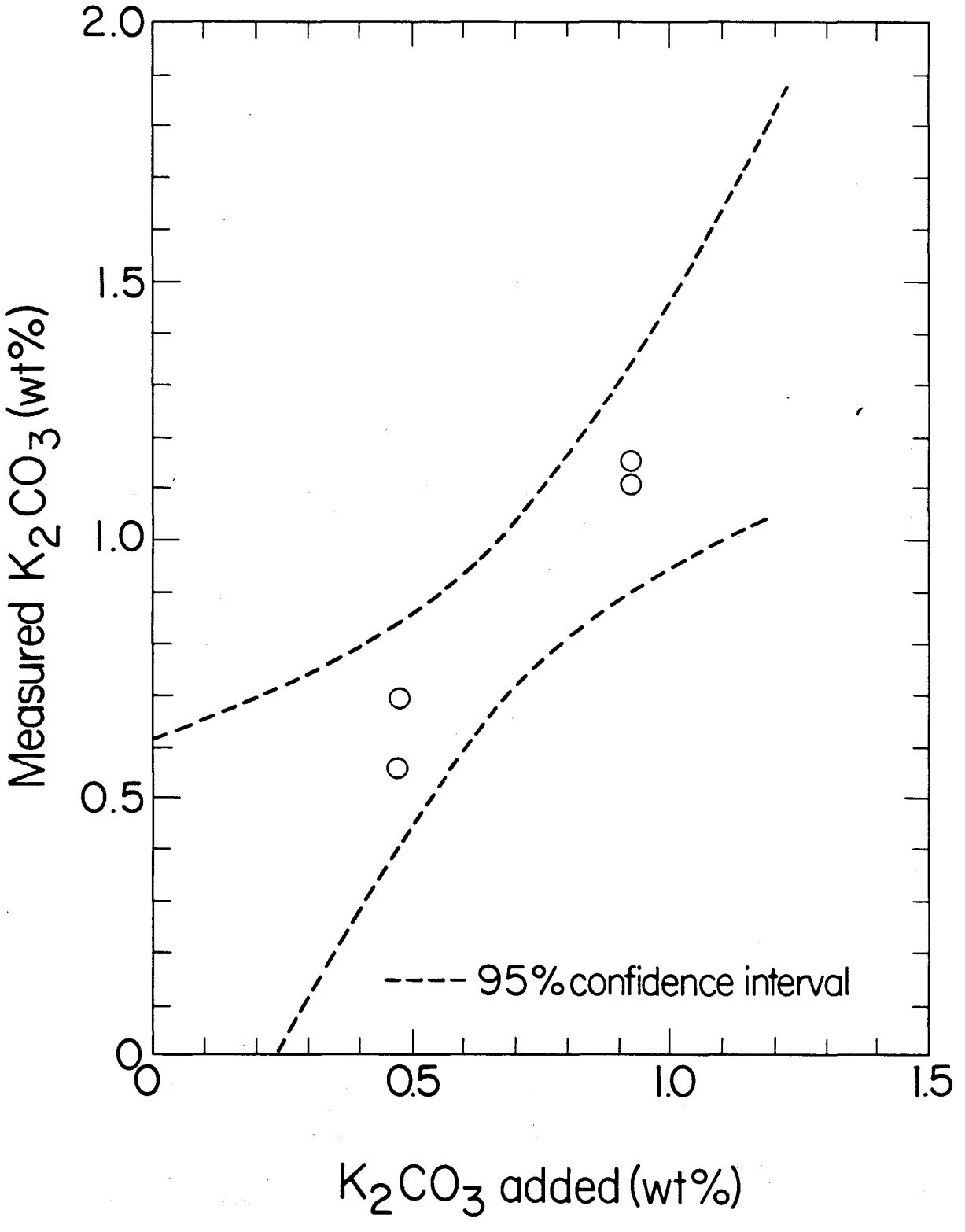

Figure D-1. Titration for Carbonate in Zn-free 46% KOH Electrolyte.

mass measurements. Most of the hydroxide was neutralized with 0.1 M HCl. As the pH 8.3 endpoint was approached, a 0.01 M HCl titrant was used to bring the solution to the endpoint. The 0.01 M HCl was also used to continue the titration to pH 4.

The variation in the quantity of argon appeared to vary by 1% of the sample mass which would cause unacceptable 1% variation in the hydroxide analysis. The carbon dioxide in the 125 mL flask would amount to a 3% bias in the measurement at the 0.5% level, or 30% at the 0.05% level. This was remedied by using a 10 gram sample for which a 0.1 M HCl titrant could be used rather than the 0.01 M HCl. Only the carbonate was determined from the 10g sample; and the hydroxide was determined from a separate 1g sample.

This modified method was used on the 30% KOH-1% LiOH electrolyte. A carbonate composition of 0.053 wt% ± 0.009 wt% K_2CO_3 was determined which verifies the improved accuracy expected from this method over the method used to obtain the data shown in Figure D-1; it is <u>much</u> better than the Ba-EDTA method. The KOH concentration in the separate 1g sample was measured to be 30.22 wt% ± 0.20 wt% for an expected value of 30 wt% KOH ± 0.08 wt%. The complete results of the hydroxide and carbonate analysis are presented in Chapter III, Section 4.

4. Alternate Carbonate Analysis in the Presence of Zinc

For alkali electrolytes containing dissolved ZnO, the carbonate content could be determined by an alternate procedure when the only dissolved acid gas is CO_2. The electrolyte sample could be neutralized and

made sufficiently acidic to allow the carbonate to be purged from the solution as CO_2. The CO_2-containing purge gas would then be scrubbed with a KOH solution sufficiently alkaline to efficiently absorb the CO_2. The carbonate content in the scrub solution would be determined by the titration procedure presented in Section 3.

The electrolyte sample must be free of other dissolved acid gases such as F^- or $S^=$. These would carry over to the scrub solution and interfere with the carbonate titration. The scrubbing solution must be sufficiently low in carbonate so as not to mask the CO_2 absorbed. This requirement implies a large electrolyte sample or a high carbonate content in the sample.

Low carbonate concentrations could be analyzed by a similar method where the alkaline scrubbing solution is replaced by commercially available CO_2 analysis equipment capable of quantitatively measuring μg amounts of CO_2.

Neither of these methods was investigated, but they may be worthy of further investigation. The use of an alkaline scrubbing solution would require careful design to optimize the quantity of scrubbing solution and the sample size.

5. References

1. R.B. Fischer and D.G. Peters, "Chemical Equilibria," W.B. Saunders, Pub., Philadelphia (1970).

2. S.U. Falk and A.J. Salkind, "Alkaline Storage Batteries," John Wiley and Sons, New York (1969).

3. D.A. Otterson, NASA Tech. Report TND-8007, Cleveland, Ohio (1975).

4. Steven Fong private communication, December 1980.

5. G.E.P. Box, W.G. Hunter and J.S. Hunter, "Statistics for Experimenters," John Wiley and Sons, New York (1978).

6. I.M. Kolthoff and V.A. Stenger, "Volumetric Analysis, Volume II Titration Methods," Interscience Pub. Inc., New York (1947).

TECHNICAL INFORMATION DEPARTMENT
LAWRENCE BERKELEY LABORATORY
UNIVERSITY OF CALIFORNIA
BERKELEY, CALIFORNIA 94720